A Mathematical Framework to Optimize Methods for De-noising and Features Extraction of EEG Signals and Perspectives on Applications of Experimental Observations

A Thesis
submitted in partial fulfillment of the requirements for the degree of
Doctor of Philosophy

by

Balbir Singh
(Student Number: 14899001)

Kyutech
Kyushu Institute of Technology

Graduate School of Life Science and Systems Engineering
Kyushu Institute of Technology
Japan

March , 2017

A Mathematical Framework to Optimize Methods for De-noising and Features Extraction of EEG Signals and Perspectives on Applications of Experimental Observations

by

Balbir Singh

Submitted to the Graduate School of Life Science and Systems Engineering
in partial fulfillment of the requirements for the degree of

Doctor of Philosophy

Author . . . .
Graduate School of Life Science and Systems Engineering
March , 2017

Certified by . . . .
Hiroaki Wagatsuma
Associate Professor
Thesis Supervisor

Accepted by . . . .
Kiyoshi Natsume
Chairman, Department Committee on Graduate Thesis

at the

Kyushu Institute of Technology

March 2017

This doctoral thesis has been examined by a Committee of the Graduate School of life Engineering Department:

Professor Kiyoshi Natsume..
Chairman, Thesis Committee
Professor of Human Interaction and Brain Function

Professor Masaaki Nagahara..
External Member, Thesis Committee
Professor of Automatic Control, Artificial Intelligence, Sparse Modelling and Applied Mathematics

Associate Professor Hiroaki Wagatsuma..............................
Thesis Supervisor, Thesis Committee
Associate Professor of Intelligence Systems and Emergent Design

Associate Professor Keiichi Horio..................................
Member, Thesis Committee
Associate Professor of Intelligence Systems and Emergent Design

A Mathematical Framework to Optimize Methods for De-noising and Features Extraction of EEG Signals and Perspectives on Applications of Experimental Observations

by

Balbir Singh

Submitted to the Graduate School of Life Science and Systems Engineering
on March , 2017, in partial fulfillment of the
requirements for the degree of
Doctor of Philosophy

Abstract

Electroencephalography (EEG) data inevitably contains a large amount of noise particularly from ocular potentials in tasks with eye-movements and eye-blink, known as electrooculography (EOG) artifact, which has been a crucial issue in the brain-computer-interface (BCI) study. The eye-movements and eye-blinks have different time-frequency properties mixing together in EEGs of interest. This time-frequency characteristic has been substantially dealt with past proposed denoising algorithms relying on the consistent assumption based on the single noise component model. However, the traditional model is not simply applicable for biomedical signals consist of multiple signal components, such as weak EEG signals easily recognized as a noise because of the signal amplitude with respect to the EOG signal. In consideration of the realistic signal contamination, we newly designed the EEG-EOG signal contamination model for quantitative validations of the artifact removal from EEGs, and then proposed the two-stage wavelet shrinkage method with the undecimated wavelet decomposition (UDWT), which is suitable for the signal structure.

The features of EEG-EOG signal has been extracted with existing decomposition methods known as Principal Component Analysis (PCA), Independent Component Analysis (ICA) based on a consistent assumption of the orthogonality of signal vectors or statistical independence of signal components. In the viewpoint of the signal morphology such as spiking, waves and signal pattern transitions, A systematic decomposition method is proposed to identify the type of signal components or morphology on the basis of sparsity in time-frequency domain. Morphological Component Analysis (MCA) is extended the traditional concept of signal decomposition including Fourier and wavelet transforms and provided a way of reconstruction that guarantees accuracy in reconstruction by using multiple bases being independent of each other and uniqueness representation, called the concept of "dictionary". MCA is applied to decompose the real EEG signal and clarified the best combination of dictionaries for the purpose. In this proposed semi-realistic biological signal analysis,

target EEG data was prepared as mixture signals of artificial eye movements and blinks and iEEG recorded from electrodes embedded into the brain intracranially and then those signals were successfully decomposed into original types by a linear expansion of waveforms such as redundant transforms: UDWT, DCT,LDCT, DST and DIRAC. The result demonstrated that the most suitable combination for EEG data analysis was UDWT, DST and DIRAC to represent the baseline envelop, multi frequency wave forms and spiking activities individually as representative types of EEG morphologies.

MCA proposed method is used in negative-going Bereitschaftspotential (BP). It is associated with the preparation and execution of voluntary movement. Thus far, the BP for simple movements involving either the upper or lower body segment has been studied. However, the BP has not yet been recorded during sit-to-stand movements, which use the upper and lower body segments. Electroencephalograms were recorded during movement. To detect the movement of the upper body segment, a gyro sensor was placed on the back, and to detect the movement of the lower body segment, an electromyogram (EMG) electrode was placed on the surface of the hamstrings and quadriceps. Our study revealed that a negative-going BP was evoked around -3 to -2 seconds before the onset of the upper body movement in the sit-to-stand movement in response to the start cue. The BP had a negative peak before the onset of the movement. The potential was followed by premotor positivity, a motor-related potential, and a reafferent potential. The BP for the sit-to-stand movement had a steeper negative slope (-0.8 to -0.001 seconds) just before the onset of the upper body movement. The slope correlated with the gyro peak and the max amplitude of hamstrings EMG. A BP negative peak value was correlated with the max amplitude of the hamstring EMG. These results suggested that the observed BP is involved in the preparation/execution for a sit-to-stand movement using the upper and lower body. In summary, this thesis is help to pave the practical approach of real time analysis of desired EEG signal of interest toward the implementation of rehabilitation device which may be used for motor disabled people. We also pointed out the EEG-EOG contamination model that helps in removal of the artifacts and explicit dictionaries are representing the EEG morphologies.

Keyword

Brain-computer-interface (BCI), Electroencephalography (EEG), Electrooculography (EOG), Electromyogram (EMG), Undecimated Wavelet Decomposition (UDWT), Wavelet Shrinkage, EEG-EOG Contamination Model, Morphological Component Analysis (MCA), Discrete Cosine Transform (DCT), Local Discrete Cosine Transform (LDCT), Discrete Sine Transform (DST), DIRAC and Bereitschaftspotential (BP).

Acknowledgments

First of all, I praise God for providing me this opportunity and granting me the capability to proceed successfully. After an exhaustive period of nine months, I write this note for acknowledgment in my thesis. It has been a period of intense learning for me in scientific arena as well as personal level. I would like to imitate on the people who have unceasing supported with suggestion in various direction and helped me so much throughout this period. First I offer my sincerest gratitude to my supervisor, Associate Professor Hiroaki Wagatsuma, who has supported me throughout my thesis with his knowledge whilst allowing me to work in my own interest. I would particularly thanks to Professor Kiyohisa Natsume, who has given the opportunities to conduct the EEG behavioural experiment and continuous research discussion. I would like to thanks the member of PhD committee Professor Kiyohisa Natsume, Professor Masaaki Nagahara, Associate Professor Hiroaki Wagatsuma, Associate Professor Keiichi Horio for their excellent suggestion and detail review during the thesis evaluation. In addition, I would like to thank my tutor and friend Dr. Kazuma Komoda for valuable guidance and help. I thank to my all lab members for their support and help. I am grateful to Akiko Yanagimoto, for assisting me in many different ways and handling the paperwork. I would also like to thank my parents and family for their wise counsel and sympathetic ear. Thank you so much, you always there for me. Finally, thanks to all my friends, we were not only able to support each other by deliberating over our problems and findings and relative, we Thank you very much, everyone who directly or indirectly supported and helped me.

Balbir Singh

Contents

List of Figures

List of Tables

Chapter 1

Introduction

Advancements in modelling of mathematical methods and computational science has been playing an important role for manufacturing the biological systems. There has been a great interest in the effective and precise model that contributing to solve the fundamental problem of many applications in daily life. The electrical signal called electroencephalography (EEG) measured from the brain is one of the biological aspects that has much more probability to assist and bring convenience to our daily life. Many researcher and engineers are widely used EEG signals in neuroscience, cognitive science, cognitive psychology and psychophysiological research etc. EEG signals are used for clinical application , biometric systems and brain computer interface (BCI), *e.g.* a smartphone display the brain activities in time and frequency domain. There are many more application that has a great interest from medicine to military objective[1, 2, 3, 4, 5, 6].

1.1 Motivation

During last few years, EEG-driven applications have been increased day by day. The basic principle of these applications is work in real-time and may be used as portable device. The BCI system [7] is one of the best example that communicate between the device and EEG signal taken from scalp. It is independent of its normal output pathway of peripheral nerves and muscles. The BCI system is allowed the user to interface with the device and is based on real-time analysis of EEG signals associated with the recognition of the event related task. The BCI system is depend on intermediary functional components, the control signals, and feedback loops. An intention of the user relies on the brain state to generate a signal that has the input signal for the BCI system. There were a lot of studies done by researcher throughout the world for the accuracy, online analysis etc. And much more research is required to achieve the sustainable goal.

Rehabilitation device is one of the option that may be used for motor disabled and healthy people. However, every EEG-driven application has its own particularity (*e.g.* under the condition which is during body movements, or in an almost still state without any motion but intensive brain activities) therefore prediction of the brain activities through EEG become a huge and highly attractive field of research. It is very crucial to understand the principles by which neural ensembles encode sensory, motor and cognitive information [8] and how to extract these features from EEG signals that may be used for particular EEG-driven application. It is equally important that the physiological features of neuron and which areas of the brain are involved [9]. To overcome all these as a general framework is difficult. The more EEG-driven application means the more meaningful feature from EEG signals. The EEG study is assessed in term of frequency and time series analysis. The EEG in time series [10, 11, 12] are used to measure the nonlinear dynamic behaviour, sparsity pattern of the brain, understanding the time sequences, model the time series and estimate the brain behaviour and it help to design the BCI system. The individual EEG frequency bands reveal the information of neurophysiology in frequency analysis of the brain [13]. The EEG signal features extraction have not clearly identified, such as which frequency band is used or which event-related potential (ERP) to be tested during the practical implications. So it is very important to specify the original purpose before talking about EEG-driven application although there may exist some common point between these EEG-driven applications. The brain activities is measured during a task and removal of EOG artifact and feature extraction by decomposition is described in next section.

1.2 Objective of Dissertation

The main objective of this dissertation is a signal/noise separation in biological system. For that a mathematical framework is proposed to optimize methods for denoising and features extraction of EEG signals during voluntary movement related task. To achieve this objective, this work is divided in three steps:

- A mathematical framework to optimize "signal decomposition with high visibility".
- To discriminate " true biological signal" from noise clarification of information representation.
- Pursuit of what kind of "information" can be obtained in the specific motion control task.

This dissertation describes a robust methodology to denoise and decompose the EEG signal into its component and an experimental paradigm provides the EEG information for rise to stand-up behavior. In experimental paradigm, the EEG component "negative going potential called bereitschaftspotential (BP)" based on movement related cortical potentials (MRCPs) are efficient and practically may be used for rehabilitation device for the functional movement disorder. The most prominent problems are removing artifacts and robust algorithms for extracting the features from EEG signal that is consider as the input for BCI system. A general view of this dissertation is illustrated by Figure 1-1.

The highlighted block in Figure 1-1 is the new methodology based on sparsity to improve the practicability of EEG analysis for real time. The main purpose is to explored the morphological diversity of the component feature in the EEG signal. Each component feature reveals the different morphological characteristics.

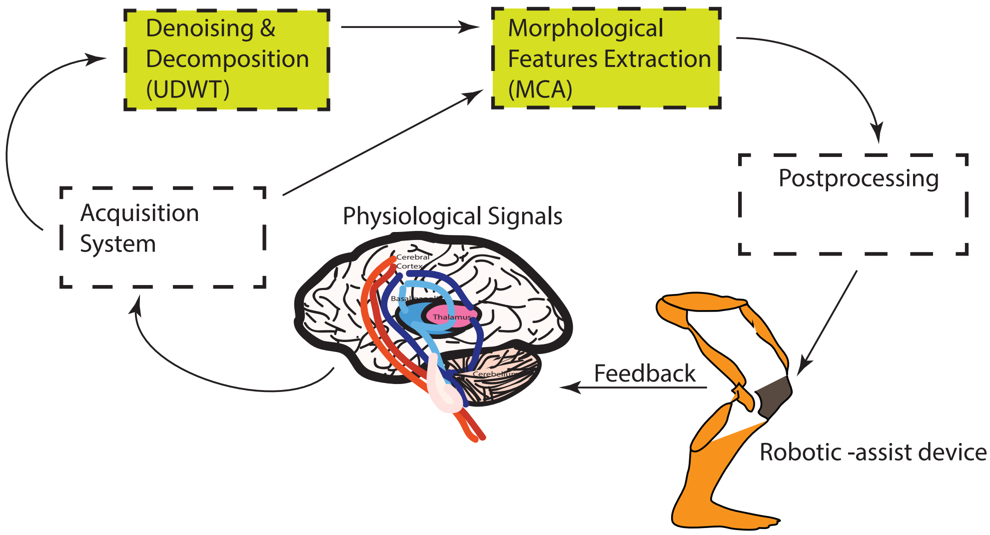

Figure 1-1: A proposed scheme for Denoising & removal of EOG artifacts using 'UDWT' and Morphological Features Extraction using 'MCA' for neurorobotics rehabilitation, first of all the Physiological signal taken from the voluntary participant performs rise to stand-up task. Then remove the artifacts and extract the features based on morphology.

1.3 Organization of this Dissertation

This dissertation is organized in two major parts *i.e* mathematical framework and new experiment paradigm for rise to stand-up. The first part consists of methodology & algorithms for EEG denoising and decomposition. The second part consists of detail study of experimental paradigm and decomposition of the raw EEG signal using MCA.

Chapter 2: This chapter comprises all preliminary knowledge and information related to human brain. The brain activity and their properties is mentioned that includes the characteristics of EEG in term of frequency. The different types of artifacts affect the EEG and the sources of artifacts.

Chapter 3: The eye-movements and eye-blinks have time-frequency properties mixing together in EEGs. This time-frequency characteristic has been substantially dealt with past proposed denoising algorithms relying on the consistent assumption based on the single noise component model. In consideration of the realistic signal contamination, we newly designed the EEG-EOG signal contamination model for quantitative validations of the artifact removal from EEGs, and then proposed the two-stage wavelet shrinkage method with the undecimated wavelet decomposition (UDWT), which is suitable for the signal structure.

Chapter 4: The advantage of a sparse representation of EEG signal has used to extract the feature of EEG signal. In the viewpoint of the signal morphology such as spiking, waves and signal pattern transitions, we proposed a systematic decomposition method to be able to identify the type of signal components on the basis of sparsity in time-frequency domain. Morphological Component Analysis (MCA) extended the traditional concept of signal decomposition including Fourier and wavelet transforms and provided a way of reconstruction that guarantees accuracy in reconstruction by using multiple bases being independent of each other and uniqueness representation, called the concept of dictionary". MCA is applied to decompose the real EEG signal and clarified the best combination of dictionaries. The different types of redundant dictionaries ('UDWT', 'DCT', 'LDCT', 'DST' and 'DIRAC) is used to decomposed the sparse feature of EEG signal. In this part of the dissertation to decompose the EEG signals in different morphological features and extract the useful information.

Chapter 5: This chapter comprises human brain information for a rise to stand-up behavior experimental paradigm. The detailed study of EEG and EMG activity of this experiment is recorded. It contains the Bereitschaftspotential as preceded the motor related cortical potential. Here, the most important point to understand the properties of the brain activities in a rise to stand-up behavior. The slow cortical potential particularly Bereitschaftspotential is one of the parameters to be used for rehabilitation BCI device. The EEG and EMG have been used to implement the complex, dynamic and voluntary behavior for developing the robot-assisted device for motor disabled person to stand-up.

The rest of the dissertation includes the summary and conclusion in Chapter 6. Chapter 3, 4 and 5 include the main contribution of this dissertation.

Chapter 2

Research Background and Preliminaries

This chapter is explained the brief overview of the human brain structure and their different functional activities. The short description of brain measuring activity and recording techniques. The different types of artifacts that usually contaminates in the EEG signal.

2.1 Human Brain

The human nervous system is divided into two parts: the central nervous system (CNS) and peripheral nervous system (PNS) [14]. CNS comprises of the brain and spinal cord. The brain defined as an integration of many functional activities like thought, emotion organ control. The spinal cord defined as the transmission medium of sensory information to and from the peripheral nervous system. The PNS consists of the afferent and efferent fibres. To be specific, the human brain structure organization is a complex hierarchical network which comprises with billions of neurons [15]. The hierarchical network is split into various circuits, columns and functional areas. Even the brain is distinguished in two hemispheres; they are separated by the central sulcus and commutate with each through corpus callosum and anterior commissure and further it can divide into four lobes frontal, parietal, temporal and occipital.

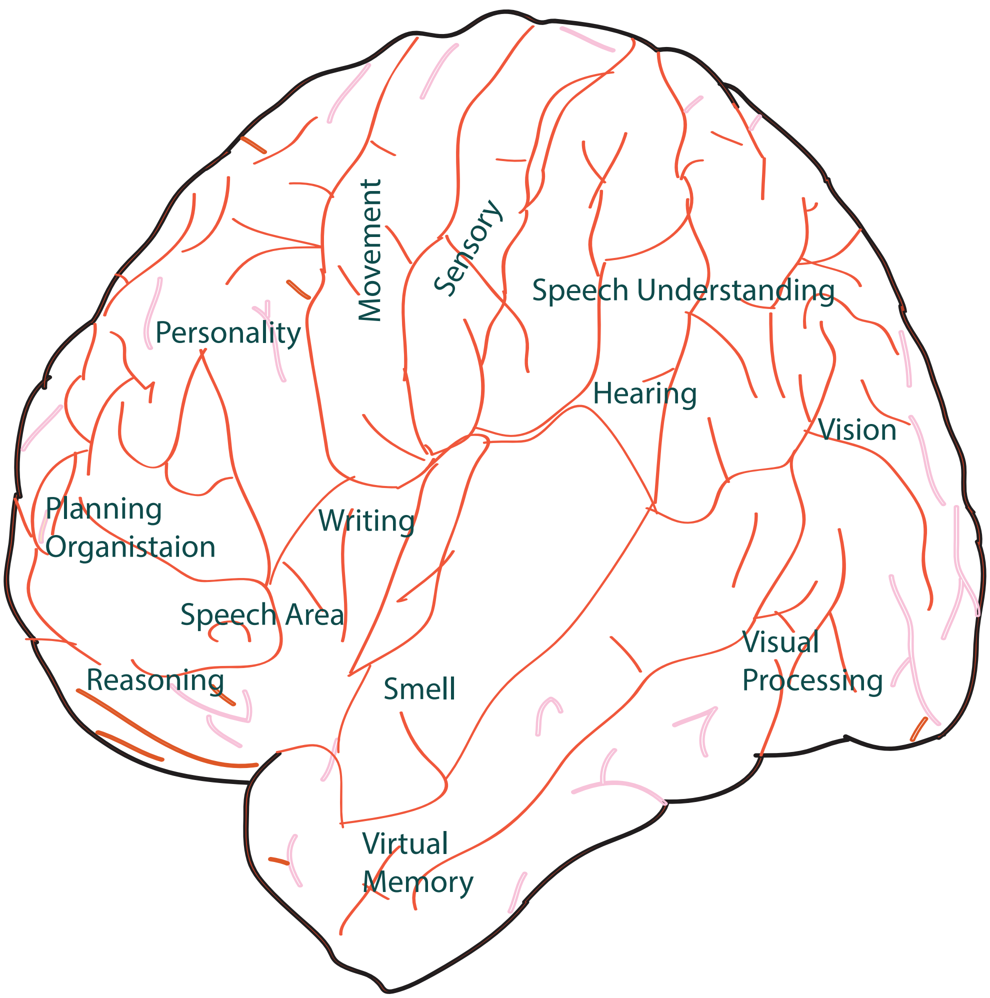

Figure 2-1: A schematic representation of functional areas of human brain.

The Figure 2-1 is cover the whole brain structure that illustrates the location of the functional areas. The topological of the whole human brain is a functional networks [16] and these networks separating into modules, each module is connected with internal or intra-modular. The gray matter, white matter, axons and cell bodies are the major components of the human brain. The gray matter is distributed over the surface of the cerebral hemispheres. The motor cortex is a region of the cerebral cortex associated with planning, control, and execution of voluntary movement.

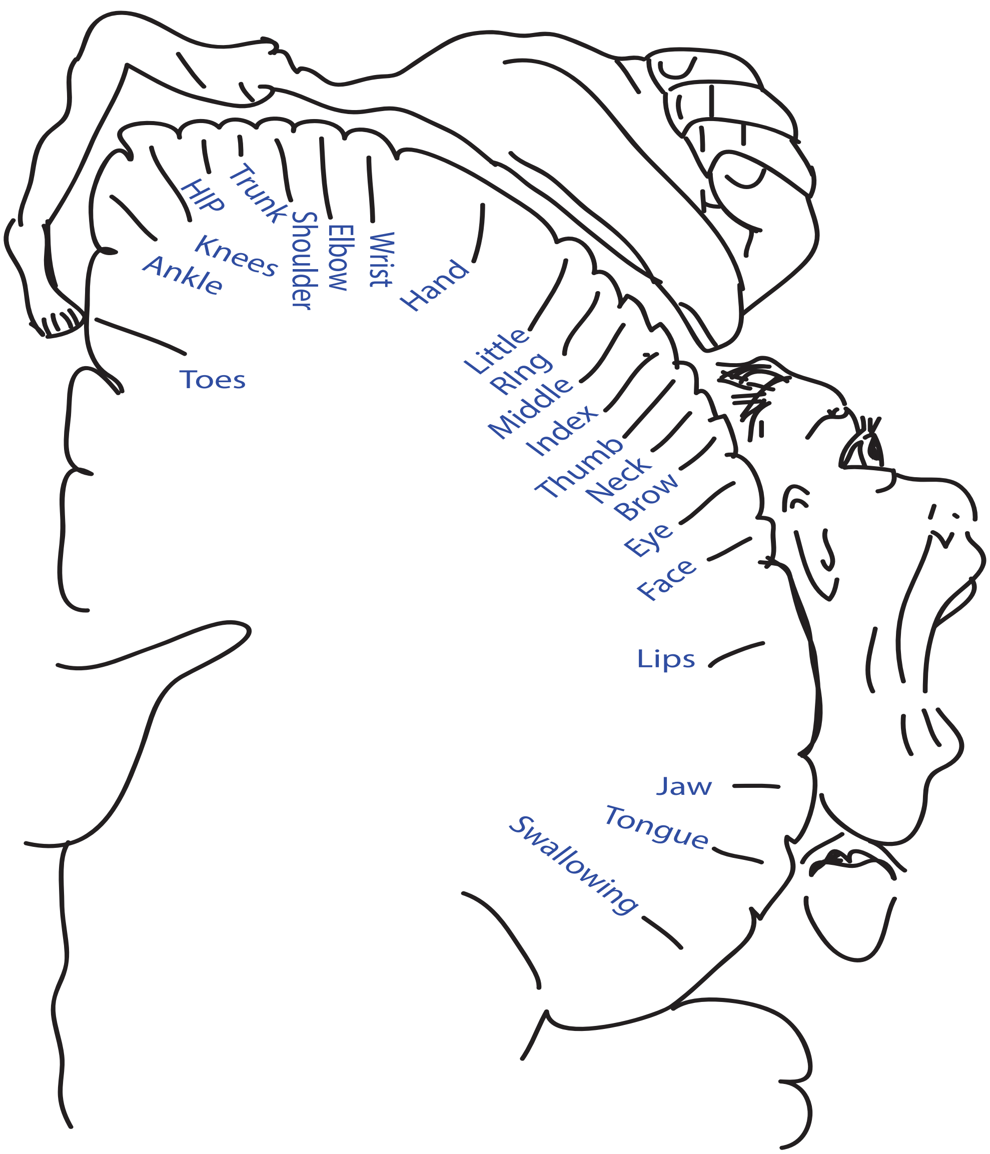

Figure 2-2: Organization of different parts of the body on the motor cortex.

The Figure 2-2 shows the motor cortex area according to the Penfield and Rasmussen theory. And area on the cerebral are activated during preparation, posture control and task execution of voluntary movement and are widely used in BCI as non-invasive EEG [17]. There are several parts of brain those are contributing from preparation to execution of voluntary movement that shown in Figure 2-3 [18].

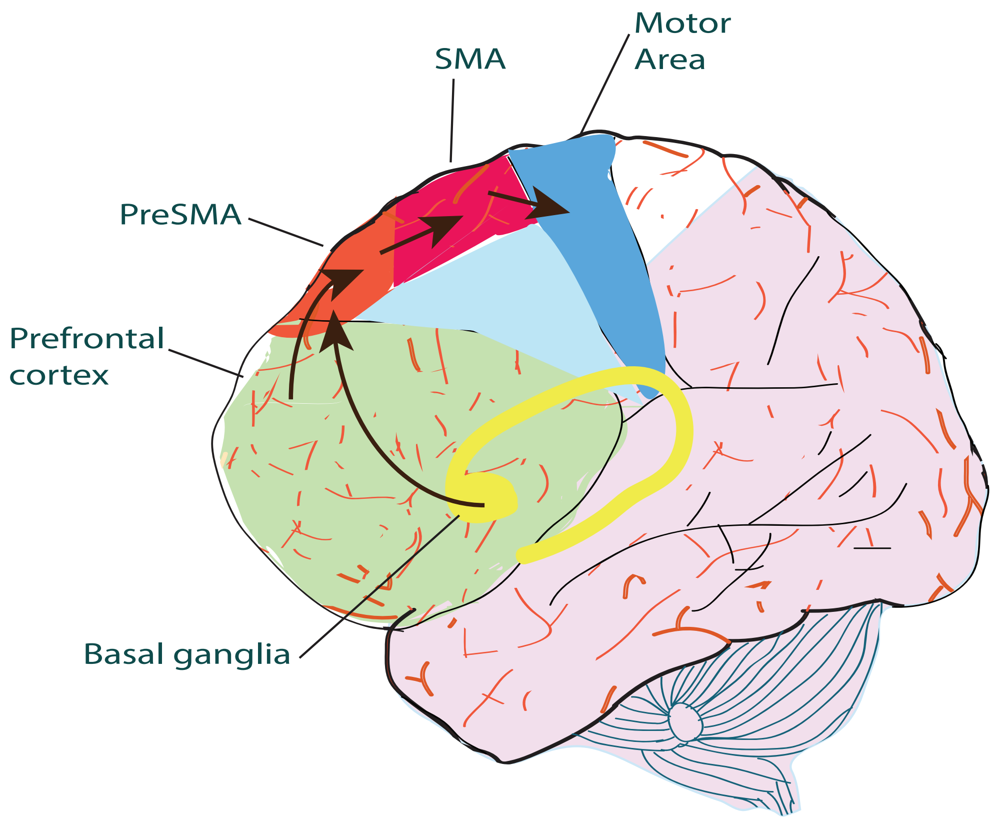

Figure 2-3: From basal ganglia to prefrontal cortex, PreSMA, SMA to motor for preparation of voluntary movement.

In voluntary movement, the motor cortex receives two input, one from the supplementary motor area that flow from basal ganglia to prefrontal cortex and pre supplementary motor area and second input receives from sensory cortices that flow from parietal cortex [18]. The parietal premotor circuit is associated with object oriented action such grasping, sensory input and voluntary behaviour [18].

2.2 Brain Measuring Activity

A biosignal may be defined as the description of a physiological phenomenon, irrespective of the nature of description[19] and are classified in electrical and non-electrical signals. The EEG, ECG, EMG, EOG and much more are categorized as electrical signals. The biosignals are non-stationary, continuously measured and monitored. In this dissertation, we focus on classifying the brain state for various mean by using EEG signal. In 1920, the first EEG recorded from human scalp demonstrated by Berger.

2.2.1 Brain rhythms

The brain is composed of billions of particular neurons and nerve cell or brain cell. The neuron receives information from cells and transmits to other cells. Neuron consists of nucleus and cell body, cell body is extensions to dendrites which bring the information to the cell body and on opposite side of neuron extension called axons which transmit the information to another neuron through axon terminals. The information flows from dendrites to axon as shown in Figure 2-4.

The Figure 2-4 [20, 21] is illustrated the mechanism of electrical activity passes from one end of a nerve cell to another cell that carries information about the intensity of the nerve cell. Every neuron maintains a voltage difference between its membranes and a significant voltage difference called the action potential or nerve impulse is generated by ensembles of neurons at different spatial scales that reflect the activity of few nearby nerves cells. The neuronal activity is connected through the spike across the cortical regions that create local oscillations and establish their coherence between distant cortical areas [22]. The electrical activity is measured as a wave called brain wave or brain rhythms[20, 21]. The brain rhythms [23] are generated various forms of rhythms by a central nervous system. These electric activities in the human brain are capable of firing in specific patterns which cause rhythms and rhythms are ubiquitous features of brain dynamics oscillation [24]. The functional task is associated with physiological rhythms but generation mechanism of these rhythms remain a mystery.

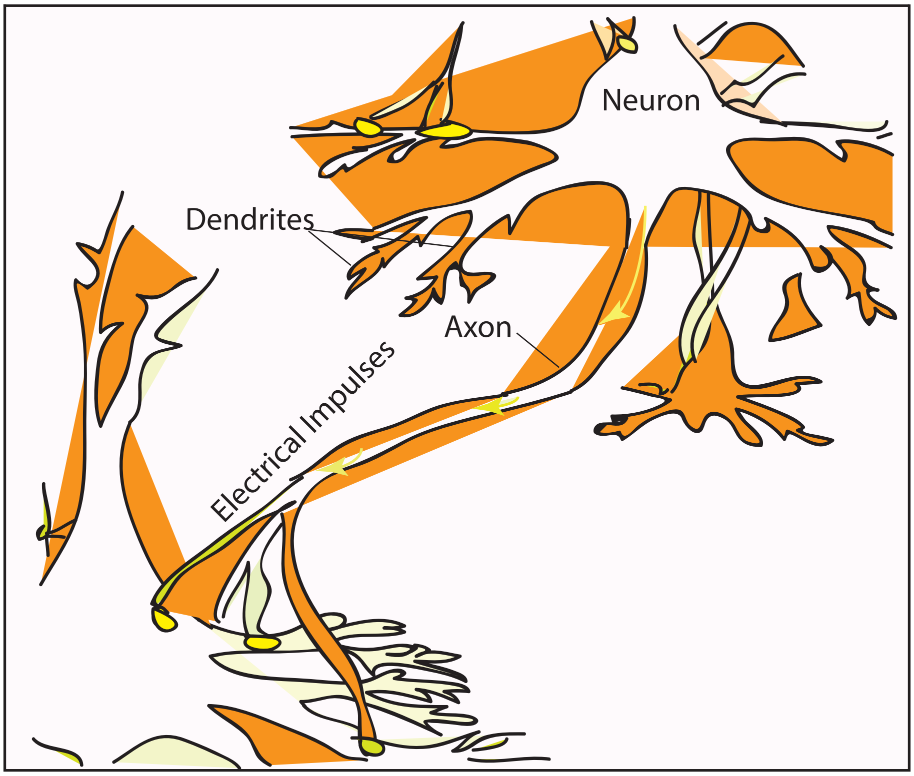

Figure 2-4: Synaptic transmissions.

The brain rhythms play an important role to facilitate the internal and external behaviour. The rhythms in the brain are initially and superficially uncovered in the EEG measurement.

The undulation electrical potential is brain waves, monitoring and recording are called EEG [25, 26]. The continuous electrical activity of the brain is measured from the scalp by various recording apparatus (EEG, MEG, fMRI, TMS, PET etc.). These apparatus are classified on their temporal and spatial resolution. EEG is a high temporal resolution, low cost and easy to implement. The imaging techniques such functional magnetic resonance imaging (fMRI) have the spatial resolution. The combined implementation of fMRI and EEG is to grab the gap between temporal and spatial resolution, but it is a sophisticated method to implement. Other imaging techniques such transcranial magnetic stimulation (TMS) and magnetoencephalography (MEG) is provided with the high temporal and spatial resolution. MEG measures the electromagnetic fields that are generated by electrical currents in the intracellular fluid. However, MEG is the temporal resolution similar to EEG. It has the ability to identify neural generators but it is expensive and time-consuming. TMS directly stimulates the cortical regions using magnetic waves. TMS is good in spatial resolution, fMRI is superior to TMS. The simultaneous recording of EEG and fMRI or EEG and TMS are improved the temporal and spatial resolution to identify the neural activity [27, 28]. The intensity and pattern of electrical activity are determined by the level excitation of different parts of the brain. Much of the time brain waves are irregular and no specific pattern can distinguish in the EEG and MEG[29, 30, 31]. Due to the advancement of recording techniques, it is possible to monitor and record the neuronal activity in the brain simultaneously. Mostly EEG is examined from the scalp by electrodes that are not directly from neuron tissues. The indirect contact is established by an electrolyte bond formed by electrode gel in between electrode and skin. EEG is used to diagnose and analyse symptoms. EEGs has an advantage that the EEG test contains vast information without an invasive procedure. The EEG monitoring is proving the effective in the diagnosis of epilepsy, tumor, cerebrovascular lesions, ischemia and many others brain disorder associated with the brain.

2.2.2 Brain rhythms frequency

The brain wave is the superimpose of many action potentials by the neuron in the brain measured by monopolar and bipolar techniques. The first Human EEG was recorded by the Hans Berger in 1924. The EEG wave is relatively small and measured in microvolts (μV). The human brain rhythmic is distinguished based on relevant frequency bands. These frequency bands are used for classification. The rhythmic activity within a certain frequency band of EEG is varied from 0.1 to 100 Hz for clinical purpose and sometimes it have a strict band that varies from 0.5 to 70 Hz. Every brain rhythmic is distributed over the scalp and it has a certain biological significance. The range of relevant frequency bands of the EEG is used for measurement or analysis is known as delta, theta, alpha, beta and gamma.

Delta: Delta frequency band tends to be the highest amplitude and slowest waves (has frequency range of 0.5 - 4 Hz) [32]. It is normal as the dominant rhythm in infants up to one year and mainly characterized during deep NREM in stages 3 and 4 of sleep [33, 34]. It may occur focally with the subcortical lesion and in general distribution with diffuse lesions, metabolic encephalopathy hydrocephalus or deep midline lesions. It is usually most prominent frontally in adults and posteriorly in children.

Theta: Theta frequency band is the frequency range of 4 - 7.5 Hz [34] and defined by slow wave activity. It is normal in children and in sleep but abnormal in awake adults. It is associated with emotion [35] and memory [36]. The midline frontal activity is linked to low anxiety and increased approach related to behaviour [37]. It is considered as a manifestation of focal subcortical lesions; it may be seen in generalized distribution in diffuse disorders such as metabolic encephalopathy or some instances of hydrocephalus.

Alpha: Alpha frequency band is the frequency range of 7.5 - 14 Hz and associate with relaxed wakefulness state with closed eyes. It is generated in the occipital and anterior regions [38, 39]. The higher amplitude is seen in the posterior regions. It disappears when opening the eyes or calculating or thinking. It is the major rhythms seen in normal relaxed adults. It is presented during most of life especially after the thirteenth year.

Beta: Beta frequency band is the frequency range of 14 - 30 Hz and described as a fast activity. It is a symmetrical distribution on both sides usually and is most evident frontally. It may be absent or reduced in areas of cortical damage. It is observed as a normal rhythm. It is dominant rhythms in patients who are alert or anxious or have their eyes open [40, 41].

Gamma: Gamma frequency band is the frequency range of 30 - 100 Hz. It is associated with visual perception and cognition and related to cognitive task execution and many researchers consider for working memory [42]. It is involved in the formation of memory, language processing, internal thought, behaviour, actions, attention, arousal and object recognition.

2.2.3 Artifacts in brain rhythms

EEG artifacts are non-cerebral in origin that considered as extraneous signals appeared in the desired waveform. Although the artifacts are often recognised by the experts due to their morphology and distribution. The systematic approach of recognition, source identification and elimination of artifacts are an important process to reduce the chance of EEG distort and limit the potential for adverse clinical consequences. These artifacts are divided into two types physiological and non-physiological based on their origin. The non-physiological artifact arises from the external electrical interference and internal electrical malfunctioning of the recording system (recording electrodes, electrode positioning, cables, amplifiers etc.). The non-physiological (Extaphysiologic) artifacts [43] are based on the origin of the source given below:

- **Electrode Artifacts:** The electrode artifacts are various types such as electrode pop, electrode contact, electrode movement, perspiration, salt bridge and lead movement. The electrode artifact [44] is brief transients and restricted to one electrode and low-frequency rhythms across the scalp region. The brief transient is spontaneous electrical potential discharging, it is happened due to the electrode and skin interface to act as capacitor and store electrical charge across the electrolyte gel [45, 46]. The electrode movement is produced the slow wave. The salt bridge artifact is due to smearing of the electrode paste and electrodes [45] and it produced the unwanted electrical connection by forming a channel in between the electrodes.

- **External Interference Artifacts:** The external interference artifacts [47, 48] are produced from the electrical fields, magnetic fields, mechanical effects on the body and another form of external device noise. Due to this the high amplitude, irregular, spike-like signals are accumulated in the EEG signals. These artifacts have high frequency, static morphology and periodically repetition rate in nature. The Mechanical devices such as ventilators and circulatory pumps are usually produced artifacts with slower components than other electrical devices. The artifact is typically repeated at fixed intervals and a slow or complex wave includes a mixture of frequencies superimposed on a slow wave. It is a great complex job to recognized the specific variety features of the artefacts that each device may produce based on its setting. Usually, the artifacts from external devices have produced the waveform that is highly dissimilar to cerebrally generate waveform, therefore unusual waveform should always be suspected as the artifact. The most common external artifact is due to alternating current present in the electrical power supply. This artifact is usually medium to low amplitude and has fixed frequency of the current, which may be 60 Hz and 50Hz depends on the location of the world. It may present in all channel or in the isolated channel due to poorly matched impedance.

The physiological artifacts arise from the movement (head, body and scalp), bio-electrical potentials (potentials generated due eye, tongue and pharyngeal muscles movements, the scalp muscles, heart or sweat glands), and change in skin resistance as described below:

- The cardiac artifact are generated by the heart and mixed with EEG across the head and left ear, particularly over-weighted participants or patients. It is timely locked to cardiac contractions and easy to identify by their synchronization with ECG channel.

- The pulse wave artifact is a periodic wave of smooth or triangular shape may be picked up by an electrode on or near a scalp artery as the result of the pulse wave. This is more likely to happen with the electrode in the frontal and temporal areas. It is recognized by it usually regular occurrence or by touching the electrode producing it.

- Skin potential is generated due to change in skin and produced the perspiration artifact and galvanic skin response. The perspiration is caused the slow shift of the electrical base line by changing impedance or contact between the electrode and skin. It is revealed as low amplitude and beyond the frequency range of

EEG. The sweat artifact is characterized by low frequency (0.25 to 0.5 Hz). Slat bridge artifact are different from perspiration artifact by lower in amplitude and typically including only one channel.

- The head and body movements are caused the movement artifact. It is rhythmical in tremor, chewing and sucking, breathing and cardioballistographic [49]. These movements are produced artifacts during the EEG recording by mean of the electrical field generated by muscle and this movement is effected on the electrode contacts and their leads.

- Muscle artifact [50, 51] is one of the most common and significant source of artifacts in EEG signal. The muscle artifacts have high amplitude and frequency as compared to EEG signal. Muscle artifact has appeared in beta frequency band or spikes if high frequencies filter is used. EMG signal has a more disorganized appearance because the individual myogenic potential overlaps with each other. The duration of muscles artifact is varied according to the duration of the muscle activity *i.e.* from one second to entire recording. EMG artifact has most commonly occurred in channels including the frontal and temporal electrodes.

- Ocular artifact [52, 53, 54, 55] is due to slow roving eye movement and blinks; each eyes inherent 10 mV electrical dipole. The slow eye movement has occurred with the drowsiness and has an involuntary and repeated horizontal ocular movement; has a constant period phase reversal due to eye dipoles. The electric field due to dipole has occurred with eye gaze, eye opening and eye closing become relevant to EEG recording; and myogenic potential has occurred due to eyelid movement with eye opening and closing may also contribute ocular artifacts. Due to rapid up and down movement of eyes are caused the blinking artifacts. A slow wave ocular artifacts have occurred due to repetitive blinks and it resemble with delta rhythms. These artifacts are may distinguished by its morphology.

The experienced researcher are easily distinguished between the EEG signal and artifacts. By visually reviewed the entire EEG recording and selected the artifact segments is one of the often to remove the artifacts by expert researcher. It is time consuming and it became reader fatigue due to multichannel recording. There various algorithms or methods are used to remove the artifacts but it quit difficult to remove completely. The EEG analysis is limited to certain frequency bands, according to that an algorithm can be designed to analyse in particular band, for example 1 to 20 Hz band pass filter to remove muscle artifacts. Therefore this kind of algorithms cannot be used for entire bandwidth of EEG as artifacts can be occurs at any frequency varies from .5 to 100 Hz. The filtering processes is altered the appearance of EEG signal and the artifacts identification become more difficult.

The EEG signals are the most complex electrical activities generated by the cortical neurons in the brain. The scalp electric change representing collective spike activities is very weak rather than electric changes from other biological signals, such as electrooculography (EOG) and so on. However artifacts from various body sources such as the heart, muscle movements are easily contaminated into EEG signals and then the noise removal is an important issue. The ocular artifacts are potentially in the range of 100 V that is much larger than EEG and low-frequency band. Ocular artifacts are happened especially near stimulation onset distort baseline and the invoked potentials greatly. It is possible to improve the signal-to-ratio by signal averaging, evoked potentials are usually very weak (for example < 10 V). The ocular artifact doesn‘t follow any statistical distribution that is also one of the drawbacks. The influence of ocular is suppressed by increasing the number of trials. The EOG is overlapped the lower frequency band of EEGs and make the low-frequency component of EEG unclear during spectrum analysis. These EEG data inevitably contains large amounts of noise particularly from ocular potentials in tasks with eye-movements, which is an inevitable issue in the brain-computer interface (BCI) study. To remove the artifacts from EEG signals depends on their characteristics, which they hold. Every artifact has different characteristics that make difficult to model as a universal artifacts removal. And artifacts from various body sources interference to EEG signal which produce nonlinear and non-stationary signals. However, the artifacts have become a serious problem in the daily BCI application.

In this dissertation, we focused on wavelet and morphological based method to remove the artifacts and to identify the particular artifacts and separate from the EEG signals. These algorithms may be adapted for each kind of patient.

Chapter 3

Introduction of Morphological Component Analysis

This chapter explained the overview of the denoising, artifacts removal, feature extraction and classification methods applied to the EEG signal. The brief overview of the morphological component analysis method. The morphological component analysis is allowing us to decompose/separate the source components of a biological signal which have different morphological component.

3.1 Overview of EEG Signal Analysis Methods

There are various methods with a different approach has been used in the EEG signal analysis and still in going state because of the complicated mechanism of physiological behaviour or principles. Therefore, it is difficult to say one method is the best method for EEG signal analysis. Moreover, there is no standard approach or method can be used to compare with a new approach. Research are developing the methods considering some assumption and verification theories to explore the representation of neuron activities. The EEG signal is non-stationary signals. They have been considered the approach in time-domain, frequency domain and time-frequency domain. The removal of artifacts is the most prompting problem.

3.1.1 Methods for detection and rejection of artifacts

The various methods for detection and rejection of artifacts [56, 57] are given below:

- To detect the period and reject the EEG signal is the simplest approach to remove artifacts. The artifacts related non-stationary behavior need to select the method parameters.

- we can consider the energy operation for the sudden change in EEG signals spikes and they are sensitive to instantaneous fluctuation. Due to moving subtle change in signal spectrum become less sensitive.

- Autoregressive (AR) model of the signal within Kalman filter setting to predict future of time series and examine data for significant deviation from their predictions.

3.1.2 Methods for suppressing artifacts

- The muscle artifacts cannot eliminate the EMG artifacts in the frequency selective filters (low-pass, high-pass, band-pass used in artifacts processing band-stop) due to their broad spectrum.

- To measured the reference signal in the Dual channel rejection scheme. The EEG and the reference signal can be processed to remove the artifact. This can be achieved by using time-domain regression, wiener filters, frequency domain regression or adaptive filtering.

- The limitation of such approaches are the quality of the reference measured signal and cross contamination by the EEG signal of interest provides an absolute limit on performance.

- For EMG artifacts removal the regression analysis and wiener filtering have been used.

- Adaptive filtering has been used to remove EOG from general EEG signal.

- The frequency selective filtering ha been applied on each channel independently and dual channel methods exploit a dedicated reference channel.
- An ICA approach has been exploited the multichannel character of most EEG signals to decompose the data into a set of random variables which are maximally independent.

3.1.3 Feature extraction

The features extracting from a signal of interest is often carried in the time series EEG analysis. And the feature can be defined as parameters which provide information about the underlying structure of a signal. The feature can be classified in various category:

- Temporal features:
  - Temporal features are characteristics obtained from the signal in the time domain Instantaneous statistics: it is the simplest features which frequency used temporal features in sleep EEG analysis. These statistics include measures derived from moments of the waveform including the mean absolute amplitude standard deviation/ variance skewness and kurtosis as well measures relating to the probability density function of the waveform such as mode, median or the entropy.
  - Zero crossing and period amplitude analysis (PAA) Zero crossing are the points at which the waveform crosses the x-axis they are simple to compute and zero crossing rate encoding the frequency information PAA approach can be adopted within the frequency band to mitigate the effects of noise and to reduce the issues associated with signals comprised of multiple components.
  - Hjorth parameters The parameters are based on the variance of the derivatives of the waveform and have been used for some time to characteristics EEG waveforms. Three Hjorth parameters defined to describe activity

mobility (shape) and complexity of EEG signals Hjorth parameters are sensitive to noise.

  - Detrended fluctuation analysis (DFA) DFA is a method to characterise long-range temporal correlation in time series and used as a measure of self-similarity. It is based on identify trends in the signals variance when analysed with different block length and is inherently suitable for the analysis of non-stationary noisy signals.

- Spectral features:
  - The most commonly extracted features are the spectral features from EEG. They are an essential parameter which characterises the signals in frequency domain.
  - The fast Fourier transform is the most common spectral analysis of non-parametric methods for spectral estimation.
  - The multiple signals are used to measured the cross -spectral analysis is called coherence analysis. It reflects the degree of synchrony between the frequency component of two signals and can provide estimates of functional connectivity in the brain. A related approach is the directed transfer function method (directly coherence) which provides information about causation and so is suitable for investing functional connectivity in the different brain region. DTF is sensitive to the phase shift between signals but robust in the presence of noise.
  - The parametric spectral estimation based model to spectral estimation are used the digital filter excited by white noise, methods based on auto-regressive (AR) modelling.
  - The subspace methods are the form of parametric spectral estimation. They are based on assumption that the signal consists of sinusoids in white noise and exploits the Eigen structure of the resulting correlation matrix. MUSIC multiple signals classification algorithms EEG application

underlying model for there methods is not well matched to practical EEG signals.

  - Higher order spectral analysis(HOSA): The principle behind the power spectral analysis have natural extensions to a higher order. A significant problem when applying HOSA is that they require considerable quantities of data in order to obtain good estimates.

- Time-frequency features: Time-frequency analysis is a powerful tool which allows decomposition of signals into both time and frequency.

  - The short time Fourier transform compute the signal of interest in uniformally segmented manner into many short duration overlapping portion. The time-frequency resolution of STFT is directly determined by the segment size, the smaller the segment the higher the time resolution and the lower the frequency as resolution.

  - The wavelet transform is closely related to the STFT whilst STFT can be regarded as representing a signal as a set of windowed sinusoids of different frequencies, the wavelet transform represent a signal using a function which is scaled and shift in time. The scaling factor and time respectively it uses variable size windows to achieve time-frequency decomposition short duration function representing high frequency components and long duration function representing low frequencies. Orthogonal discrete wavelet transform is generally not time shift invariant. The different time shifts in the input don't results in time shifted in the input don't result in time shifted version of the decomposition but a different decomposition which may limit its use in certain application.

  - Matching Pursuits it is more recently developed time-frequency analysis methods. It is based on signals description via collection of mathematically function (commonly Gaussian modulated sinsusoids) called dictionaries. An advantages of MP is the large dictionary size which is not not limited to acertian form of function (as opposed to the Fourier transform which uses only sinsuoids or the wavelet transform which employ a mother wavelet function .MP achieves time-frequency decomposition by finding the best matches that fit structure of the signal from the dictionary. The parameter of the identified matches in time , frequency amplitude and energy results in a complete decomposition of the signals. A possible shortcoming of the methods is its high computational cost which may limits it use in real time application.

  – The Empirical mode decomposition (EMD)is a heuristic decomposition technique which provides a signal representation. The signal is broken down into basis function(IMF Intrinsic mode function) which have distinct oscillatory modes.

- Non-linear features In non-linear feature methods assumed that EEG signals are generated from stochastic processes EEG signals may be generated from a deterministic nonlinear process. There are some non-linear methods such as Fractal dimension (FD), Correlation dimension, Entropy measures and Lyapunov exponents.

3.1.4 Features classification

The features are measurable characteristics of a time series used to reduce the signals dimension and methods such as Neural networks classification, clustering (unsupervised learning) self organizing maps or kohonen maps. And the statistical classification such as the Linear discriminant analysis (LDA), support vector machines (SVM), Hidden markov model, Fuzzy classification and the combined classification.

3.2 Morphological Component Analysis

The decomposition of signal component into its constructed component is one of the great interests for many applications. In this kind of problems, there is an assumption that any given signal/image is a linear combination of several source components of more coherent origin. There is a lot of research to draw the attention. A signal S is a linear combination of the different component generated by a various source. Here, we describe the EEG signal in this way

$$S = B \times X \tag{3.1}$$

Most of the researcher used the various method such as ICA, PCA, wavelets and much more to decomposed a signal into its constructed components. PCA methods compute the orthonormal basis to minimizing the average linear approximation error over of a signal component. Suppose the S is a signal that has to decompose in k component of the raw signal, except that all component have unit variance. In the case of the blind source separation methods, the aim is to blindly estimate both the mixing matrix B and the X from the known S signal only. This problem is called ill-posed problem which requires the prior knowledge of mixing matrix and the source components to be recovered. There is a classical approach (discriminant information or diversity between the source components) for this kind of problem. Therefore the ICA methods are work by assuming the statistically independent of the source components.

Due to the advancement of Harmonic analysis and applied mathematics, the morphologically sparse modelling of signals has attracted a lot of interest. We assumed that each source can be sparsely decomposed in some basis, waveform dictionary or some signal representation. The MCA is recently developed methods to decomposed the signal and image into it different component, Now the component depends upon the types of dictionaries it is based on the signals description in the form of mathematical function. The sparsity methods are typically used for the separation of signal mixtures with varying degrees of success. The morphological component analysis is used to morphologically decompose / separate the building component of the signal. This method relies on the sparsity and over-completeness dictionary; An over-complete dictionary $\Phi \in R^{n \times k}$, where k morphological component coefficient of signal for $\{\phi_k\}_{k=1}$ and a signal S is sparse linear combination of source components.

The over-complete dictionary Φ is a set of redundant transforms /mathematical function that represents the specific waveform/signal source components or designed by adapting its coefficient to fit a given set of signal that leads to sparse representation. A dictionary/redundant transform can reproduce the specific source components of the signal using the sparse representation. The sparsity and over-completeness dictionary concept benefits the signal decomposition extends to source component extraction and more. Extraction of the sparest representation is a hard problem that has been extensively investigated in the past few years.

The dictionary is usually used for sparse representation or approximation of the signal/image and dictionary learning or training in the signal processing. A dictionary is a collection of elements and n length elements are the real column vector. A finite dictionary can be represented by $n \times L$ matrix of L elements. The dictionary such as discrete sine transform (DST) is a Fourier transform similar to the discrete Fourier transform (DFT) but using a purely real matrix and the dictionary discrete cosine transform (DCT) which is equivalent to a DFT of real and even function. There are various types of transforms such as DCT, Orthogonal Wavelet transforms, Bi-orthogonal wavelet transforms and lifting scheme. Redundant transform such as Local DCT, Undecimated Wavelet Transform, Isotrophic Undecimated Wavelet Transform, Ridgelet Transform, Curvelet Transform. Basically, these transforms are filtered coefficients.

The limitation of traditional tools such as linear systems and Fourier analysis for solving the geometry based problem because they don't directly address the issues of how to quantify the shape and the size of the signals. A complex signal such as EEG signal often are not well represented by a few coefficients in single basis, therefore, large dictionaries in cooperating more pattern can increase sparsity and thus improve the application to compression, denoising, inverse problem and pattern recognition. The important thing to finding the set of k dictionary coefficients that approximate a signal with minimum non-deterministic polynomial-time (NP) hard error in redundant dictionaries. Therefore we can compute the redundant dictionary of $n \times L$ which minimizes the average non-limitation approximation error of signals.

NP-hard but greedy optimization are possible. The best combination k approximation, $\Phi = \{\phi_k\}_{k\in\Gamma}$ be a over-complete dictionary of k basis coefficients in signal space. The type of dictionary includes a combination of orthonormal basis (Fourier basis, Dirac delta basis, wavelet DCT and Gabor dictionary. The Gabor dictionary is constructed by scaling, modulating and translating a Gaussian window on the signal-sample grid on the basis of time and frequency translation-invariant. The n elements of the waveform ϕ_k are discrete time signals. Depending on the dictionary, the parameter k can have the interpretation of indexing frequency, in this case, the Fourier dictionary. Time scaling indexing the dictionary is a time scale dictionary, time-frequency indexing the dictionary is a time-frequency dictionary. Dictionaries are complete or overcomplete in that case they contain exactly n elements or more than n elements but continuum dictionaries containing an infinity of atoms and under complete dictionaries for special purposes, containing fewer than n elements, many of interesting dictionaries have been proposed over last few years. Suppose that a ϕ discrete dictionary of j waveform and we consider all these waveforms as columns of $n \times p$ matrix and the decomposition is given by

$$S = \sum_{k=1}^{j} \phi_k \beta_k \tag{3.2}$$

When the dictionary furnishes a basis then ϕ is an $n \times n$ non-singular matrix and we have the unique representation $\beta = \phi^{-1}s$, when the elements are mutually orthonormal, then $\phi^{-1} = \phi^T$. The difference between the synthesis waveform $S = \Phi\beta$ and the analysis waveform $\tilde{\beta} = \Phi^T S$.

A signal S as a linear combination of different component generates by the various source with the desired source the representation of these signals are sparse over the augmented dictionaries Φ. Blind the source separation by MCA to determine the original source set of signals, where each signal is assumed to be a linear mixture of the source, disadvantage the component do not necessarily only contain artifacts data, but also contains underlying EEG data removing this lead to loss of EEG data. The morphology of signal can be used for recognized and based on the separate from the combined signal. The sparsity, morphological diversity play an important role in decomposing. It is devised the quantitative measures of diversity to extricate between the sources. The signals with different morphology have disjoint significant coefficients in a sparsifying dictionary. The linear mixture with additive Gaussian noise and the mixing mixing matrix criterion measures a deviation between the true mixing matrix and estimate source components. To extend the spatial and spectral sparsity constraints. Morphological component analysis consist of mathematical and theoretical concepts for signal analysis, nonlinear signal operator design methodologies and application system that are related to mathematical morphology.

A over-complete dictionary as collection of waveforms $\{\Phi_k\}_{k\in\Gamma}$, assume that EEG signal is linear combination of a small number basis elements ϕ_k. It would be expressed as one dimension $S \in R_N$ and combination of many signals, $S = s_1 + s_2 + \cdots + s_k$, where s_1, s_2, $\ldots$ and s_k represents different types of morphology of the signal to decomposed. The signal S approximation decomposition into its building components can be expressed as

and to estimate k unknown source components of a signal from m linear mixture with $m > /n$

$$\begin{aligned} S &= \textstyle\sum_{i=1}^{k} \phi_k \beta_k + W \\ &= \phi_1\beta_1 + \phi_2\beta_2 + \cdots + \phi_k\beta_k + W \\ &= s_1 + s_2 + \cdots + s_k + W \end{aligned} \tag{3.3}$$

We expressed equation above without external noise as

$$S = \sum_{i=1}^{k} \phi_k \beta_k \tag{3.4}$$

And we need to solve, this is given by

$$\begin{aligned} &\{\beta_1^{opt}, \beta_2^{opt}, \cdots, \beta_k^{opt}\} = \underset{\beta_1,\cdots,\beta_k}{\arg\min} \textstyle\sum_{i=1}^{k} \|\beta_i\|_0 \\ &\text{subject to: } S = \textstyle\sum_{i=1}^{k} \beta_i \phi_i. \end{aligned} \tag{3.5}$$

The above equation suffered with several drawbacks,therefore to minimized the drawbacks the source coefficients are defined as follows [58]

$$\begin{aligned} &\{\beta_1^{opt}, \beta_2^{opt}, \cdots, \beta_k^{opt}\} = \underset{\beta_1,\cdots,\beta_k}{\arg\min} \textstyle\sum_{i=1}^{k} \|\beta_i\|_1 \\ &\text{subject to: } S = \textstyle\sum_{i=1}^{k} \beta_i \phi_i \end{aligned} \tag{3.6}$$

Here the l_2 norm as the error norm is intimately related to the assumption that the residual behaves like a white zero-mean Gaussian noise. The functions in dictionaries subdirectory provide fast implicit analysis and synthesis operation. All dictionaries are normalized such that elements have unit l_2 norm. To estimated the source coefficients by solving the above equation in iterative manner. The iterative algorithm is used to estimate the sparse source EEG signals as proposed by Starck et al [58]. The mathematical derivation of the methods and algorithms is given in article [58].

1. Initialize $= I_{max}$, number of iteration and threshold $\delta = \lambda * I_{max}$.

2. Perform J times:

3. For $k = 1, \cdots, K$:

   Update of s_k assuming all $s_i, i \neq k$, are fixed:

   - Calculate the residual $r_k = S - \sum_{i=1,i\neq k} s_i$
   - Calculate the transform T_k of s_{k+r} and $\beta k = T_k(s_k + r)$
   - Calculate $\phi_k = \tilde{x_k} T_k$
   - Soft threshold the coefficients

     $beta_k$ with threshold δ and obtain $\hat{\beta_k}$
   - Reconstruct s_k by $s_k = R_k \hat{\beta_k}$
   - Apply the constraint correction by $s_k = s_k - \mu_\gamma \frac{\partial C_k\{s_k\}}{\partial s_k}$
   - The parameter μ is chosen either by a line search minimizing the overall.

4. Update the threshold by $\delta = \delta - \lambda$.

5. If $\delta_k > \lambda_k$

   Return to Step 2. else finish.

In the decomposition process normalize the threshold has an important impact. The signal processing and function approximation, overcomplete can help the researcher to achieve a more stable robust or more compact decomposition than using a basis. Based on above theory question rose in mind, how we can embed MCA methodology in the biomedical signal especially EEG signal. A new MCA method has been used to identification of component on the basis of time-frequency of EEG recording. As we already mention the dictionary and requirement of MCA methodologies that lead the success of arbitrary EEG signal decomposition. The effectiveness of MCA is mostly clarified in image processing [58, 59, 60, 61, 62].

Chapter 4

Two-Stage Undecimated Wavelet Shrinkage Method

In this chapter, EOG artifacts are removed from the recorded EEG and denoising the EEG signal. The artifacts are an inevitable issue in the brain-computer interface study. The scheme of EEG-EOG signal contamination model is proposed and the two-stage wavelet shrinkage method with undecimated wavelet decomposition is used for quantitative validations of the artifacts removal from EEGs, which is suitable for the signal structure. A hundred dataset of open-source clinical intracranial EEGs in each behavioural condition is introduced to the validation to be raw EEG before the contamination of artifacal EOGs. The EEG signal reconstruction is validated according to the frequency spectrum profile representing a specific brain state. Numerical analyses demonstrated that the first stage is pursued the signal envelop with high amplitude fluctuations provided by artificial EOGs and the significant EEG spectrum was reconstructed in the second stage, which exceeded the performance of the conventional shrinkage, suggesting threshold values properly set depending on the individual amplitudes of multiple signal sources in the proposed method. The present results are focused on actual amplitude-frequency structure in the polygenetic signal and contributed to not only provide the decomposition performance but also revealed how they are mixed together in the viewpoint of a standard model for robust validations.

4.1 Introduction

EEG signals are very popular tool to observe the brain activity for clinical purpose like reflecting sensation, recognition, action plans even with mental imagination, neuroscientific investigation and BCI in recent demand [63, 64, 65]. The EEG signals are recorded from the scalp and are susceptible to external interference such electric power noise or other electromagnetic radiation sources. These artifacts are easily removed from EEG signals depending on signal electrical characteristics. However, the artifacts from various sources such as EOG, ECG and EMG are easily contaminated with the EEG signals because multiple electrophysiological mechanisms exist in the brain and other biosignals [66, 67, 68], which makes the EEG signal nonlinear and non-stationary. Therefore the artifacts removal and denoising become a very important issue in EEG signal need to be solved. Many time-frequency analyses have been studied such as fast Fourier transform (FFT), wavelet transform (WT) [69] and eigenvectors for EEG signal features extraction [70]. The speed and accuracy of feature extractions are the critical issue in EEG signal and wavelet methods have been discussed as a solution for unstable signals if the mother wavelet is appropriately introduced. The subspace projection methods such as principal component analysis (PCA) and independent component analysis (ICA) are frequently used to remove the artifacts. But every method has some limitation and not used for real time analysis. A PCA is a sophisticated method as it influences the overall data space based on the principal components (PC) therefore it is difficult to suppress the artifacts and component that represent the artifacts. To identify PC requires the prior knowledge as the artifact [52, 66]. ICA based methods were getting popular in the purpose of the signal decomposition into independent components having high order statistics. It works after the recording as an offline analysis under the sufficient computational power, which assures a high reliability in accuracy while the selection of components of interest requires a classification by human experts to be semi-automatic or heuristic approaches [71]. Secondly it does not confirm the extracted component have original scale and sequence. More over EEG recording can be rather noisy and since ICA is based on a measure of independence, the noise in the input channel can be even amplified by ICA, which again makes the detection of the true EOG component rather difficult most ICA methods are blind to Gaussian noise and spread the noise among the extracted components which is undesired [67, 68, 72, 73].

An adaptive filtering [74] is a powerful technique to suppress the artifacts from the EEG signal. The spectral distortion is the main limitation in filtering method that harms the further application. The artifacts are removed by decomposition method EMD (Empirical mode decomposition) from the EEG signals has been used [75]. It is represent the non-stationary signals as sums of zero-mean amplitude modulation frequency modulation components [76]. The artifact are suppressed by adaptive filtering approach from EEG signals [77]. The EMD method is used the time domain filter to the extract the artifacts. The EMD makes no priori assumption about the composition of the signal. It is used the spline Interpolation between maxima and minima to generate the IMF (Intrinsic Mode functions). Each IMF will be a single periodic oscillator and cannot be predicted empirically from the signal. The number of IMF cannot be predicted before the decomposition is based on a signal feature and doesnt depend on a basis function and therefore it makes difficult to work.

The above methods are suggested that they are not process on-line in comparison of time-frequency analyses such as WT and another subspace projection methods that do not preserved original signal amplitudes in decomposed components, which is a serious lack in some clinical cases because a diagnosis is analyzed based on EEG waveform abnormalities [78, 79, 80] and then those methods were used for the pre-filtering before the time-frequency analyses [81]. The FFT based methods are obtained consensus for being assured detection methods of specific disorders, e.g. epileptic seizures and attention-deficit/hyperactivity disorder (ADHD) [82, 83, 84]. WT based on-line approach for signal decomposition have high expectations with less computational costs. The time-frequency characteristics of EEG signal is preserved to maximum extent, and radically improved FFT analyses [85, 86, 87, 88, 89].

As discussed above that EEG is composed with different characteristics in time-frequency domain and have specific waveform. Similar, the noise source and artifacts can be represent with time-frequency characteristics that different from EEG signals. Therefore, focusing on the denoising and artifacts removal in EEG signal. WT which removes the high frequency components, the undecimated wavelet transform (UDWT) is the perfect method to denoising and artifact removal and an effect of the UDWT was preliminary reported by Lang et al. [90] in 1995, and recently it is applied to bio-signal recordings [91]. The wavelet shrinkage is effectively used in the image processing application to reduce the contaminated noise and it works for data size compression, which is known in the JPEG2000 standard for image compression [92]. In principle, wavelet denoising was defined in the continuous wavelet transform (CWT) mathematically and evaluated in comparison with the discrete wavelet transform (DWT) to test how much accurately the original signal can be reconstructed by Lang et al. [90] which suggested the importance of the shift-invariance property in the UDWT. Starck [91] demonstrated the effectiveness of the UDWT in various cases and noted that the threshold value is not simply determined in general, rather it requires to tune carefully the level depending on the target signal.

4.2 Wavelet Shrinkage and Denoising

The decomposition of EEG signal using WT also known as decimated wavelet transform as one of the best technique in analyzing non-stationary EEG signals.The information is lost in the process of denoising based on thresholding and resulting improper reconstruction of signals. The DWT which down samples the approximation coefficients and details coefficients at each decomposition level but UWDT doesn't incorporate the down sampling operation, thus the approximation coefficients and details coefficients at each level have the same length as original. The UWDT up samples the coefficients of the low pass and high pass filter at each level. The up sampling operation is equivalent to dilating wavelets. The resolution of the UWDT coefficients decrease with increasing levels of decomposition, therefore we have to choose proper levels for decomposition. The approximation coefficients and details coefficients of EEG signal length will not decreased and at the same time no aliasing information is present after the decomposition of EEG signals. The Figure 4-5 shows the decomposition scheme of EEG signals at different levels by UWDT.

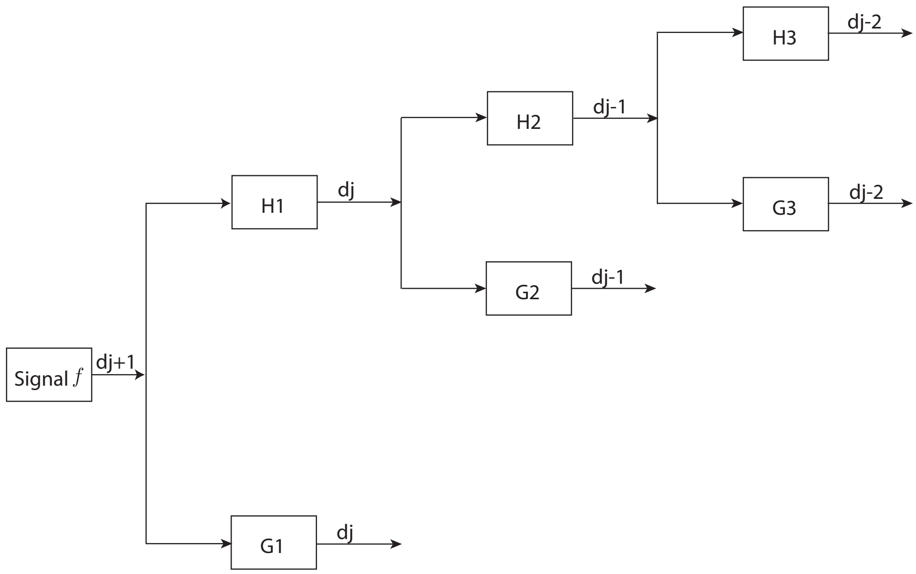

Figure 4-1: A wavelet decomposition scheme.

In addition to the UWDT has the translation or shift invariant property. If the two signals have shift version with respect to each other, then the UDWT results also have shifted version each other while it does not exist in an ordinary DWT. UWDT gives more amount of information compared to DWT. The translation invariant property is important for feature extraction in EEG signals. Denoising with UWDT also is shift invariant and the denoising result with UWDT is better balance between smoothness and accuracy than DWT [90, 91, 93]. UWDT is supported both the real and complex signal as compared to DWT used for real signals. The drawback of UWDT is that it requires higher computational memory and redundancy in the coefficients. UDWT modifies the DWT decomposition scheme by changing the low pass and high pass at each level [93]. It is imitated the sub-sampling of the filtered signal by including zeros between each of the filter coefficients to up-sampling the low-pass filter at each level. The UDWT is based on the 'a trous' algorithms. The UDWT using the wavelet filters of a 1-D signal [91, 94].

4.2.1 Denoising

The denoising signal model initially formulated by Donoho [95, 96, 97, 98, 99, 100] defined as the output signal y of a function f with a white noise z, described by equation 5.1

$$\begin{aligned} y_i &= f(t_i) + \sigma z_i \ (i = 1, \ldots, n) \\ &= f_i + \eta_i \end{aligned} \tag{4.1}$$

where $n = 2^{J+1}$, the the unit interval $t_i = i/n(t \in [0,1])$, z_i is a Gaussian white noise, and σ is the noise level. The Figure 4-2is schematically illustrate the denoising signal model. The recording signal in the double lined box in the Figure 4-2 is obtained as the summation and then it can be decomposed by the denoising method [95, 96, 97, 99, 100] if the relationship between the signal f and noise η satisfies $f \gg \eta$.

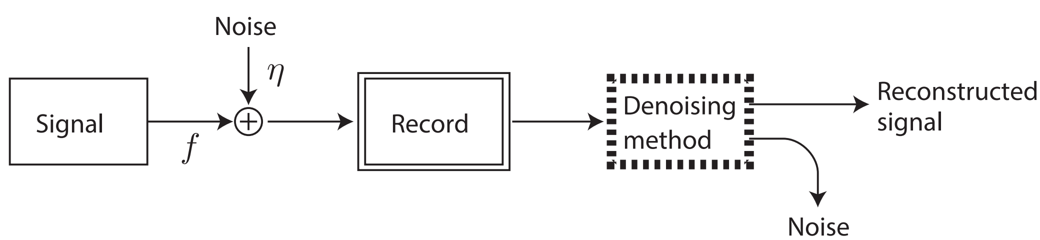

Figure 4-2: Typical signal model f with a noise η in the form of the linear combination.

To design denoising algorithms [90, 91] with adaptive thresholds, three following steps can be applied,

1. pyramid wavelet filtering of Cohen et al. [101] to the coefficient of signal $\beta_{J+1,k} = y_k/\sqrt{n}$, yielding noisy wavelet coefficients $w_{j,k}$ $(j = j_0, \ldots, J;\ k = 0, \ldots, 2^j - 1)$

2. the wavelet coefficients are passed through thresholding protocol either with soft-threshold operation $s(w)$ or hard-threshold operation $h(w)$ with a certain threshold level λ, yielding renewed wavelet coefficients $w_{\lambda_{j,k}}$

3. the signal $\hat{f}(t), (t \in [0,1])$ is recovered by inverting the wavelet transform using the renewed coefficients for $j > J$

Here the soft-thresholding is given as

$$s(w) = \begin{cases} \mathrm{sgn}(w)(|w| - \lambda) & |w| \geq \lambda \\ 0 & |w| < \lambda \end{cases} \tag{4.2}$$

and the hard-thresholding is given as

$$h(w) = \begin{cases} w & |w| \geq \lambda \\ 0 & |w| < \lambda \end{cases} \tag{4.3}$$

as non-linear operations, as illustrated in Figure 4-3. Hard-thresholding, called "keep-or-kill": a wavelet coefficient w with an absolute value under the threshold λ is replaced by zero and soft-thresholding: coefficients with magnitude above the threshold are shrunken, contributing to preservation of the smoothness of the original signal [102]. The difference clearly appears in the error magnitude curve with respect to the threshold level.

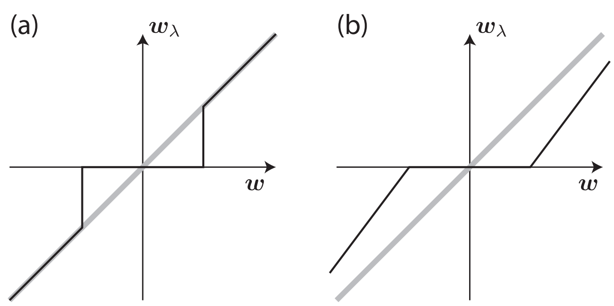

Figure 4-3: Noise reduction by wavelet shrinkage, where gray and black lines respectively denote the original and shrunken wavelet coefficients. (a) Hard-thresholding, (b) Soft-thresholding

There are various ways to define the optimal threshold such as Minimax and rigorous SURE, we used the universal threshold,$\lambda_{univ} = \sigma\sqrt{2log(n)}$, known as larger than the Minimax for any particular value of n [68]. According to Donoho and Johnstone [97, 99], the threshold can be consider as

$$\lambda = \sqrt{\log n} \cdot \gamma \cdot \sigma / \sqrt{n} \tag{4.4}$$

where γ is a constant if the empirical wavelet transform of f is denoted as $W_n^n f$ that is quasi-orthogonality [99]. The multiplier factor of the threshold of the threshold value is depended on the target signal. And the universal thresholds [96] value can be given as $\lambda = \hat{\sigma}\sqrt{\log n}$ where the error $\hat{\sigma}$ is set as

$$\hat{\sigma} = \frac{\text{median}(|w_{J-1,k})| : 0 \leq k < 2^{J-1})}{0.6745} \tag{4.5}$$

If the noise is a Gaussian white noise [69, 98]. However this model is not simply applicable for the signal f if f contains multiple signal sources with different amplitude levels.

4.2.2 Shift invariant effect in UDWT

The theoretical viewpoint by Coifman and Donoho [102] mentioned clearly that the shift invariant property in wavelet analysis is crucial for denoising the signal. The self generated artifacts are generated in the conventional DWT according to the Gibbs phenomena, it is due to discontinuities in the neighboring coefficients that reflect the lack of translation invariance of the wavelet basis. This drawback is effectively suppressed in the UDWT and stationary wavelet transform and then proposed the cycle-spinning over the range of all circulant shifts in order $n \log_2(n)$ time for denoising equivalent to UDWT and stationary WT. The aliasing effect occurs in DWT in the details coefficients at different level of decomposition therefore the information is lost while denoising based on thresholding and improper reconstruction of coefficients [90, 91] is take place.

Due to shift invariant advantage in UDWT , the biomedical signals are tested for validations in the proposed iEEG-based validation framework. In the effect, it is simply expected that the quick pursuit is relied on the Hard-thresholding and the smoothness is on the Soft-thresholding as is illustrated in Figure 4-3 according to the definition of Eq. 4.3, which needs to be investigated in the real EEG signals.

4.3 EOG-EEG Signal Contamination

We consider that the electrophysiological mechanism is coupled with myogenic potential evoked by ocular movements in the nervous system [55, 103]. The generation of amplitude is depending on the degree of eyeball rotation [104, 105], which is observed as the staying potential of approximately 500 μV as maximum from the EOG recording in the 4-20 Hz range [106], known as the corneo-retinal dipole. The saccade movements phenomena have been in investigated in past studies [71, 107, 108]. The overall biological mechanism is schematically illustrate in Figure 4-4. The EEG

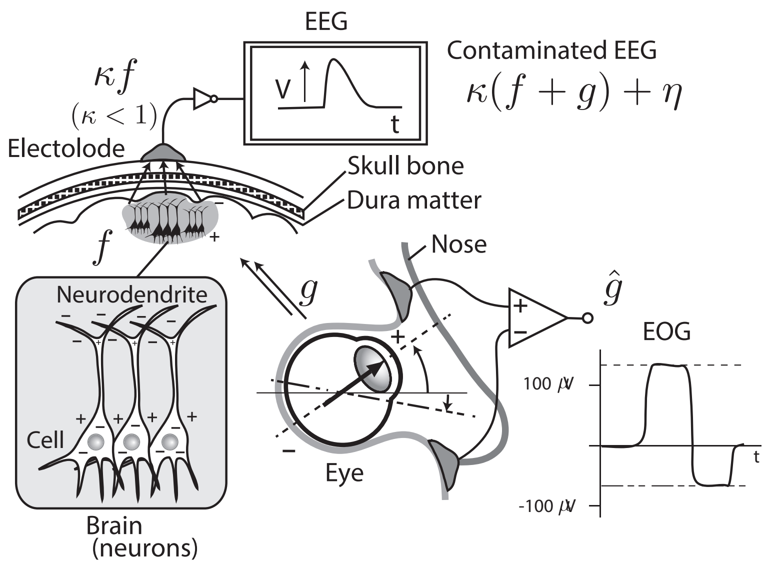

Figure 4-4: Schematic process in the signal contamination of EEGs and EOGs with respect to the biological structure. Note that arrows with g simply represent an strong influence to EEG but this does not indicate the direct pathway such as a traveling wave.

signals consider the representation which ‘information’ is reflected by the individual neuronal spikes in the brain, the collective process is important as is observed a specific range of neuronal oscillations, rather than individual spikes, and the fact has extended the possibility of EEG/MEG measurements [109]. According to the inevitable decay of the signal amplitude from the inside of the scalp to the outside, the signal f can be considered κf where $\kappa < 1$. In accordance with electrophysiological evidences of the simultaneous recording between the scalp EEG and intracranial EEG (iEEG) [110, 111, 112, 113, 114], the reduction ratio of EEG signals is estimated as

$\kappa \simeq 0.25$ in the simplest way. In addition, EOG ($\hat{g}$ in the figure) ranges from 200-500 μV and the scalp EEG level is about 10-50 μV in the ERP studies [71, 115], which implies the ratio of EOG and scalp EEG, $\hat{g}/\kappa f$, in 10-50 as is observed in the scalp EEG measurement and quite less in the intracranial [116]. Consistently, the ratio of intracranial EEG and EOG can be estimated in the same manner as $\kappa \simeq 0.25$ and then $f \gg g$.

4.4 Two-Stage Signal Model

There is a serious risk in the EOG-EEG signal contamination framework as discussed in section 4.3 [95, 96, 97, 98, 99, 100]. And the decomposition of the signal and noise will be treated respectively κg and $\kappa f + \eta$ so that

$$\begin{aligned} y &= \kappa\,(f + g) + \eta \\ &= \kappa g + (\kappa f + \eta) \\ &= \hat{g} + (\kappa f + \eta) \end{aligned} \tag{4.6}$$

where the EOG $\hat{g}$ ($\sim 500\mu V$) $\gg \kappa f + \eta$ ($\sim 10\mu V$) in the most serious case.

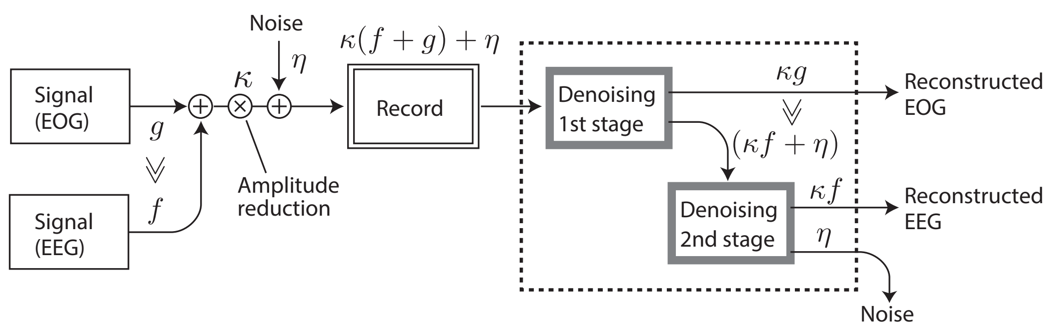

Figure 4-5: Two-stage signal model of f and g with the condition $f \gg g$, which is focused on our proposed method and frequently happens in the signal contamination of EEGs and EOG (Figure 4-4). In this figure, the amplitude reduction ratio κ is used as the single constant but if two signals are contaminated after the amplitude reduction (passing the scalp) κ can be considered as the average of κ_1 for EEGs and κ_2 for EOGs. The same extension can be considered in multiple noise factors on η.

In this dissertation, we proposed the two-stage wavelet shrinkage to improve the effectiveness of the potential risk to remove necessary EEG components as noise if it is mixed with EOGs. Thus, we hypothesized that the efficacy of the decomposition of the two signal sources is improved in comparison with the conventional single-stage method to fit for the requirement of the EEG data analysis. The proposed two-stage wavelet shrinkage scheme is summarized in Figure 4-5, which is an extended version of the single-stage scheme in Figure 4-2 according to the above theoretical background.

4.5 iEEG Based Validation Framework for Semi-Artificial Signals

In the dissertation study, We analysis the multifrequency signals with a intracranial electroencephalography (iEEG) with small amplitude and scalp recorded EEG obtained by real human EEGs and the step function is defined by Eq. 4.7 to reproduce a large amplitude potential frequently generated in the saccade eye movements is used and then the mixed signal provides a smooth curve with baseline changes unexpectedly. As the results in image processing [93, 117] is validated whether the proposed method is effective or not in the biomedical signals because the signals are spontaneously generated from the biological system inside and it is difficult to determine what is 'true signal'. Therefore, the validation remains in practical applications in past studies [118, 119, 120, 121] by using their own biomedical data to be a special case, rather than numerical analyses or quantitative validation. In the purpose of the establishment of the standard validation method for biomedical signals especially for EEG studies, we addressed the standard noise model as the framework how the EEG-EOG signal contamination data can be provided to be able to validate systematically and numerically. It provides a standard numerical validation in EEGs available for the comparative study of similar methods.

The semi-artifical EEG-EOG contamination data set is newly introduced by considering the requirement of the efficacy validation of our proposed method using the real human data of iEEGs by Andrzejak et al. [122]. This dataset is obtained from epileptic patients in the Department of Epileptology at the University Hospital of

Bonn [123] under the ethical procedure. The iEEGs data is contained a hundred dataset of open-source clinical intracranial EEGs in each from five behavioral conditions. In this dissertation, we used the dataset in the eye-closed condition after removal of the epoch of epileptic seizures. According to Andrzejak et al. [122], the iEEGs were recorded at a sampling rate of 173.61 Hz through the 12 bit analog-to-digital conversion with the band-pass filter of 0.53 – 40 Hz. The existence of a sharp peak in the alpha frequency band (9 - 11 Hz conventionally) of EEGs when subjects are closing their eyes is the useful criterion to verify whether or not the necessary EEG components is preserved after the noise removal. We assumed the iEEGs as 'true EEG' and used it to be f, and then stationary EOGs with slow changes is set artificially to mimic random eyeball rotations, which is given as

$$\hat{g}(t) = V_k^g \quad (T_k \leq t < T_{k+1}) \tag{4.7}$$

where the time length of k-th period $D_k = |T_{k+1} - T_k|$ and the potential magnitude of the EOG V_k^g are respectively given by random variables in $[-1, 1] \cdot 2^J \cdot L^{sub}$ and $[-1, 1] \cdot V^{max}$ with the uniform distribution.

4.6 Results

4.6.1 Threshold level control

As we described the denoising in section 4.2.1, in past studies [95, 96, 97, 98, 99, 100]. The threshold level is not determined completely because of the existence of the multiplication constant γ [97, 99], which may be related to data dimension. The multiplier γ dependency with different threshold definitions in the denoising is investigated with the comparison of UDWT and DWT by using the artificial EEG with a EOG step function provided by Eq. 4.7 (an example is shown in Figure 5-3). The Haar wavelet as mother wavelet is used for the this chapter.

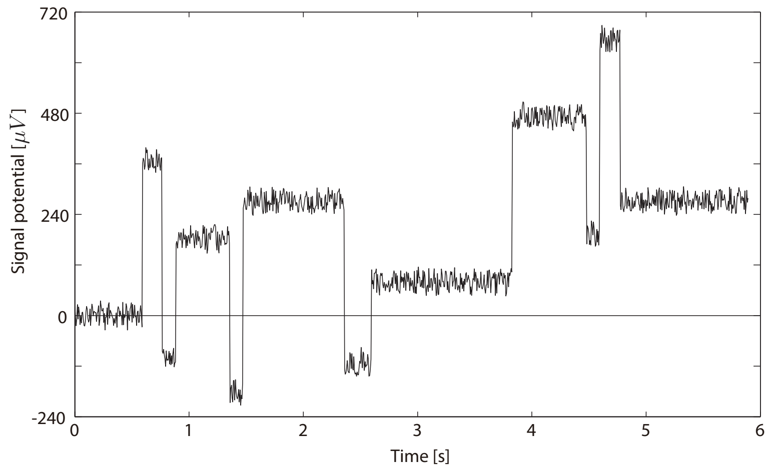

Figure 4-6: An example of the target signal for denoising, including the artificial singe wave EEG, a EOG step function and white noise.

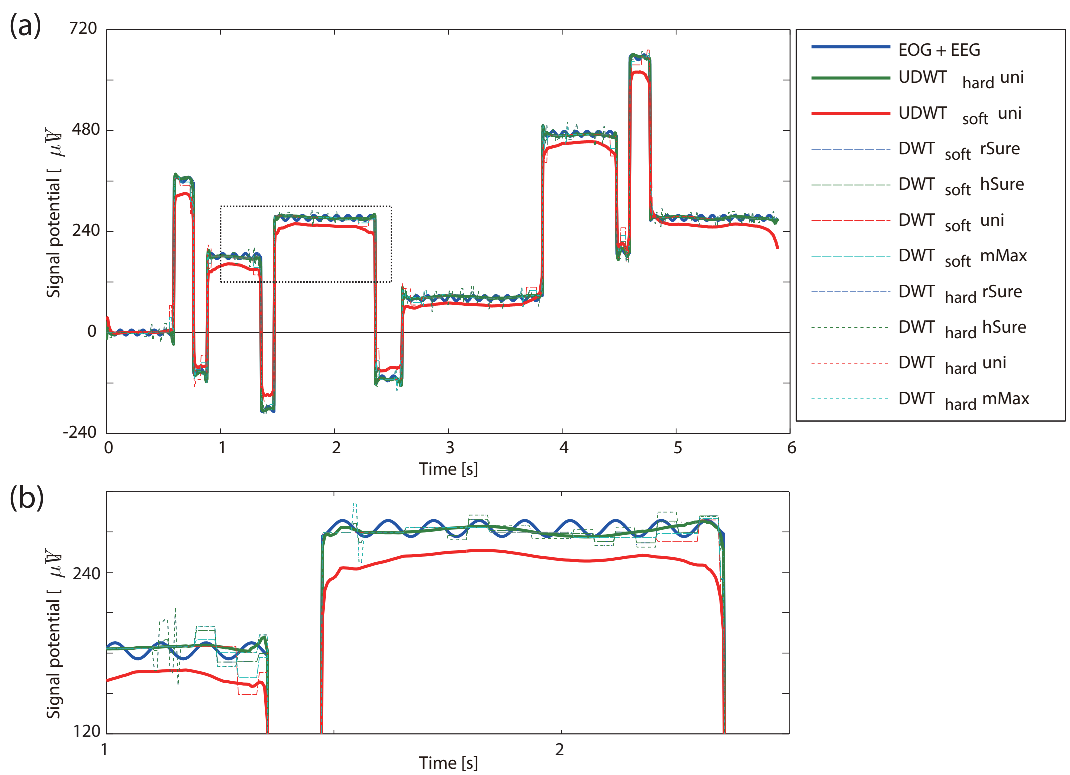

Figure 4-7: Denoised signals in the first stage applied to the artificial singe wave EEG with a EOG step function. Right panel denotes individual setting of the denosing method either UDWT or DWT, thresholding method either soft or hard, and threshold value criterion ('uni' : universal threshold is $\sqrt{2\log_2 N} \cdot \sigma$, 'rSure' : adaptive threshold selection using principle of Stein's Unbiased Risk Estimate, 'hSure' : heuristic variant of the first option, 'mMax' : mMax thresholding). (b) Enlarged view marked by the dotted line in (a).

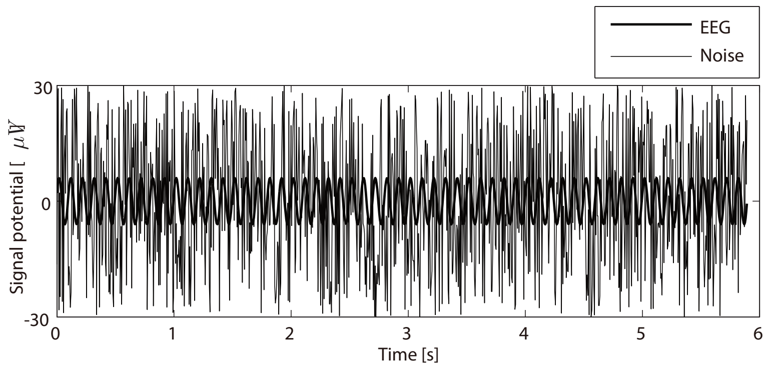

Figure 4-8: Comparison between the artificial EEG signal amplitude (10 Hz sine wave in $\pm 6\ \mu V$) and the white noise ranging $\pm 30\ \mu V$, which was provided to the numerical analysis before the denoising experiment in Figure 5-4. Due to the weakness of the EEG signal, noise amplitudes sometimes exceeds the signal amplitude level in the actual human brain measurement.

4.6.2 UDWT v.s. DWT

The quantitative analyses is discussed in the following section with the specification of the iEEG dataset by Andrzejak et al. [122]. The sampling rate is mentioned as 173.61 Hz (0.00576 s/sample) and then 2^{10}(=1024) samples are corresponded about 6s (5.89824s). The artificial EEG signal is assumed to be a single wave with 10Hz for while. The results of signal denoising in comparative analyses with combinations of wavelet types (UDWT/DWT), thresholding method (soft/hard) and threshold value criterions as shown in Figure 5-4. This simple result is demonstrated the effectiveness of the UDWT rather than DWTs even with different threshold value criterions, and the UDWT soft-threshloding provided smoothing effect to the signal excessively. In this preliminary test consequence, the reconstructed signal by the UDWT hard-threshloding was closest to the EOG signal. On other hand, the first-stage by UDWT denoising is correspond to the conventional wavelet denoising and then the method completely ignore the EEG wave because of the weakness of the signal amplitude with respect to the noise amplitude (Figure 5-5), this suggests that the necessity of the second-stage as is discussed in Figure 4-5.

Here, we introduced a criterion for sake of numerical evaluations that determines how much the signal can be reconstructed finely. In accordance with the EOG signal assumption by using the step function, the flatness without moments of stepping is evaluated. The rate of change $(\hat{g})'$ of $\hat{g}$ represents differences in signal along the time and then the differences without moments of change $\{t\ |(\hat{g})' > 0\}$ should be 0. Thus, the definition of the EOG smoothness is described as

$$(\hat{g})'_I = (\hat{g})'_I(t) = \begin{cases} (\hat{g})'(t) & (\hat{g})'(t) = 0 \\ 0 & (\hat{g})'(t) > 0 \end{cases} \tag{4.8}$$

where $I = \{t\ |(\hat{g})' = 0\}$ leads $(\hat{g})'_I \equiv 0$ according to its definition as shown in Figure 5-10 (a) (bottom). Therefore the quality of the reconstructed EOG abbreviated as $\hat{g}^{\mathbf{WT}}_{h/s:\mathbf{th}}$, where h/s denotes either Hard or Soft thresholding, $\mathbf{WT}$ is either UD (UDWT) or D (DWT) and $\mathbf{th}$ is the type of threshold value criterion, can be estimated in the minimization of $(\hat{g}^{\mathbf{WT}}_{h/s:\mathbf{th}})'_I$, which is zero if the reconstructed EOG is equivalent to the original EOG signal. As is demonstrated in Figure 5-10 (b-c), the UDWT finely reconstructed the EOG signal rather than DWTs in the viewpoint of the criterion.

4.6.3 Multiplier effect

The Pearson's correlation coefficient (**cc**) is introduced for the serious evaluation as

$$\rho^{\mathbf{WT}}_{h/s:\mathbf{th}} = \rho\left(\hat{g}, \hat{g}^{\mathbf{WT}}_{h/s:\mathbf{th}}\right) = \frac{1}{N-1}\sum_{i=1}^{N}\left(\frac{\hat{g}-\mu_{\hat{g}}}{\sigma_{\hat{g}}}\right)\left(\frac{\hat{g}^{\mathbf{WT}}_{h/s:\mathbf{th}} - \mu_{\hat{g}^{\mathbf{WT}}_{h/s:\mathbf{th}}}}{\sigma_{\hat{g}^{\mathbf{WT}}_{h/s:\mathbf{th}}}}\right) \tag{4.9}$$

where $T = 2^J$ is used for comparisons between two time series. According to the section 4.6.1 result, we focusing on the simple EOG artificial signal for the EOG smoothness, or flatness. The minimization of the summation of $(\hat{g}^{\mathbf{WT}}_{h/s:\mathbf{th}})'_I$ in the whole period of I such as the averaged fluctuation evaluator,

$$\left\langle (\hat{g}^{\mathbf{WT}}_{h/s:\mathbf{th}})'_I \right\rangle = \frac{1}{T}\int_{I=\{t|(\hat{g})'=0\}} |(\hat{g}^{\mathbf{WT}}_{h/s:\mathbf{th}})'(t)|dt \tag{4.10}$$

The reconstructed EOG smoothness in time domain (shortly 'EOG smoothness in time domain') is considerable in the first phase. On other hand, the criterion is required to evaluate the quality of the reconstruction with respect to the shift invariant

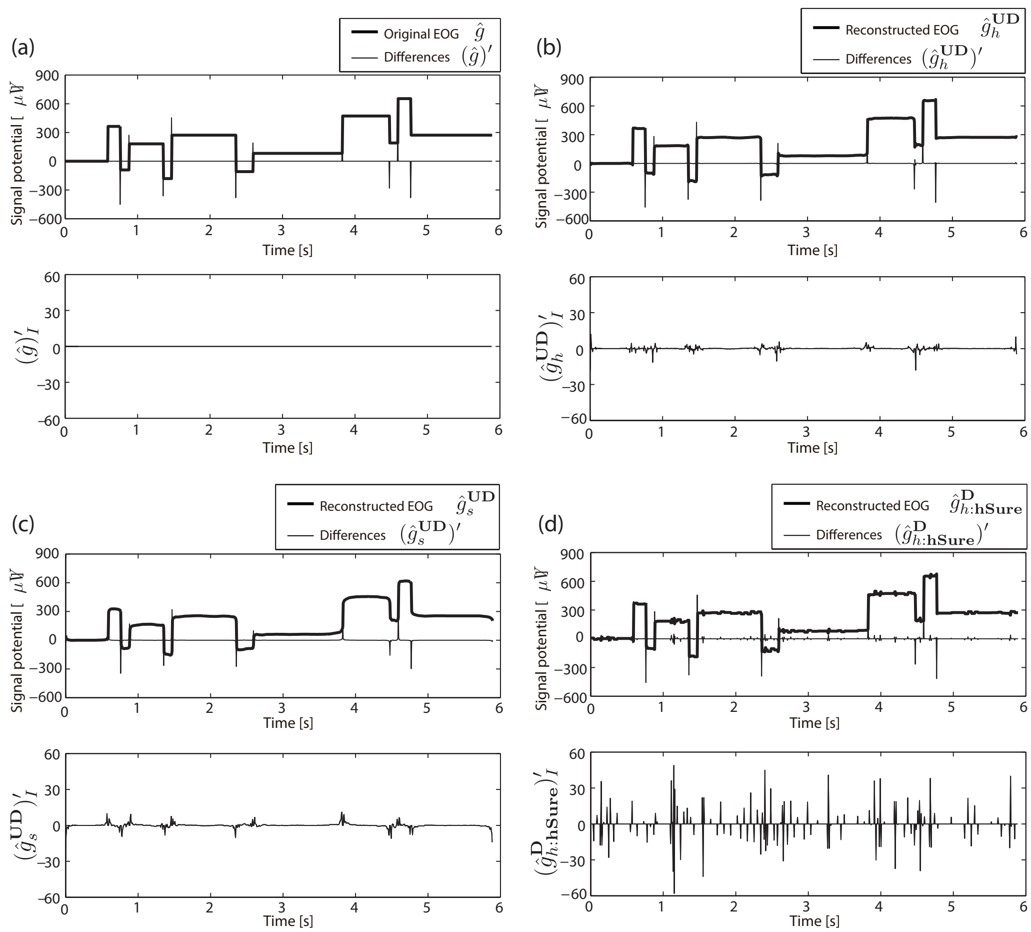

Figure 4-9: An example of the target signal for denoising, including the artificial singe wave EEG, a EOG step function and white noise.

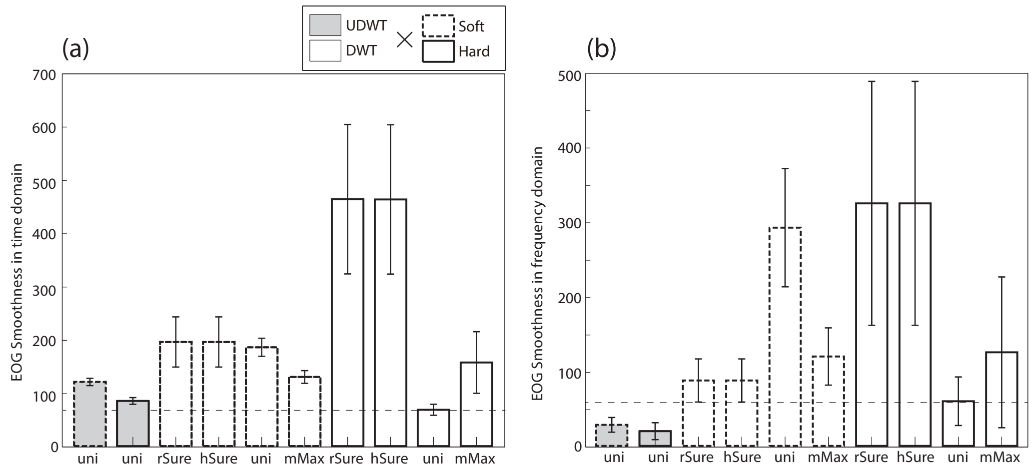

Figure 4-10: Comparison of errors in two criterion between the original EOG and reconstructed signal. Statistical evaluation was analyzed from data with 50 different white noise components. (a) In the case of the EOG smoothness in time domain. (b) In the case of the EOG smoothness in frequency domain. Abbreviations of threshold value criterion are consistent with the description in Figure 5-4.

effect, which appear in the difference between UDWT (Figure 5-10 (c)) and DWT (Figure 5-10 (d)) results. In the simple summation of **cc**, the existence of high frequency spikes in the DWT reconstructed signal is estimated as less difference with the original signal with respect to the UDWT in some cases. As shown in Figure 5-11 (a), the comparison among different denoising methods including UDWT and DWT, by using the EOG smoothness in time domain defined as $\left\langle (\hat{g}^{\mathbf{WT}}_{h/s:\mathbf{th}})'_I \right\rangle$. The result is indicated the criterion does not effectively works for the evaluator.

In the second phase, the flatness of the averaged fluctuation evaluator can be evaluate in the frequency domain is called the reconstructed EOG smoothness in frequency domain (shortly 'EOG smoothness in frequency domain'), which is given as

$$\left\langle (\hat{g}^{\mathbf{WT}}_{h/s:\mathbf{th}})'_I \right\rangle^{F} = \frac{1}{T_f} \int_{I_f} |(\hat{G}^{\mathbf{WT}}_{h/s:\mathbf{th}})'(f) - G'(f)| df \tag{4.11}$$

where

$$(\hat{G}^{\mathbf{WT}}_{h/s:\mathbf{th}})'(f) = \int_0^{2^J} (\hat{g}^{\mathbf{WT}}_{h/s:\mathbf{th}})'(t) e^{-i2\pi ft} dt,\ G'(f) = \int_0^{2^J} g'(t) e^{-i2\pi ft} dt. \tag{4.12}$$

The comparison of reconstructed signals with multiple methods of the EOG smooth-

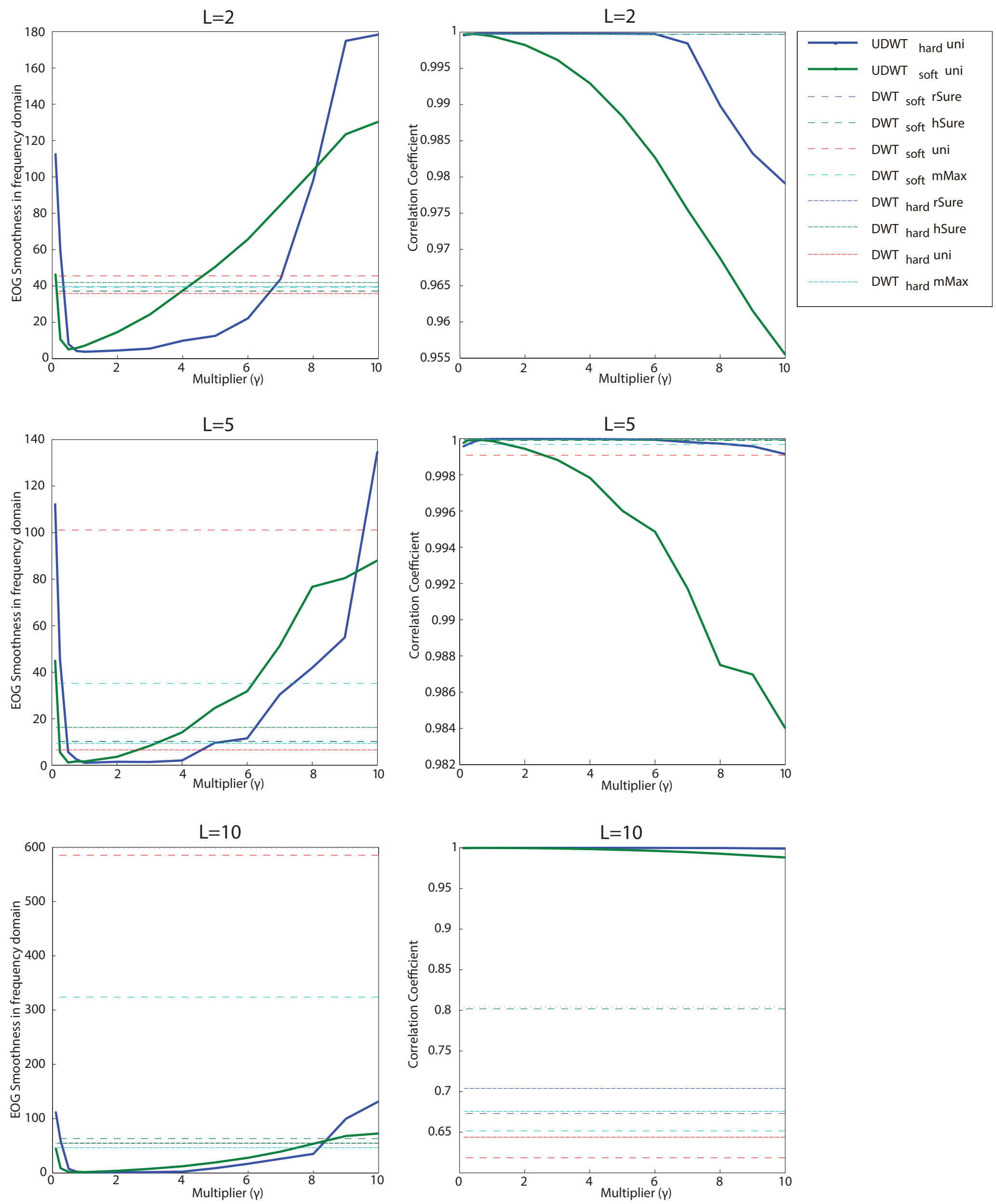

Figure 4-11: Multiplier γ dependency in UDWT denoising methods evaluated by **cc** and EOG of smoothness in frequency domain $\left\langle (\hat{g}^{\mathbf{WT}}_{h/s:\mathbf{th}})'_I \right\rangle^F$. (top) Decomposition level $L = 2$. (middle) Decomposition level $L = 5$. (bottom) Decomposition level $L = 10$.

ness in frequency domain is shown in Figure 5-11 (b). As the Figure 5-10 is visualized that the UDWT reconstructed has smooth line with less spikes especially in the zone in-between up-and-down transition points and the criterion focusing on the frequency domain $\left\langle (\hat{g}^{\mathbf{WT}}_{h/s:\mathbf{th}})'_I \right\rangle^F$ clearly demonstrated the validity. If the high frequency spikes is remain in the EOG signal before going to the second stage, it contains a part of EEG signals and then it influences the lack of EEG signals in the reconstructed process of the second stage.

Table 4.1: Statistical difference between reconstructed EOGs evaluated by the EOG smoothness in time domain. The mark * denotes the significant difference (T test; p < 0.05).

			UDWT	
			Hard	Soft
UDWT	Hard			* ($p = 3.09 \times 10^{-47}$)
	Soft		* ($p = 3.09 \times 10^{-47}$)	
DWT	Hard	rSure	* ($p = 9.42 \times 10^{-35}$)	* ($p = 1.70 \times 10^{-31}$)
		hSure	* ($p = 9.57 \times 10^{-35}$)	* ($p = 1.74 \times 10^{-31}$)
		uni	* ($p = 5.63 \times 10^{-16}$)	* ($p = 6.50 \times 10^{-51}$)
		mMax	* ($p = 5.48 \times 10^{-14}$)	* ($p = 2.36 \times 10^{-5}$)
	Soft	rSure	* ($p = 5.07 \times 10^{-30}$)	* ($p = 3.65 \times 10^{-19}$)
		hSure	* ($p = 5.13 \times 10^{-30}$)	* ($p = 3.70 \times 10^{-19}$
		uni	* ($p = 6.36 \times 10^{-62}$)	* ($p = 1.35 \times 10^{-44}$)
		mMax	* ($p = 4.28 \times 10^{-42}$)	* ($p = 5.64 \times 10^{-6}$)

The efficacy of the UDWT denoising method is significantly different from results of DWT methods as shown in Table 4.1 and 4.2. In consideration of the definition of the criterion, the EOG smoothness in frequency domain is required to be used and the efficacy is validated with the significantly difference (T test; $p < 0.05$). Therefore, the multiplier γ dependency in the UDWT denoising are evaluated (Figure 5-12)

Table 4.2: Statistical difference between reconstructed EOGs evaluated by the EOG smoothness in frequency domain. The mark * denotes the significant difference (T test; p < 0.05).

			UDWT	
			Hard	Soft
UDWT	Hard			* ($p = 1.3 \times 10^{-04}$)
	Soft		* ($p = 1.3 \times 10^{-4}$)	
DWT	Hard	rSure	* ($p = 2.01 \times 10^{-23}$)	* ($p = 1.12 \times 10^{-22}$)
		hSure	* ($p = 2.01 \times 10^{-23}$)	* ($p = 1.12 \times 10^{-22}$)
		uni	* ($p = 7.57 \times 10^{-13}$)	* ($p = 2.16 \times 10^{-9}$)
		mMax	* ($p = 5.93 \times 10^{-11}$)	* ($p = 9.33 \times 10^{-10}$)
	Soft	rSure	* ($p = 4.01 \times 10^{-28}$)	* ($p = 1.06 \times 10^{-24}$)
		hSure	* ($p = 4.01 \times 10^{-28}$)	* ($p = 1.06 \times 10^{-24}$)
		uni	* ($p = 5.89 \times 10^{-43}$)	* ($p = 6.71 \times 10^{-42}$)
		mMax	* ($p = 2.70 \times 10^{-32}$)	* ($p = 8.67 \times 10^{-30}$)

by using **cc** and $\left\langle (\hat{g}^{\mathbf{WT}}_{h/s:\mathbf{th}})'_I \right\rangle^F$. The result is demonstrated the moderate number of decomposition level such as $L = 5$ is appropriate for keeping the less error with respect to the change of the the multiplier γ. According to the concept of the two-stage model (Figure 4-5),the large value of the multiplier γ has a less risk to preserve EEG signal in the reconstructed signal in the first stage, while the reconstructed signal if $\gamma > 4$ is getting worse to reproduce the EOG signal. Thus, the appropriate γ is placed in the range from 3 to 4.

4.6.4 Wavelet shrinkage and denoising

The true EEG signal is taken from the iEEG data set [122] to validate the proposed method. We considered the EEG signals which is contaminated with noise and EOGs, is decompose up to N (N=5) level and the threshold is applied to EEG signal for denoising at each level. The EEG samples is taken from open open eye and close eye

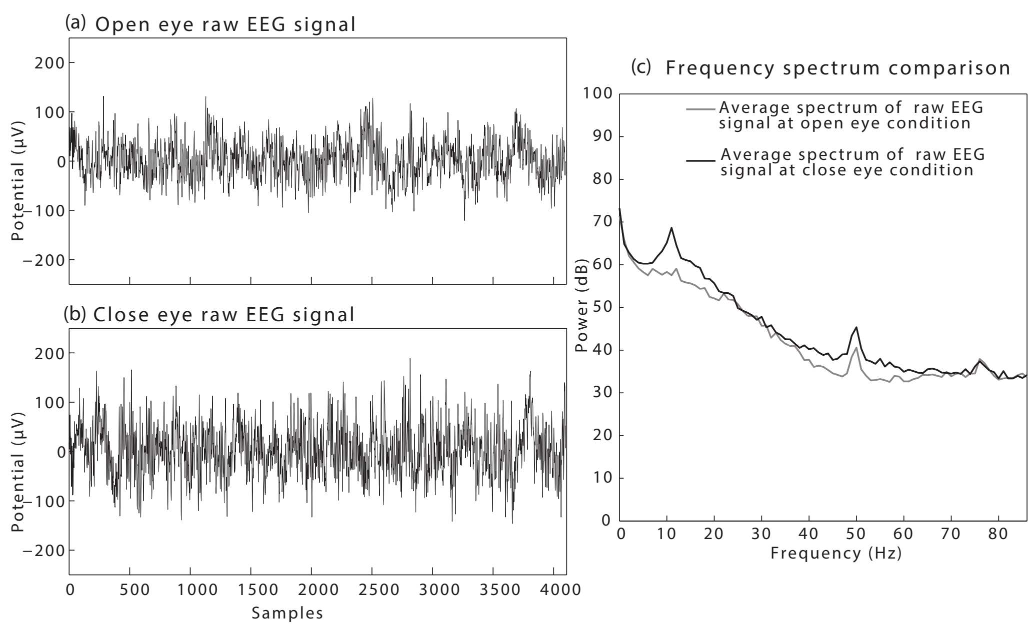

Figure 4-12: Two samples of iEEG signals and averaged frequency spectrum of the signals from ‘Open Eye’ and ‘Close Eye’ at awake state condition. In the close eye condition, there exists a sharp peak around 10Hz, which is used for the following validation whether this profile preserved in the reconstructed EEG signal successfully.

at awake state condition have shown in Figure 4-12(a) and (b). In the time domain, the EEG samples have same kind of tendency as shown in Figure 4-12(a) and (b). In the close eye condition, it is known that a sharp peak around 10 Hz appears [122], and the closed eye condition EEGs is used for the validation of proposed method whether the peak clearly preserved in the reconstructed signal without any other pseudo peaks in the frequency profile. The averaged frequency spectrum is exhibited the peak at the low frequency range as shown in the Figure 4-12 (c). The time series difference of two EEG samples is unclear in time domain (Figure 4-12(a-b)) but they are different with respect to the peak profile in the frequency domain (Figure 4-12(c)). The close eye signal has the power peak at the lower frequency but it is absent at open eye, this kind of tendency is difficult to recognized in the time domain. In this section, the first and second stages are abbreviated as stage-I and stage-II respectively.

The amount of white Gaussian noise is selected based on the amplitude percentage of the EEG signals.

The different amount (η_m :$[\eta_1, \eta_2, \ldots, \eta_8] = [0, 0.1, 1, 5, 10, 20, 50, 100]\%$) are categorized with respect to the maximum of EEG amplitude. Thus, the amount of noise potential mixed with the EEG signal is denoted by η. The Figure 4-13 is showed an example of the Combined EEG signal with artificial EOG and white gaussian noise. And this mixed signal is the input of the stage-I

The Figure 4-14 is showed the reconstructed artificial EOG and noisy EEG after the stage-I by UDWT and DWT methods. The threshold value for hard and soft as per $\lambda = \sqrt{\log n} \cdot \gamma \cdot \sigma / \sqrt{n}$ where γ is a constant related to the quasi-orthogonality [99]. As we discussed above about the multiplier factor of the threshold is played an important role in reconstruction of the EOG signal. And here, the multiplier factor γ 3 is used consistently. The Figure 4-14 (a) and (b) are showed the fluctuating noisy EEG signal at different level of noise. The fluctuating EEG is subtracted from the reconstructed EOG signal. The EOG signal is removed from mixed EEG signal at the stage-I, but still have noise, which is corresponding to the traditional single stage denoising.

Therefore, we proposed the stage-II to remove the small potential noise in section 4.4. The performance of the EEG signal reconstruction after the stage-II is compared between UDWT and DWT denoising.

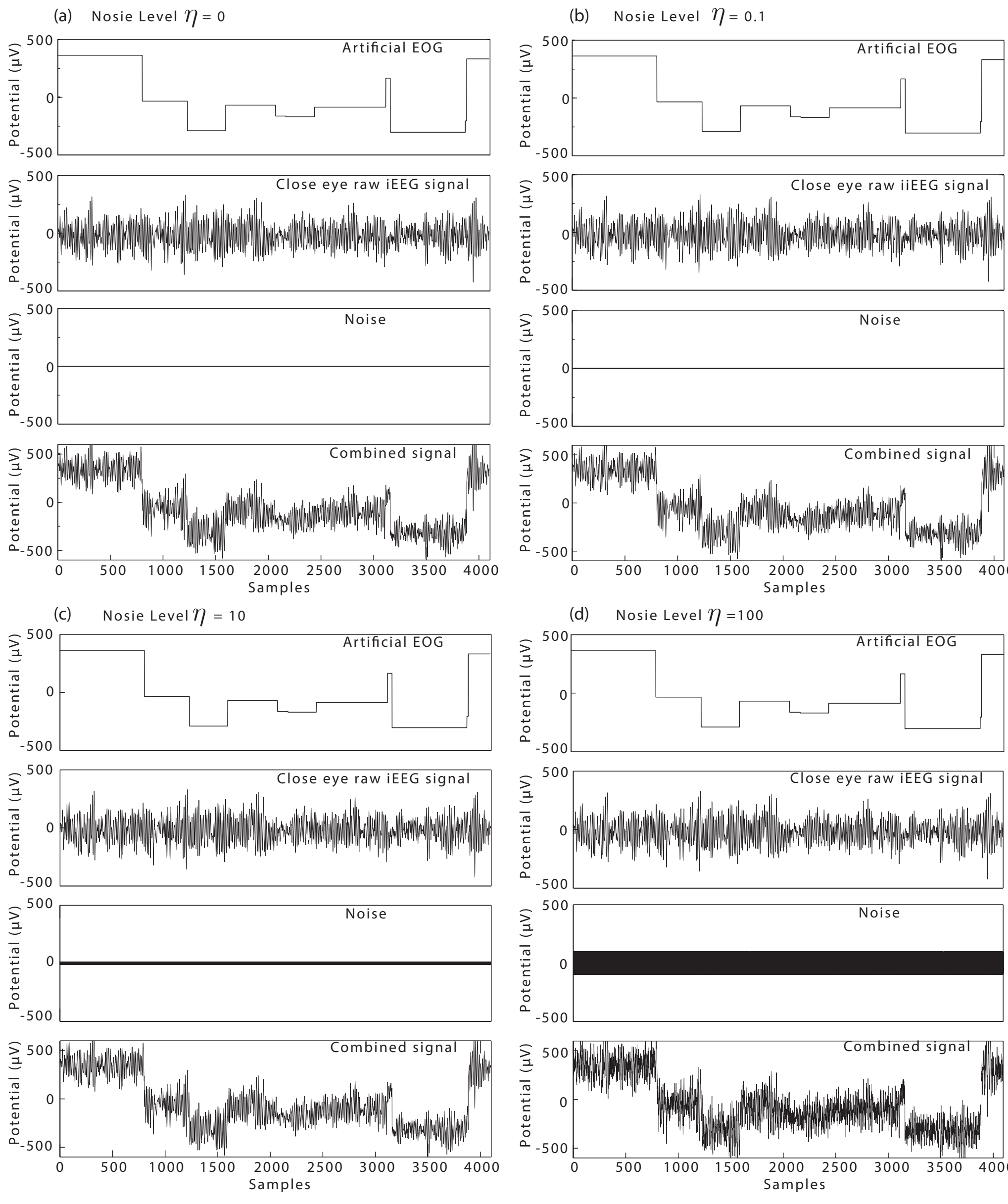

Figure 4-13: An example of the combined EEG, artificial EOG and the white noise. (a) $\eta = 0$. (b) $\eta = 0.1$. (c) $\eta = 10$, (d) $\eta = 100$. Numerical analysis were done with 2000 data set (100 iEEG set) with the white noise in each η condition.

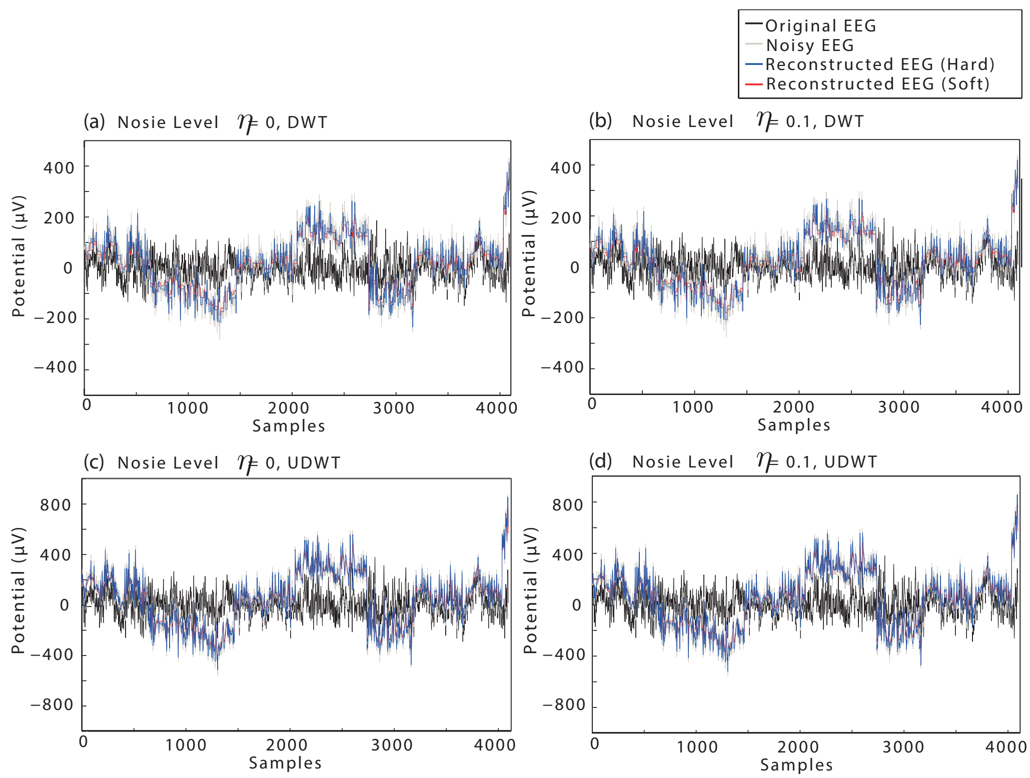

Figure 4-14: Reconstructed EEG signals by using DWT and UDWT denoising methods with hard and soft thresholding after stage-I, which correspond to the conventional single stage denoising. (a) $\eta = 0$. (b) $\eta = 0.1$. Reconstructed signals of DWT and UDWT tended to pursuit the Noisy EEG (iEEG + artificial EOG + white noise), by changing the baseline, which indicates the failure of the removal of the EOG artifact.

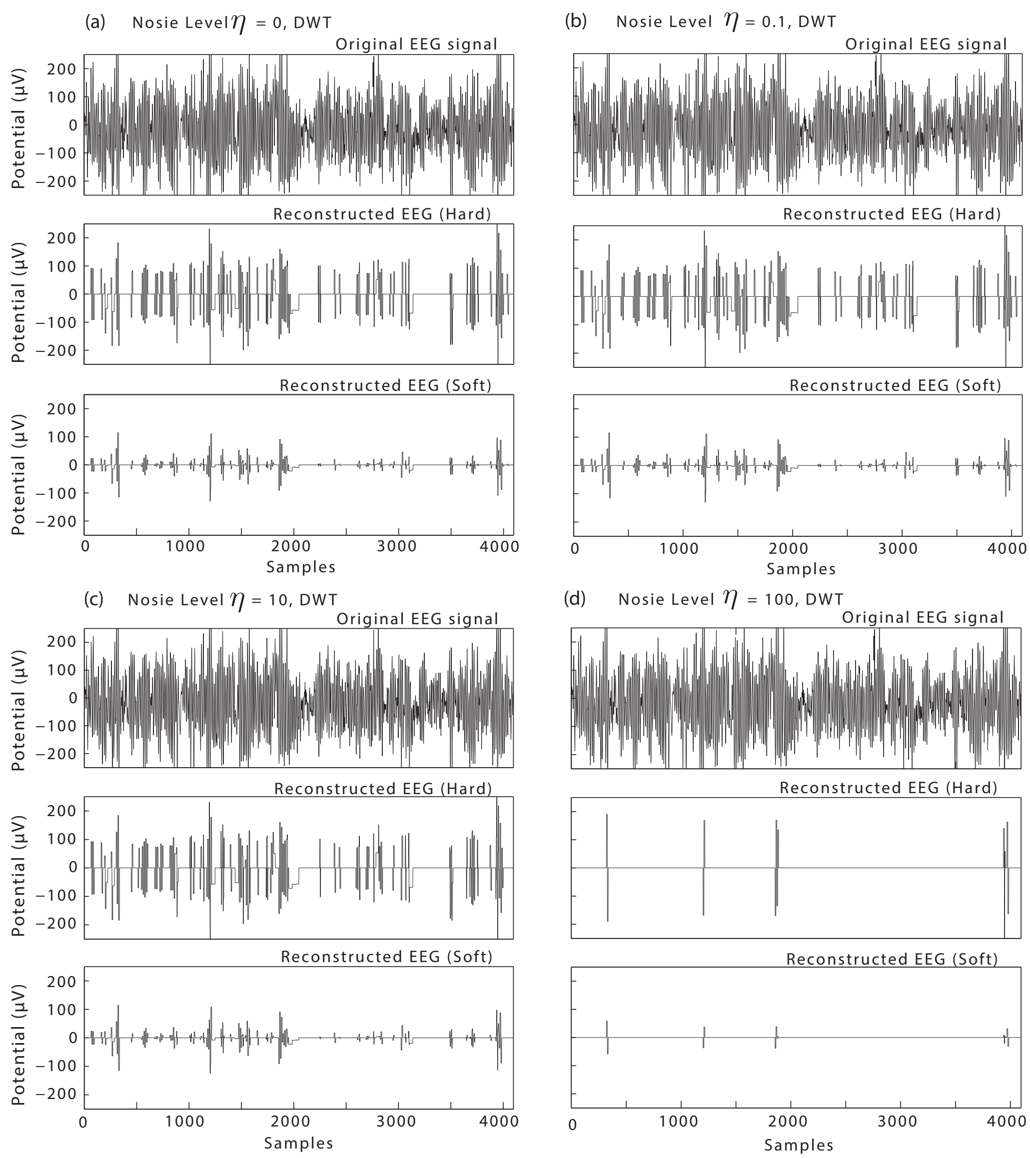

Figure 4-15: Reconstructed EEG signals by using DWT denoising methods with hard and soft thresholding after stage-II, which is originally proposed in the present study. (a) $\eta = 0$. (b) $\eta = 0.1$. (c) $\eta = 10$, (d) $\eta = 100$. The reconstructed signal formed a step-like function.

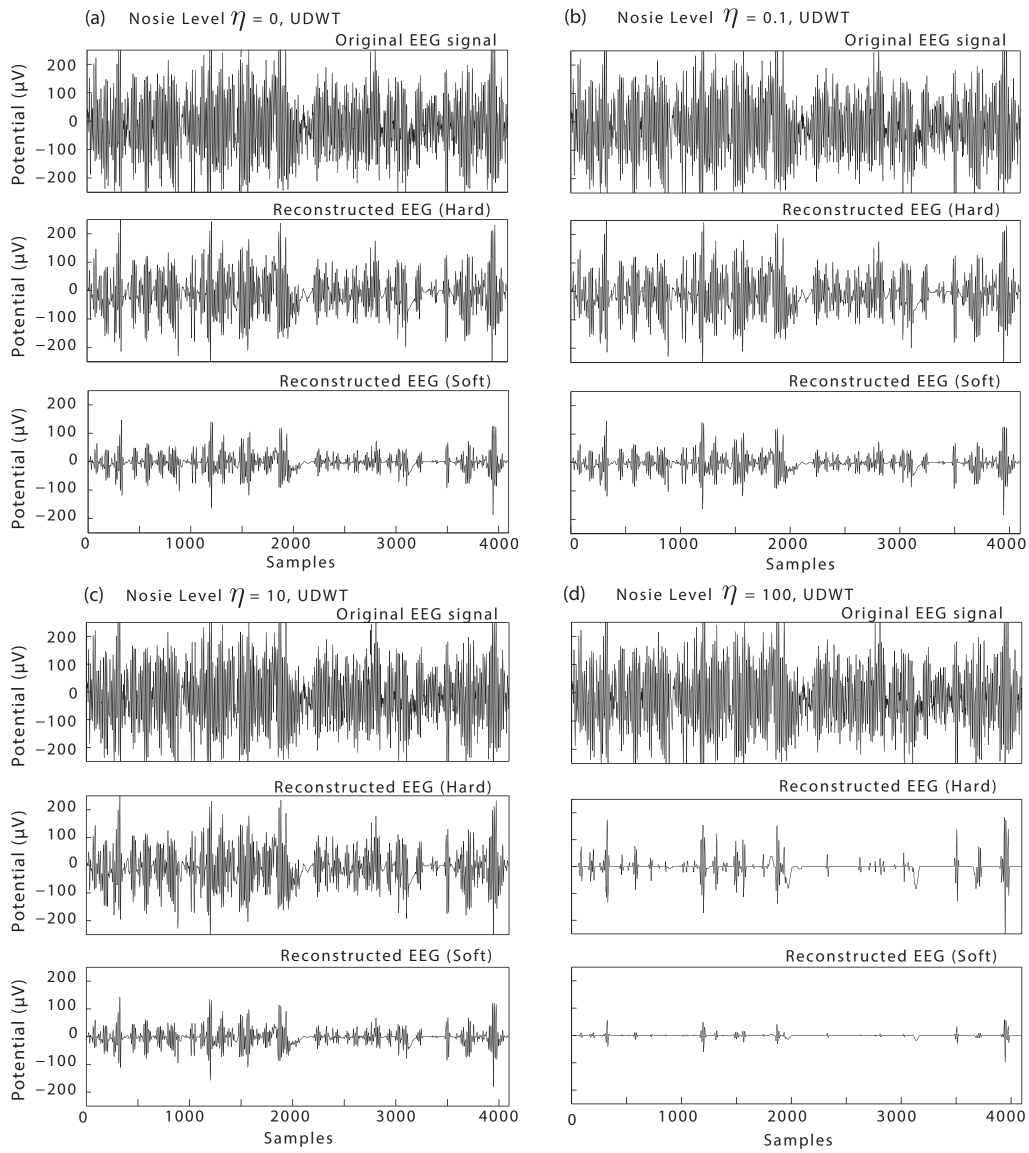

Figure 4-16: Reconstructed EEG signals by using UDWT denoising methods with hard and soft thresholding after stage-II, which is originally proposed in the present study. (a) $\eta = 0$. (b) $\eta = 0.1$. (c) $\eta = 10$, (d) $\eta = 100$. The reconstructed signal clearly reproduce a consistent form with respect to the original signal in the condition $\eta \leq 10$.

The reconstruction of denoised EEG signal with DWT and UDWT is shown in the Figure 4-15 and Figure 4-16 respectively. As seen in the time course, the reconstruction using UDWT is seemed to be better than DWT because of the similarity of the temporal profile. For the quantitative analysis, the data set $(8 \times 20 \times 100)$ is prepared as the combination of 100 iEEG signal, 20 artificial EOGs and 8 noise level. And the reconstructed EEGs are evaluated with the correlation coefficient **cc** between the reconstructed signal and the original EEG in frequency domain. The Figure 4-17 is showed the averaged frequency spectrum of original EEG and reconstructed EEG using UDWT and DWT. The result is demonstrated that UDWT clearly reconstructed the consistency in the frequency spectrum profile with the single peak around 10Hz, yet DWTs is not upto mark because it has the less height of the peak and reproduced unnecessary peaks in the high frequency range.

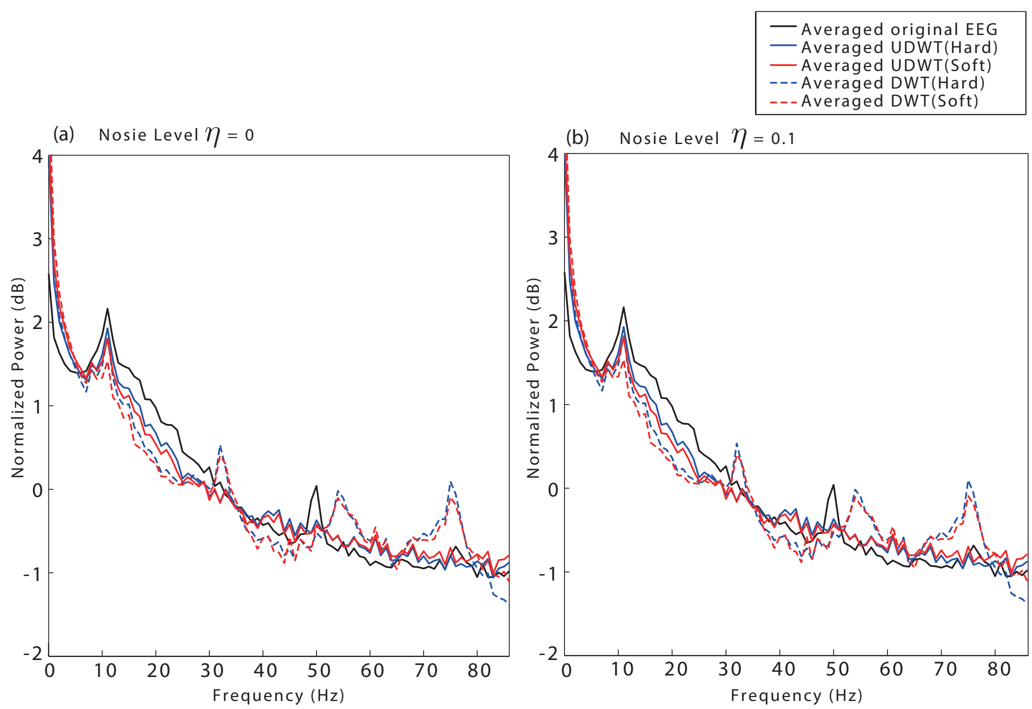

Figure 4-17: Frequency spectrum of reconstructed EEG signals by using UDWT denoising methods with hard and soft thresholding after stage-II. (a) $\eta = 0$. (b) $\eta = 0.1$. UDWT clearly reconstructed the consistency in the frequency spectrum profile with the single peak around 10Hz, yet DWTs had the less height of the peak and reproduced unnecessary peaks in the high frequency range.

In the final result, correlation coefficients among all the trial EEG signals are

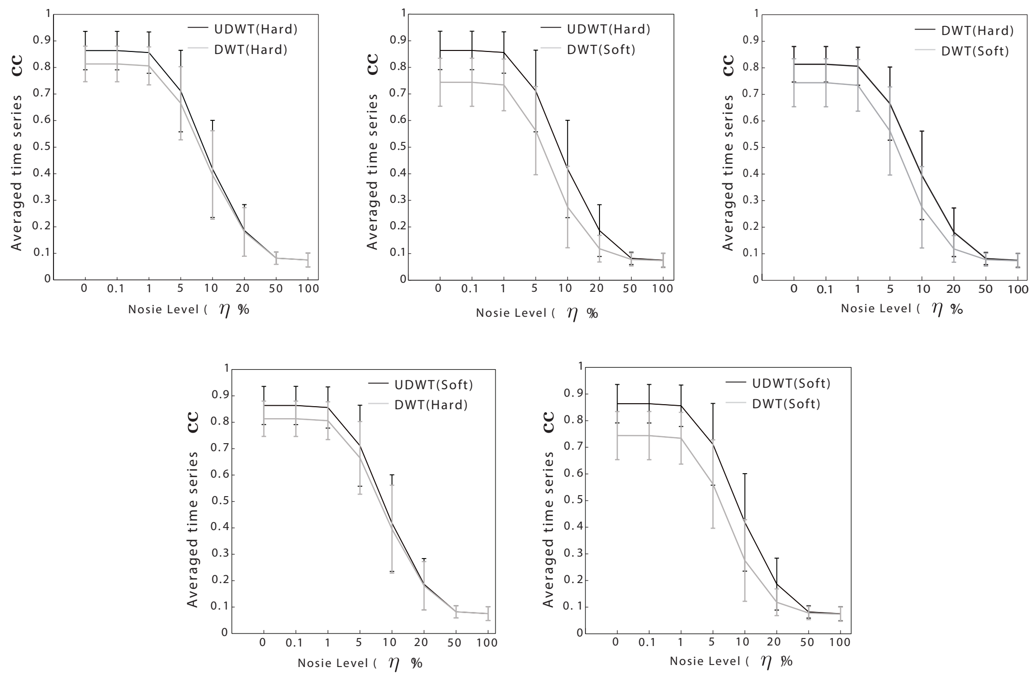

Figure 4-18: Averaged time series correlation coefficient **cc** of all reconstruction EEG signal with hard and soft threshold after stage-II. UDWT and DWT were significantly different as shown in Table 4.3.

evaluated according to the noise level in time domain (Figure 4-18) and frequency domain (Figure 4-19). Furthermore, the significant difference (Table 4.3) is also demonstrated that reconstructed EEG signal using UDWT has the advantage rather than the DWT. The results as shown in the Figure 4-18 and 4-19 are the comparison between all combination of UDWT based stage-II model, while on the other hand, the significant difference between UDWT hard and UDWT soft is not exhibited.

Thus, our hypothesis of the efficacy of the two-stage model and the sift invariant advantage of UDWT is clearly examined in the quantitative analyses and proved. Therefore, the proposed two-stage wavelet shrinkage scheme is validated as schematically shown in Figure 4-5, which represents the suitable signal is the contamination model in the case of the EEGs and EOGs.

The Table 4.3 is illustrated the significant correlation (T test; $p < 0.05$) between UDWT and DWT at different η. The calculation of the frequency spectrum correlation coefficient and is found to be significant correlation. The averaged frequency spectrum correlation coefficient is shown in Figure 4-19. The shrinkage UDWT is

Table 4.3: Statistical difference between reconstructed EEGs evaluated by the **cc** in frequency domain, including the change of the noise level η_m. The mark * denotes the significant difference (T test; p < 0.05).

<table>
<tr><td colspan="2" rowspan="2"></td><td colspan="2">DWT</td></tr>
<tr><td>Hard</td><td>Soft</td></tr>
<tr><td rowspan="2">UDWT</td><td>Hard</td><td>$\eta \leq 10^*$
$(p = 1.50 \times 10^{-3})$</td><td>$\eta \leq 50^*$
$(p = 2.27 \times 10^{-4})$</td></tr>
<tr><td>Soft</td><td>$\eta \leq 100^*$
$(p = 0.04)$</td><td>$\eta \leq 10^*$
$(p = 0.036)$</td></tr>
<tr><td colspan="2" rowspan="2"></td><td colspan="2">UDWT</td></tr>
<tr><td>Hard</td><td>Soft</td></tr>
<tr><td rowspan="2">UDWT</td><td>Hard</td><td></td><td>$\eta \leq 50^*$
$(p = 1.38 \times 10^{-4})$</td></tr>
<tr><td>Soft</td><td>$\eta \leq 50^*$
$(p = 1.38 \times 10^{-4})$</td><td></td></tr>
<tr><td colspan="2" rowspan="2"></td><td colspan="2">DWT</td></tr>
<tr><td>Hard</td><td>Soft</td></tr>
<tr><td rowspan="2">DWT</td><td>Hard</td><td></td><td>$\eta \leq 50^*$
$(p = 4.25 \times 10^{-4})$</td></tr>
<tr><td>Soft</td><td>$\eta \leq 50^*$
$(p = 4.25 \times 10^{-4})$</td><td></td></tr>
</table>

better than shrinkage DWT and above results suggested that our proposed model good for EEG signal. Only the criteria is to select the appropriate multiplier to the threshold value.

4.7 Discussion

'Blocks', 'Bumps', 'HeaviSine' and 'Dopples', some standard time series test signals with various inhomogeneities are consider in the traditional evaluation of the wavelet transform [102, 90, 91]. The 'Blocks' with abrupt changes that is similar to the horizontal and vertical eye movement that described by Patrick [52, 53]. Even though 'Bumps' may be similar to the blinks but the trigger is unexpected timings. Rest two standard test signal are not similar to the bio-medical especially EEG signal therefore it is difficult to consider them. Due to the similarity between the real EOG signal with different standard signal in time series as discussed above. We consider the block

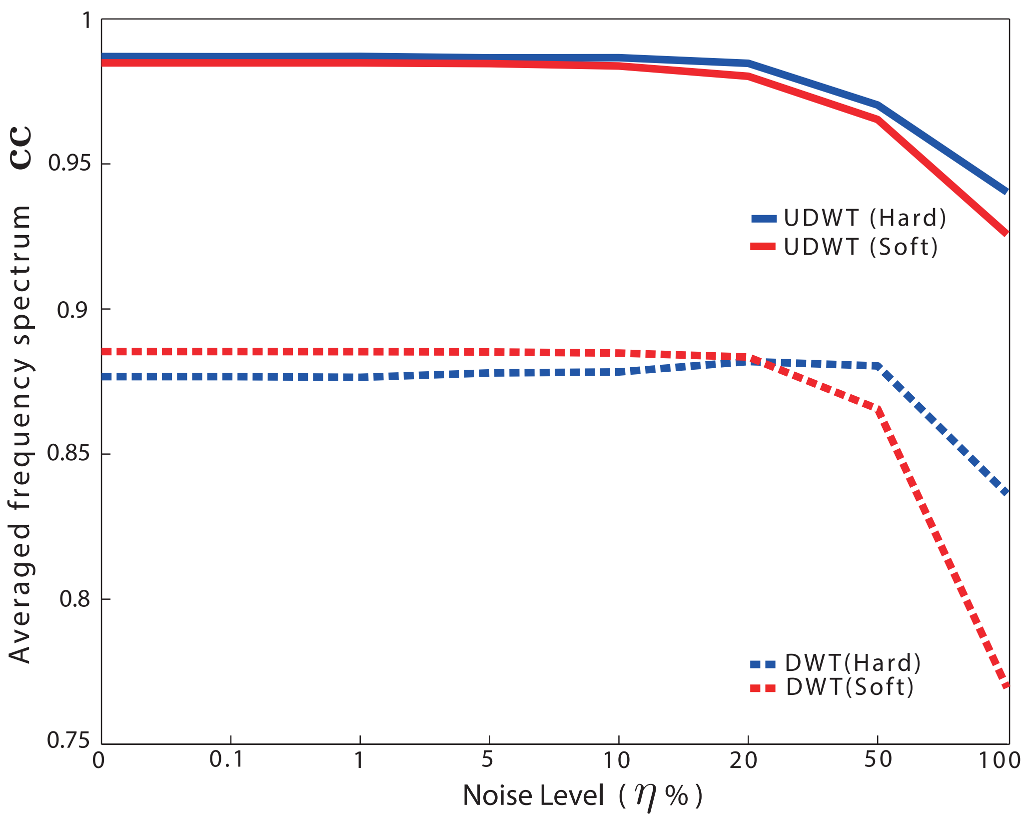

Figure 4-19: Comparison of UDWT and DWT performances after stage-II in the averaged frequency spectrum correlation coefficient **cc**. UDWTs were better than DWTs with the difference > 0.05.

signal is ideal for the proposed method with UDWT to denoise the EEG signal.

The wavelet denoising is to cut-off the coefficient values if the threshold (hard thresholding) and cut down on the threshold (soft thresholding) according to the Donoho et al [91]. The Figure 4-5 is illustrated based on the single-noise-and-single signal-source model. However, in the case of the mixed signal sources of EOGs and EEGs the assumption of EEG amplitudes to be a noise level with respect to the EOG level, illustrated in Figure 4-5. Therefore, the EOG signal removal in the first place, and then the EEG signal denoising is the plausible steps to assure preservation of signals with large amplitude differences. The Figure 5-3 is showed the combination of two signal EEG and Block (artificial EOG). The block form of is reconstructed as artificial EOG as shown in the Figure 5-4(a) is due to the advantage of shift-invariant property. Here we have to choose proper levels of decomposition. The reconstructed from UDWT using hard and soft threshold are good as compare to the DWT using different scheme. Even-though the UDWT using hard threshold is better than UDWT soft threshold as shown in the Figure 5-4(b).

We used the different types of wavelet filter coefficient for UDWT and DWT decomposition as mention earlier, in that the Daubechis filter is better for the decomposition. The approximation coefficients and details coefficients of EEG signal length is not decreased and no aliasing is take place at the decomposition of EEG signals. The Figure 4-5 is demonstrated the decomposition scheme of EEG signals at different levels by UWDT. The smoothing of EEG signal is increased as compared to other wavelet filter due to the increment in vanishes moment. UWDT gives more amount of information for feature extraction in EEG signals as compared to DWT due to the translation invariant property. The denoising result with UWDT has better balance between smoothness and accuracy than DWT [90][91], [93]. UWDT method is support both real and complex signal as compared to DWT is used for real signals.

Here, we focused on the wavelet shrinkage for the decomposition of the contaminated signals accompanied with the capability of the artifact removal. The qualitative validation is based on the standard noise contamination model. It is highly important for the comparative study of similar methods and providing clues of possible improvements. Even the one(Block test signal) has possibility which is very important because it changed the base of the EEG signal due slow eye movement that is very difficult recognized on real time basis. But at same we cannot ignore the blinks that similar is to blocks. In future we consider the blocks test signals.

Chapter 5

Morphologically Decomposition of EEG Signals

In this chapter, morphologically features are extracted by varieties of component decomposition procedures that can be efficiently summarized a wide range of problem in electrophysiology. The component analysis methods from Principal Component Analysis and Independent Component Analysis have been used for decomposition of the component but there are suffering from constraints of orthogonality or statistical independence of components. Therefore, this new method is used to overcome of those methods by identify the component on the base of sparsity in time-frequency and time-scale EEG signal is decomposed into their morphology component by using the large number of developed waveform dictionaries. The Morphological Component Analysis (MCA) extended the traditional concept of signal decomposition and reconstruction using basis which not only guarantees accuracy in reconstruction but also requires being independent of each other and the uniqueness of the representation using the basis. By admitting a redundancy in representations of the signal i.e. a way of decomposition, MCA used a concept of dictionary such as a mixture of traditional basis. The MCA is applied to decompose the real electroencephalogram (EEG) in time-frequency domain. In this analysis, the EEG signal is decomposed into signal sources that can be represented by a linear expansion of waveforms such as redundant dictionaries: UDWT, DCT, LDCT, DST, and DIRAC. These morphology decomposed components are represent the irregular spike, smooth curve in both frequency and time domain. In this chapter, we discuss the results are decomposed by MCA and suggested that the effectiveness of separation by component. And further decomposition may be useful to search for activity with a given spectral and this method may be useful for artifact recognition and removal.

5.1 Introduction

According to the electrophysiological mechanism, it is unclear that how EEG signals are generated and which information represent is what and the most plausible hypothesis is suggest that the signals are composed of synchronous spiking activities with respect to the oscillatory modulation of the local field potential [124]. Therefore, the brain state such as awake, sleep and selective attention is represented as EEG's index. It is also estimated the activation of brain region by comparison with other regions if they are located in the superior surface of the brain close to the cranial bone, like a part of the cerebrum. The most difficult issue is an uncertainty in EEG signals to discriminate the EEG signals having different morphology and noise. EEG signals is contained a multiple types of morphologies caused by different internal mechanisms such as EOG generated by eyeballs and eyelids movements, and EMG by muscular movements of body parts. The problem of true EEG signal is inevitable and it may be solve by the isolation of individual electrophysiological mechanisms. As we discussed earlier the EEG signal is known as the most noninvasive tool in particular for clinical diagnosis and neuroscience research, while medical professionals and researchers in related fields have faced the difficulty of the signal contamination. The ocular artifacts *i.e.* eye movements and eye blinks is the most serious artifacts and many past studies based on linearity and stationary signal decomposition had proposed for EOG removal [67, 72, 73]. However there are a few methods to treat nonlinear and non-stationary properties in EEG signals [125, 126, 127]. It is indicated that the traditional methods are not simply applicable to nonlinear and non-stationary signals in the purpose of artifact removals [128].

Recently the morphologically signal decomposition are highlighted due to the applicability of nonlinear and non-stationary signal properties [129, 59, 60].The blind source separation [130] has been discussed widely to separate the signal components of a linear mixture signal. The ICA and PCA are the representative methods that to be used. These methods are frequently applied [131, 132] to the EEG signal decomposition, especially in the offline analysis. The PCA is decomposed the EEG components in space/time basis. While as disadvantages, it is difficult to reconstruct overall signals by the linear combination of principal components (PCs) because of the ignorance of signals with small amplitudes and irregular changes. Therefore, the accurate reconstruction in those method are required the prior and detail knowledge to identify PCs corresponding to artifacts [52, 66]. Due to the limitation in PCA, the research trend is shifted from PCA to ICA with high order statics to specify independence in the signal. On the other hand, since the ICA is restricted to the basement on measure of statistical independence, ICA is face the difficulty to detect signal components if Gaussian noise are contaminated in the manner of spreading over the noise in an undesired way into the signal components [67, 68, 72, 73, 107].

The effectiveness in analyzation, enhancement and synthetization of signal properties include the nonlinear and non-stationary changes is the key role in a plausible EEG decomposition [133]. The ICA methods are demonstrated the performance on the decomposition of complex signals in blind source separation. But the analysis and synthesis of signal in a systematic manner is an extended concept of sparsity [134] and a methodology for separation based on redundant transforms can be introduced [61]. MCA is one of the methods in that the sparsity plays a vital role to separates different time/frequency properties or morphologies of individual signal components, which are demonstrated in the past studies [129, 135, 136]. The effectiveness of MCA noise removal is mostly clarified in image processing [59, 60, 61, 62]. However we hypothesized that the MCA decomposition is effective in the EEG artifact removal and it clarifies which kinds of signal morphologies are contaminated into the signal as true biological signals, by using redundant transform or mixed over-complete dictionary in the sense of MCA [137]. Yong et al. [138] preliminary is reported the effectiveness in the EEG artifact removal and is provided a less comprehensive analysis with MCA in the framework of verification of how EEG true signal preserved after noise removals even with various EOG fluctuations [139]. The different dictionaries based on the mathematical basis function are used to represent the evoked potentials generated by different electrophysiological mechanisms.

In this chapter, we proposed the best combination of dictionaries [61] for an EEG decomposition method based on the sparsity and over-completeness dictionary in the sense of EEG frequency properties. The reconstruction of the EEG signals have highly different representation of time/frequency features that depends on the set of dictionaries [137, 140, 141]. We used the block coordinate relaxation (BCR) algorithm to minimize error in signal reconstruction and to obtain the sparsest representation of desired features in the computer experiment. The goal of this study is to propose the systematic way of the artifact removal in EEG signals with MCA and to specify time/frequency properties to represent signal components by verifying the appropriate combination of the dictionaries.

5.2 Decomposition Methods

A linear combination of k EEG and artifacts sources in time domain, the source can be denoted as $s_1(t), s_2(t), ..., s_k(t)$, with amplitudes and time index $s_1,\ s_2, \cdots, s_k$ and t respectively.

$$\begin{aligned} s_1(t) = &\quad \Phi_{11}x_1 + \Phi_{12}x_2 \cdots , \\ s_2(t) = &\quad \Phi_{21}x_1 + \Phi_{22}x_2 \cdots , \end{aligned} \tag{5.1}$$

where, $\Phi_{11}, \Phi_{12}, \Phi_{21} and \Phi_{22}$, are the mixing parameters. Numerous methods have been used and formulated the linear combination according to the sources characteristics. Here we are formulated as the linear combination to separate or remove the artifacts from EEGs. If the EEG signal and other artifacts are statistically independent and assumed that the EEG and artifacts independent signal must have nongaussian distributions. Due the sparsity in the representation of EEG-EOG signal morphology.The artifacts can be removed by replacing coefficients representing the artifacts part with zero when the whole signal is reconstructed. The blind source separation methods like ICA and PCA commonly are used to decompose/separate the linear combination of EEG source [67, 68, 72, 73, 107, 131, 133, 142, 143, 144] . The above equation 5.1 can be given as.

$$\begin{aligned} S = &\ \Phi \times X, \\ Y = &\ W \times S \end{aligned} \tag{5.2}$$

The recorded EEGs from electrodes attached on the scalp (abbreviated as scalp EEG) S can be given by the Equation 5.2, where $X(t) = [x_1(t), x_2(t), ..., x_k(t)]$ are the coefficients in time series called signal components and Φ is the mixing matrix that to be determine the mixing way to separate S between the signal and artifacts. In ICA separation/decomposition, the mutual independence of W unmixing matrix is to satisfy $W = \Phi^{-1}$ and each row vector in Y is approximately equal to a scaled value of one row vector in X. Therefore the EEG signal are decomposed into the assumed EEG signal and artifacts components. For the ICA decomposition methods conventionally require the prior knowledge about the properties of the target components coupling with the constraints [133],as discussed in section 5.1. A heuristic factor remains to be obstacle for the full automation of the signal decomposition.

5.3 EEG-EOG Component Morphology

The cerebral cortex is located in the outer region of brain hemispheres just beneath the skull bone and therefore these activities are accessible by electrical potentials from the scalp. The cortical regions are locally separated depending on the functions such as decision-making (frontal cortex), motor control (premotor cortex), body sensations (somatosensory cortex), and processing of the sensory inputs in vision and audition (primary visual and auditory cortex). Therefore, the potentials from different positions on the scalp are contain the information of neuronal activities in different cortices if signals are clearly separated each other and from artifacts. The electric potentials from muscular, eyeball and eyelid movements are contaminated into the scalp EEG in an evitable mainour of leak potentials in the electrophysiological mechanism which connects the brain and muscular-skeletal mechanism. The electrophysiological properties in different biological mechanisms are different and the nature of electrophysiological mixing is the key to solve the complex decomposition problem. As the traditional knowledge in the medical field [145], it is known that EEG signals have specific characteristics on the shape of the waveform called morphology: "Monomorphic" is composed of one dominant activity, "Polymorphic" is composed of multiple frequencies to form complex activity, "Sinusoidal" is components to resemble sine waves, "Transient" has two types which are spikes in a duration of 20 – 70 msec and sharp waves with a pointed peak and 70 – 200 msec duration. If it is possible to decompose the recorded EEG with respect to those morphologies of interest, it brings us a large benefit because it leads the way to "true" EEGs.

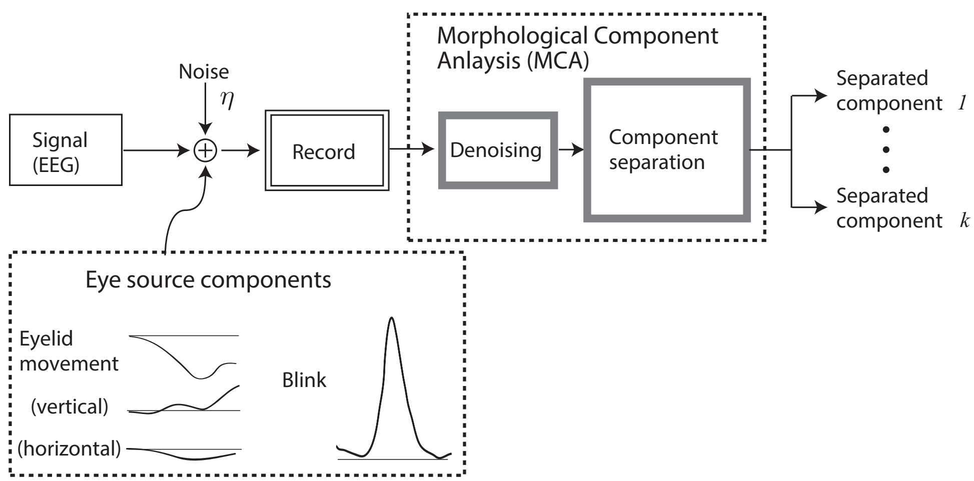

Figure 5-1: A proposed scheme for separation of morphological component representation of EOG-EEG signal.

The myogenic potential evoked by ocular movements [55, 103] is coupled with electrophysiological mechanism in the nervous system. The potential of an eyeball rotation is generated with an amplitude depending on the degree of the rotation [104], which is observed the staying potential is approximately 500 μV as maximum from the EOG recording in the 4-20 Hz range [106], known as the corneo-retinal dipole. The phenomena of saccade movements had been investigated in past studies [71, 107, 108, 115]. As above mentioned the EEG and EOGs potential have specific morphologies. Morphologies of eye movements and eye blinks can be considered as slow change with respect to the EEG time scale and a bump shape with a large peak amplitude [53, 54]. Since the presence of repetitive peaks frequently appear in the diagnosis of epilepsy [146], we assumed the single bump to be the typical eye blinks and multiple types of slow baseline changes to be eyeball rotations, as schematically shown in Figure 5-1.

5.4 Decomposition using Morphological Component Analysis

The component decomposing of a signals into their composing elements is a large expectation in the application of data size minimization for transferring the data via internet. Morphological component analysis based methods are fit for this purpose and have the advantage in the accurate reconstruction of the original data after noise removal, which relies on the sparsity and over-completeness of dictionary. The over-complete dictionary is represented by $\Phi \in R^{n\times k}$, where k is the morphological component of signal for $\{\phi_k\}_{k\in\Gamma}$, where Γ is the index set of dictionaries. According to the Chen et al. (2001) [140], the over-complete dictionary Φ is a set of redundant transforms, which are defined by a set of mathematical functions to represent the specific morphologies. Due to specific morphology representation by redundant transform, the mixed EEG signal can be defined as a sparse linear combination of component signal. Due to sparseness of signal coefficients, it is very crucial to obtain the final set of coefficients for accurate reconstruction of the original signal. In the theory, there exists a dictionary that can reproduce the specific features of the signal if the appropriate iteration method is introduced to pursue the unique sparse representation. The concept of sparsity and over-completeness dictionary has theoretically extended the traditional signal decomposition to feature extractions focusing on multiple types of morphologies simultaneously.

Due to freedom of the selection of dictionaries, the signal can be decomposed with explicit dictionary [140] and it cannot be decomposed in other form of dictionaries. A dictionary is defined as collection of waveform $\{\phi_k\}_{k\,\in\,\Gamma}$ [58] in fact, and the input signal S is assumed to be reconstructed by a linear combination of a set of basis elements ϕ_k, and then the signal S is expressed as a single vector of $S \ \in \ R^N$ and satisfies $S \ = \ s_1 + s_2, \cdots, s_K$, where $s_1, s_2, \cdots, s_k$ are subcomponent *i.e.* different morphologies. We applied this system to recorded EEG signal S as shown in Figure 5-1. The signal approximation decomposition Sinto its building components can be expressed as

$$\begin{aligned} S &= \textstyle\sum_{i=1}^{k} \beta_i \phi_i + \zeta \\ &= \beta_1\phi_1 + \beta_2\phi_2 \cdots + \beta_k\phi_k + \zeta \\ &\cong s_1 + s_2 \cdots + \ s_k \ (\zeta \ll 1) \\ &= S' \end{aligned} \tag{5.3}$$

Therefore β is the target coefficients for reconstruction of the original EEG signal based on the assumption $\zeta \ll 1$, which means that the remainder ζ is negligibly small. In the consideration that ζ represent the noise part, the Equation 5.3 without noise can be written as

$$\begin{aligned} S &= \textstyle\sum_{i=1}^{k} \beta_i \phi_i \\ &= \beta\Phi \end{aligned} \tag{5.4}$$

The Equation 5.4 is consistent with the Equation 5.2. The problem to solve is how optimized coefficients can be derived, and the equation is rewritten as follows

$$\begin{aligned} &\{\beta_1^{opt}, \beta_2^{opt}, \cdots, \beta_k^{opt}\} = \underset{\beta_1,\cdots,\beta_k}{\arg\min} \textstyle\sum_{i=1}^{k} \|\beta_i\|_0 \\ &\text{subject to: } S = \textstyle\sum_{i=1}^{k} \beta_i \phi_i. \end{aligned} \tag{5.5}$$

The problem is that how the MCA concept can be embedded in the systems to decompose biomedical signal especially for EEG signal. In this formulation is totally consistent with traditional decomposition methods which applied to the biomedical signal decomposition such as PCA, wavelets and ICA, in the sense of the single set of basis. What is an advancement of MCA is the availability of the combination of multiple basis functions, including traditional basis like wavelet decomposition as a part of the component, called redundant transforms. Thus, MCA is expected to reveal what kind of the specificity exists in time-frequency properties of EEG data. Concrete problems in this viewpoint can be addressed as

- what is the best combination of dictionaries of MCA for the EEG decomposition.
- what is the true EEG signal in the form of obtained sparsest representation based on selected dictionaries ϕ_k.

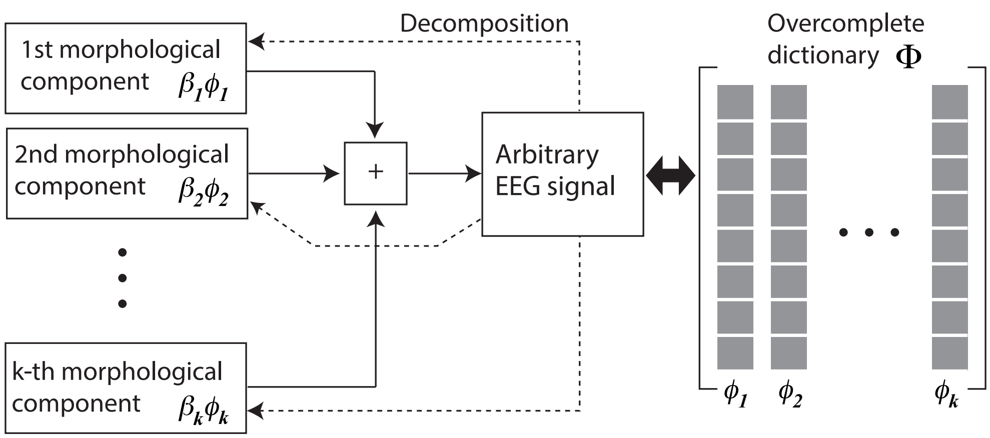

Figure 5-2: A schematic diagram for EEG signal decomposition using explicit dictionary.

The Figure 5-2 schematically illustrates the MCA scheme for an arbitrary EEG signal that is assumed to be a linear combination of k morphological component to decompose using explicit dictionaries.

We assumed three types of dictionaries ($k = 3$), the following three cases are considerable by focusing on individual dictionaries. Case 1: An over-complete dictionary ϕ_1 is representing the component s_1, $\phi_1 \in M^{N\times L_1}$, where $N \gg L_1$, N is the number of samples *i.e.* the number of time points in the recorded data.

- For s_1, $\beta_1^{opt} = \arg\min_{\beta} \|\beta\|_0$
  subject to: $s_1 = \phi_1\beta$, while solving this equation leads the sparse solution $\left(\left\|\beta_1^{opt}\right\|_0 < \left\|\beta_{12}^{opt}\right\|_0, \left\|\beta_{13}^{opt}\right\|_0\right)$.

- For s_2, $\beta_{12}^{opt} = \arg\min_{\beta} \|\beta\|_0$
  subject to: $s_2 = \phi_1 \beta$, while solving this equation leads non sparse solution.

- For s_3, $\beta_{13}^{opt} = \arg\min_{\beta} \|\beta\|_0$
  subject to: $s_3 = \phi_1 \beta$, while solving this equation also leads to non sparse solution.

Case 2: An over-complete dictionary ϕ_2 is representing the component s_2, $\phi_2 \in M^{N \times L_2}$, where $N \gg L_2$.

- For s_2, $\beta_{2}^{opt} = \arg\min_{\beta} \|\beta\|_0$
  subject to: $s_2 = \phi_2 \beta$, while solving this equation leads the sparse solution $\left(\left\| \beta_2^{opt} \right\|_0 < \left\| \beta_{23}^{opt} \right\|_0, \left\| \beta_{21}^{opt} \right\|_0 \right)$.

- For s_3, $\beta_{23}^{opt} = \arg\min_{\beta} \|\beta\|_0$
  subject to: $s_3 = \phi_2 \beta$, while this equation also have non sparse solution.

- For s_1, $\beta_{21}^{opt} = \arg\min_{\beta} \|\beta\|_0$
  subject to: $s_1 = \phi_2 \beta$, while this equation also have non sparse solution.

Case 3:

An over-complete dictionary ϕ_3 is representing the component s_3, $\phi_3 \in M^{N \times L_3}$, where $N \gg L_3$.

- For s_3, $\beta_{3}^{opt} = \arg\min_{\beta} \|\beta\|_0$
  subject to: $s_3 = \phi_3 \beta$, while solving this equation leads the sparse solution $\left(\left\| \beta_3^{opt} \right\|_0 < \left\| \beta_{32}^{opt} \right\|_0, \left\| \beta_{31}^{opt} \right\|_0 \right)$.

- For s_2, $\beta_{32}^{opt} = \arg\min_{\beta} \|\beta\|_0$
  subject to: $s_2 = \phi_3 \beta$, while solving this equation leads non sparse solution.

- For s_1, $\beta_{31}^{opt} = \arg\min_{\beta} \|\beta\|_0$
  subject to: $s_1 = \phi_3 \beta$, while solving this equation leads non sparse solution.

Theoretically by using three dictionaries MCA can divide the signal into components depending on each dictionary ϕ_1, ϕ_2 and ϕ_3 as a sparest representation of all signals, and it is described mathematically as:

$$\begin{aligned}&\{\beta_1^{opt}, \beta_2^{opt}, \beta_3^{opt}\} = \underset{\beta_1,\beta_2,\beta_3}{\arg\min} \|\beta_1\|_0 + \|\beta_2\|_0 + \|\beta_3\|_0 \\ &\text{subject to: } S = \beta_1\phi_1 + \beta_2\phi_2 + \beta_3\phi_3\end{aligned} \tag{5.6}$$

This formulation states a non-convex optimization problem for separate the component of the signal; however each ϕ_k needs to be efficient in a specific component yet non-effective in other signal components. It indicated that it is difficult to solve Equation 5.6 in a simple manner and then the Basis Pursuit (BP) method [58] was proposed based on the idea that the replacement of the l^0 norm to l^1 norm in the error minimization. According to the improvement, the BP [58] was successfully formulated to be an accurate method to represent the sparest of components, which are described as:

$$\{\beta_1^{opt}, \beta_2^{opt}, \beta_3^{opt}\} = \underset{\beta_1,\beta_2,\beta_3}{\arg\min} \sum_{i=1}^{3} \|\beta_i\|_1 + \lambda \left\| S - \sum_{i=1}^{3} \phi_i \beta_i \right\|_2^2 \tag{5.7}$$

In this system, l^2 norm consider to be the error norm based on the assumption that the residual act as a white zero-mean Gaussian noise and other important finding is the representation of noise models l^1 Laplacian noise with the consideration of l^∞ uniformly distribution noise, in the form of the optimization problem. λ represent the stopping criterion or threshold. By using the Block-Coordinate-Relaxation (BCR) method [147] the optimization problem can be solved in finite computation time. The procedure has given below:

1. Initialize $= I_{max}$, number of iteration $= L$, threshold : $\delta = \lambda * I_{max}$.
2. Perform L times:

   Part(1) update s_1, assuming s_2 and s_3 has fixed.

   (a) Calculate the residual $R = S - s_2 - s_3$

(b) Calculate $\beta_1 = \phi_1^T R$

(c) Threshold the coefficient of $\beta 1$ and obtain $\widehat{\beta_1}$

(d) Reconstruct s_1 by $s_1 = \phi_1 \widehat{\beta_1}$

Part(2) update s_2, assuming s_1 and s_3 has fixed.

(a) Calculate the residual $R = S - s_1 - s_3$

(b) Calculate $\beta_2 = \phi_2^T R$

(c) Threshold the coefficient of $\beta 2$ and obtain $\widehat{\beta_2}$

(d) Reconstruct s_2 by $s_2 = \phi_2 \widehat{\beta_2}$

Part(3) update s_3, assuming s_1 and s_2 has fixed.

(a) Calculate the residual $R = S - s_1 - s_2$

(b) Calculate $\beta_3 = \phi_3^T R$

(c) Threshold the coefficient of $\beta 3$ and obtain $\widehat{\beta_3}$

(d) Reconstruct s_3 by $s_3 = \phi_3 \widehat{\beta_3}$

3. Update the threshold by $\delta = \delta - \lambda$.

4. If $\delta > \lambda$, return to Step 2. else finish.

5.5 Hypothesis

Here, we hypothesized that an appropriate combination of three dictionaries to form an over-complete dictionary of MCA decomposition specifically for EEG recoding data are undecimated Wavelet transform , discrete sine transform and DIRAC (aka standard unit vector basis, or kronecker basis) [Fadili et al. (2009)]. The UDWT is contributed to separate slow and bump morphologies for EOG and EEG transient slow changes, DST is used for monomorphic and polymorphic EEG components (major EEG parts) and DIRAC is used for spike type activities in transient EEGs. The discrete cosine transform , discrete sine transform [148, 149], local discrete cosine transform dictionaries are used for major EEG parts in the simulated experiment for comparison. For the verification of the hypothesis, the intracranial EEG data (iEEG) to be "true EEG" signals, which was recorded from the real brain activity, and artificial EOGs including bump and slow changes were introduced and the performance of the accurate reconstruction of the true EEGs are examined. As we discussed the iEEG data in chapter 3, same types of the data is used as conditions of eye-closing and eye-opening 5.6.2. According to the neuroscientific evidence, EEGs has a clear peak in the low frequency range around 10Hz in the frequency spectrum in the eye-closing condition 5.6.2.

5.6 Results

The computer simulation is used for verification of our hypothesis, three types of the data are used, 1) all simulated data, 2) a combination of real iEEG and simulated EOG and 3) recording of real EEG-EOG data and our proposed method is validated.

5.6.1 Simulated data

The two simulated sources signals are prepared for the simple test of the proposed method in first place. Initially Yong et al. [138] had proposed a combination of wavelet, DCT and DIRAC for EEG artifact removals, while their results are unclear how much the method is effective in qualitative manner. In this experiment, the first source signal is a cosine wave, which is assumed to be a monomorphic EEG signal, and the second source is consider the blinks component with three bumps which designed as usual EOG signals. The simulated signal as a mixture of the two sources and white noise ($\eta = 20\%$) are shown in the Figure 5-3(a). where, η is defined as the percentage of the maximum amplitude of the input signal. This proposed MCA method is applied to separate the components from the simulated signal with the explicit dictionaries UDWT, DCT and DIRAC as shown in the Figure 5-3(b), as an replication test. The correlation coefficients between the simulated signal and the sum of all components has more than 0.99 and the simulated result is proved the accuracy of decomposed components by MCA with UDWT, DCT and DIRAC explicit dictionaries (Figure 5-3(c)).

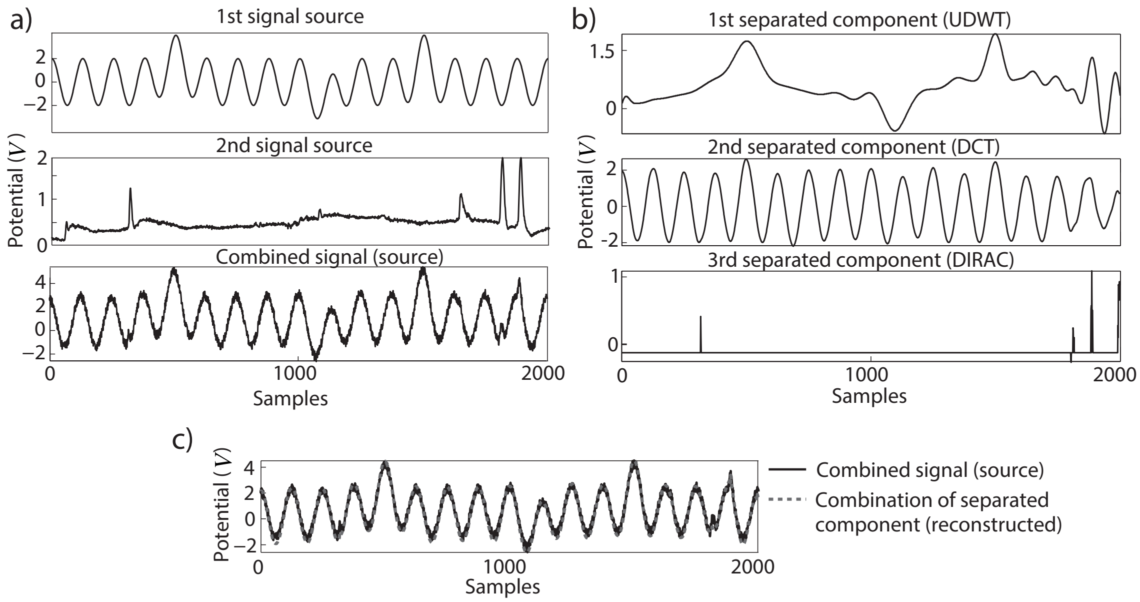

Figure 5-3: An example of simulated signal for decomposition, a) the cosine with bump and spikes signals; and combined signal with white noise ($\eta = 20\%$), b) separated components with explicit dictionaries UDWT-DCT-DIRAC, c) comparison between combined signal and sum of separated components (cc = 0.99).

5.6.2 Simulated EOG contaminated iEEG signal

The section 5.6.1 is a simple example of the simulated data. In this section, we are introduced a new validation way to test the proposed method in qualitative manner. The simulated EOG and real iEEG signal are obtained in the condition of closing eye, and the linear combination of simulated EOG , iEEG signals are simulated for the test. The iEEG signals are considered as an usual level of white noise and didn't add further noise additionally in this case. As mentioned the iEEG dataset was given by Andrzejak et al. [122] with 100 trials, and the sampling rate was at 173.61 Hz (0.00576 s/sample) and 2^{10}(=1024) samples corresponding to about 6s (5.89824s). The linear combination of simulated EOG and iEEG signals are applied for the validation.

We assumed that the different combination of simulated EOG : artificial eye movements, which is as the step function, and eye blinks by bump signal. The flatness

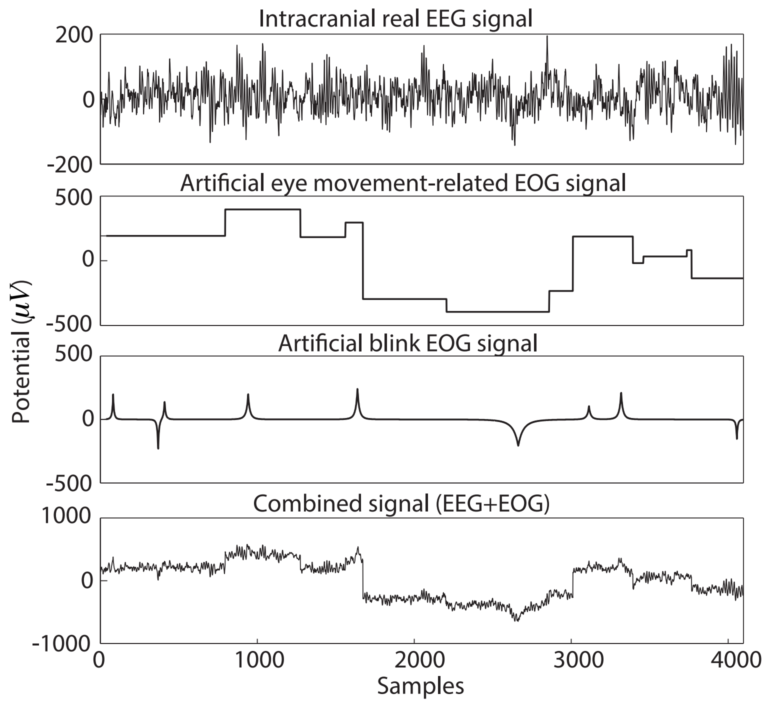

Figure 5-4: A systemic representation of different morphological signals a) intracranial EEG signal, b) artificial block EOG signal, c) artificial blink EOG signal, d) combined signal.

of signals with slow elevations in time scales with respect to the EEG time scale are represented the gaze-type eyeball rotations. This signals can be reconstructed by a mathematical function defined by the rate of change $(\hat{g})'$ of $\hat{g}$ which satisfy that $\{t \; |(\hat{g})' > 0\}$ should be 0. Thus, the definition of the EOG smoothness is described as

$$(\hat{g})'_I = \begin{cases} (\hat{g})'(t) & (\hat{g})'(t) = 0 \\ 0 & (\hat{g})'(t) > 0 \end{cases} \tag{5.8}$$

where $I = \{t \; |(\hat{g})' = 0\}$ leads $(\hat{g})'_I \equiv 0$ according to its definition as shown Figure 5-4 (b). In addition, the bumps signal is showed in the Figure 5-4(c) as assumed the blink-type EOG signal. The Figure 5-4(d) showed the schematic example for the semi-simulated signal. In same way, 100 datasets of semi-simulated signals with random combination of components in time series are used for the validation.

A set of results as shown in the Figure 5-5(a, b, c) are demonstrated the decomposition of semi-simulated signal by explicit dictionaries, depending on the combination

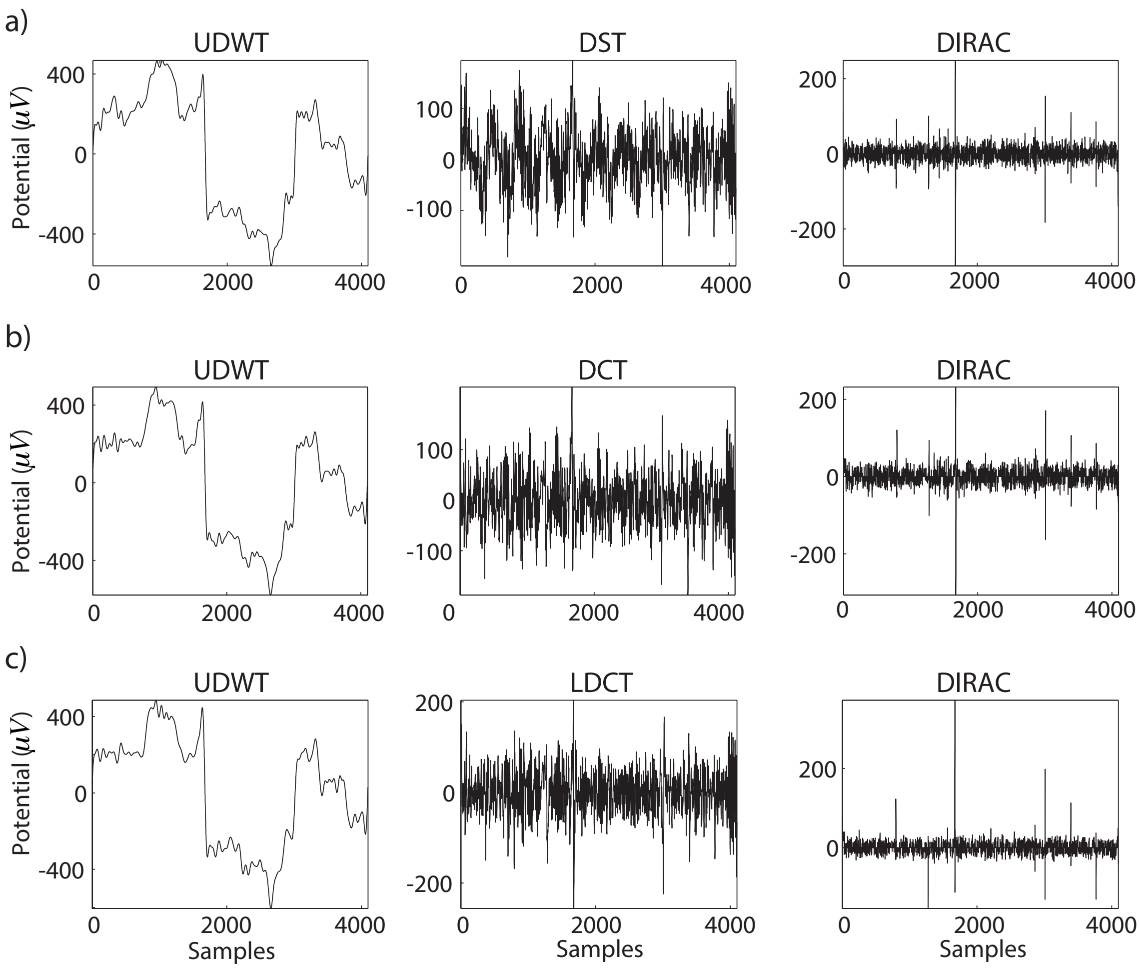

Figure 5-5: Component separation by MCA : a) explicit dictionaries are UDWT, DST and DIRAC. b) UDWT, DCT and DIRAC. c) UDWT, LDCT and DIRAC respectively at $\lambda = 4$. The original signal for decomposition is shown in Figure 5-4 (bottom) as combined signal.

of dictionaries. The stopping criterion is depend on $\lambda * threshold$ and the parameters are used of different combination of explicit dictionaries (UDWT-DCT-DIRAC, UDWT-DST-DIRAC and UDWT-LDCT-DIRAC), threshold type either a hard and soft and λ value varied from 3 to 5 in this comparative study as mentioned in section 5.4.

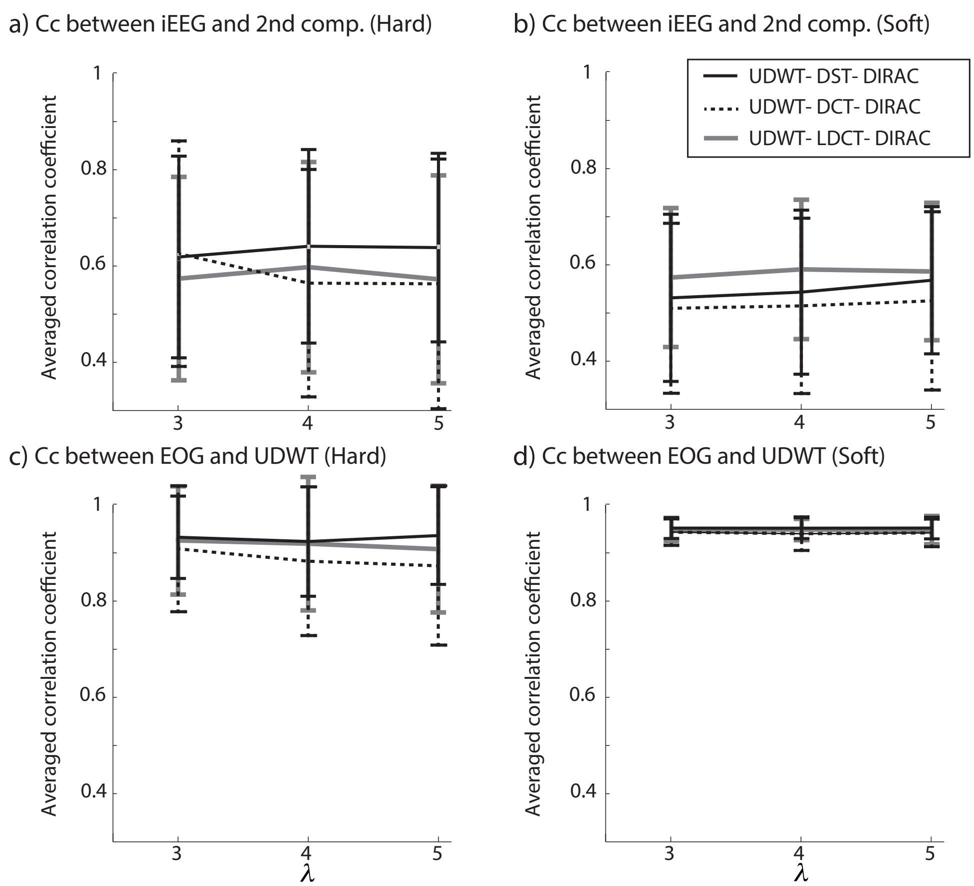

Figure 5-6: A comparison between cc of decomposed morphological component with iEEG signal and Artificial EOG with hard and soft threshold. Mean value and standard deviation are calculated from all 100 decomposed data by explicit dictionaries. a) second morphological component is decomposed by DST, DCT and LDCT with hard and, b)soft threshold respectively. c) first morphological component is decomposed by UDWT with hard threshold and d) soft threshold respectively. 100 trials of iEEG and artificial EOG are used.

The Figure 5-6 (a) and (b) are showed the averaged cc of decomposed component by respective combination of explicit dictionaries with hard and soft thresholds. The cc between iEEG and either DST, DCT or LDCT component is evaluated depending on the three combination types as shown in (Figure 5-6 (a)) for the performance of the

EEG signal decomposition. The cc between EOG and UDWT component is evaluated shown in (Figure 5-6 (b)) for the performance of the EOG signal decomposition. In comparison between hard and soft thresholds, the average value in the hard threshold is around 0.6 which is larger than that in the soft threshold, while the average value in the soft threshold is around 0.95 and less variances than that in the hard threshold. It is indicated that UDWT dictionary with soft threshold is the stable performance according to the fitness of the morphological property in this case.

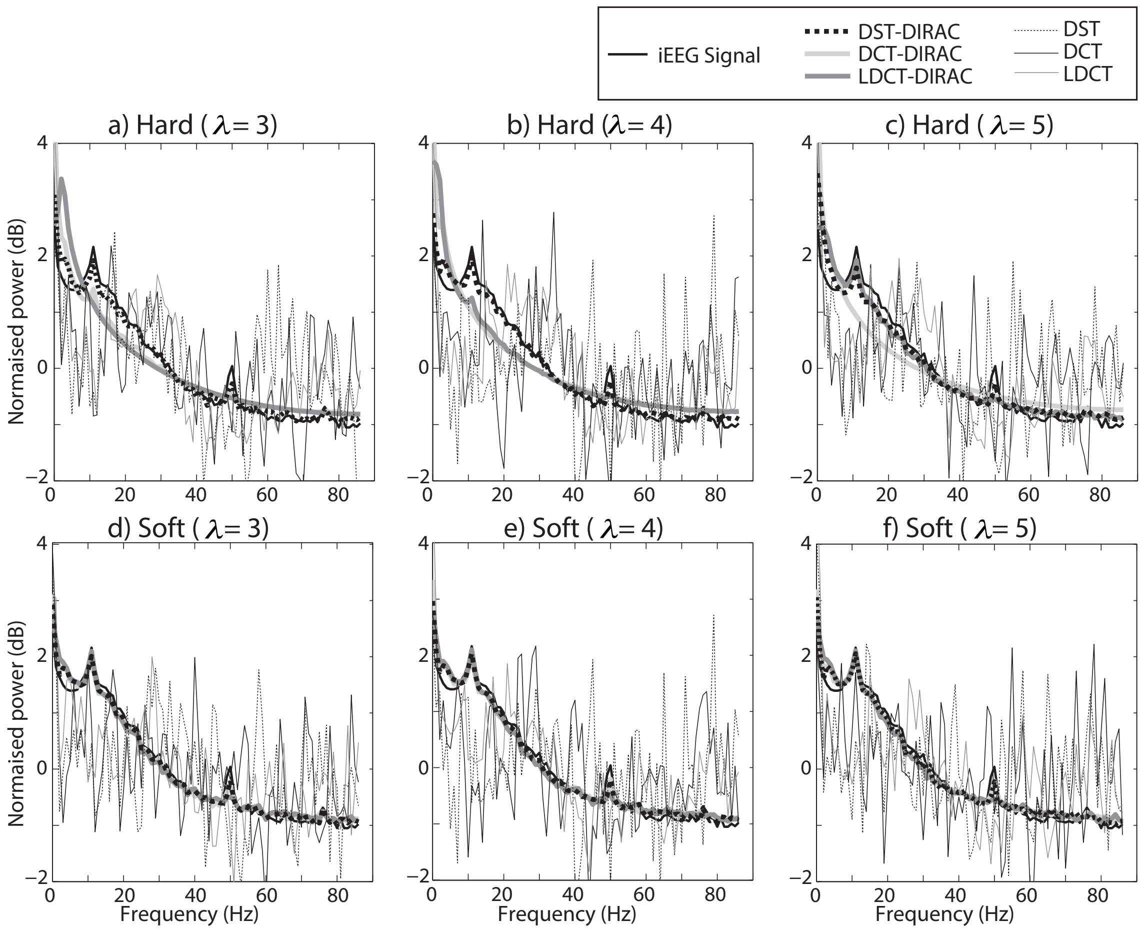

Figure 5-7: An averaged normalized FFT obtained from 100 of iEEG, combination of two morphological components and single morphological component at λ varies from 3 to 5 with hard and soft threshold.

The variances and average values are similar in the evaluation of EEG signal decomposition using the time domain, and then we introduced a measure in the frequency domain. The specific tendency of brain stage of brain can be represented through the information carry by EEG signals in the frequency domain as mentioned

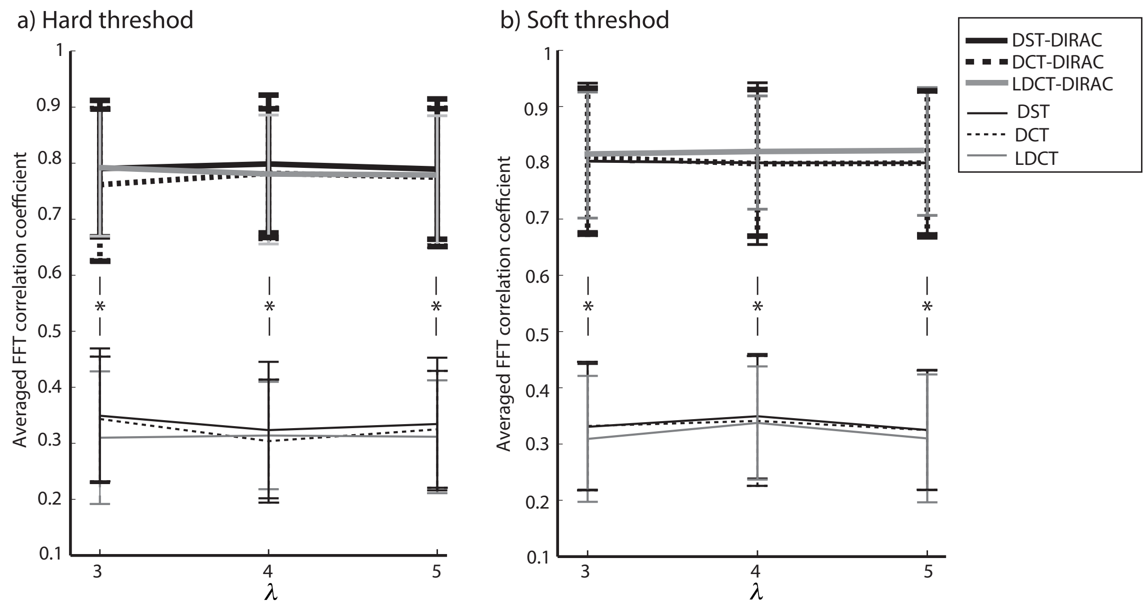

Figure 5-8: A comparison of FFT correlation coefficient between iEEG data and morphological component decomposed by explicit dictionaries. a) combined two morphological components, b) single morphological component. Mean value and standard deviation calculated from all 100 decomposed data by explicit dictionaries with hard and soft threshold.

in 5.3, such as having a synchronized neural activities by showing the existence of a peak in the frequency spectrum. A peak around 10Hz and 50Hz in closing eye condition are showed in the evaluation of the EEG data. Therefore in the frequency analysis, a 10Hz peak will be an index of how much the reconstructed signal preserves original information contained in the original iEEG data at closing eye condition. The averaged normalized FFT is showed in the Figure 5-7 as the comparison among three combinations of the dictionaries. Interestingly although DST, DCT and LDCT single components are seemed to reconstruct the EEGs because of a high cc value in the time domain. And the frequency spectrum analysis is clarified the fact that the single component cannot reproduce the necessary tendency of EEG signals as the existence of peaks. Therefore, the combination of 2nd and 3rd components which means the oscillatory and spike components are successfully reproduced the EEG signal tendency and suggesting the importance of the spike information that presumably synchronizes background oscillatory behaviors. The 10Hz peak can be reproduced depending on parameter conditions easily; however 50Hz peak is difficult especially for LDCT-

DIRAC component in every case. In the viewpoint of the tolerance in change of the threshold value, the soft threshold method showed the robust performance of the signal information preservation, which is consistent with the result of EOGs in Figure 5-6. As shown in Figure 5-8, the reconstruction accuracy of the frequency profile by two dictionaries is proved by a significant difference between results of two morphological and single morphological components (t test; p¡0.01 in both hard and soft thresholds). This evidence suggests the importance of the DIRAC component for EEG signals, which is not equivalent to the noise, or rather carrying some information.

5.6.3 Decomposition of EOG from real EEG data

EEG DATA

The real scalp EEG and EOG data are obtained from the data in the paper of Ai et al. (2016) [115]. These data were recorded from 23 EEG channels (FP1, FP2, F7, F3, Fz, F4, F8, FC5, FC1, FC2, FC4, T7, C3, Cz, C4, T8, CP1, CP2, P3, Pz, P4, O1, O2) and 7 EOG channels (V1u, V1d, V2u and V2d vertical EOG (VEOG) electrodes were placed on supraorbital and infraorbital rims of each eye; HL and HR horizontal EOG (HEOG) electrodes were on the left and right outer canthi; Vz was on the forehead approximately 25mm above the nasion) respectively, according to 10-20 international system (BrainAmp amplifier, Brain Products GmbH) from the 8 participants seated in a comfortable armchair, with the base adjusted according to a participant height. The participants were fixed their eyes straightly to the fixation cross in the center of the monitor screen. The stimulus was displayed by a CRT monitor. A chin support frame was used to keep the participant's head position and fix their head to the supporting frame without laying their chins on the supporting bar to avoid the jaw clenching artifact. The distance between eyes and monitor was set to 70cm. The sampling rate was 500 Hz. The whole details of the experiment protocols were given in Ai et al. (2016) [115].

Results with real EEG-EOG

According to Ai et al. (2015), the real EEG-EOG data are divided into 4 sessions. Each session has 12 tasks of eye movement. The two EOG signals are collected from $(V1d - V1u)$, $(V2d - V2u)$ at right and left sides of eye as shown in Figure 5-9 and both signals showed the same kind of tendency because vertical EOG propagates symmetrically in a anterior-posterior direction. The Figure 5-10 showed the real EEG signals are taken from some electrodes *e.g.* Fp1, Fp2, Cz, O1, and O2, which are represent the EOG influence depending on the frontal, central and occipital parts of the brain.

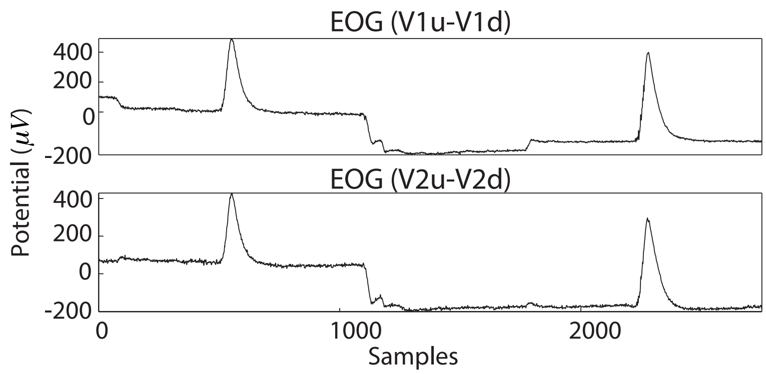

Figure 5-9: An example of EOG signal taken from right and left side of eyes.

The selected explicit dictionaries is used to represent the targeted component for the EEG and EOG signal. EEG and EOG are distinguished based on the morphology that are observed in the EEG and EOG. The lateral eye movements mostly affects frontal electrodes [55]. Therefore, Fp1 electrode is used to decompose and demonstrated the effectiveness of our proposed method with MCA as showed in Figure 5-11 and same applied to all the 23 electrodes. All EEG signals are morphologically decomposed with redundant transform.

Figure 5-11(a) is demonstrated the decomposition of components by the first explicit dictionary, it is analyzed into three different morphology of the EEG signal. Figure 5-11(b) and Figure 5-11(c) showed the second and third explicit dictionary of redundant transform respectively. The over-complete dictionary is a combination of redundant transform that characterized the component in a different morphol-

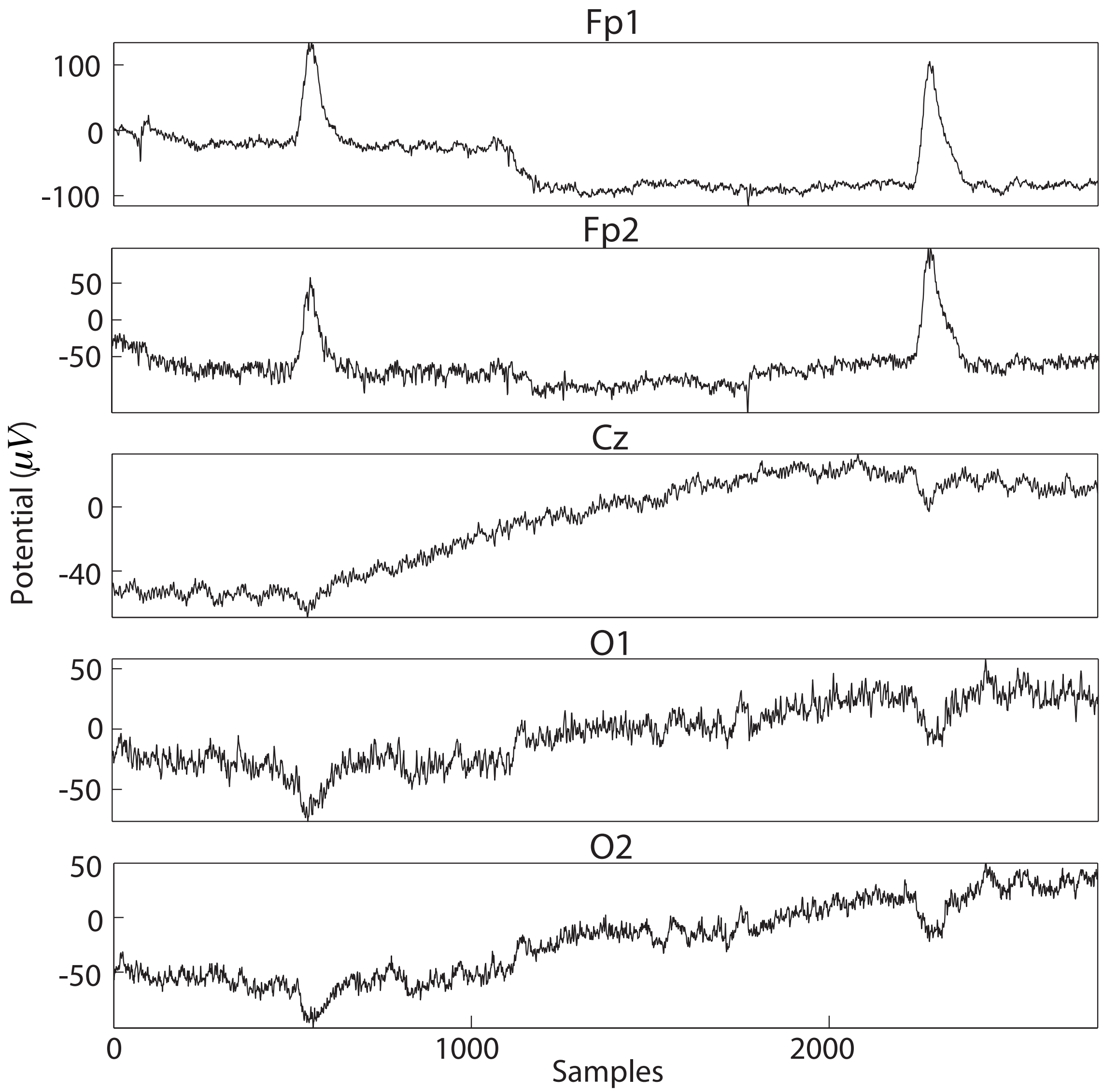

Figure 5-10: An example of real EEG signal taken from Fp1, Fp2, Cz, O1 and O2 electrode channels.

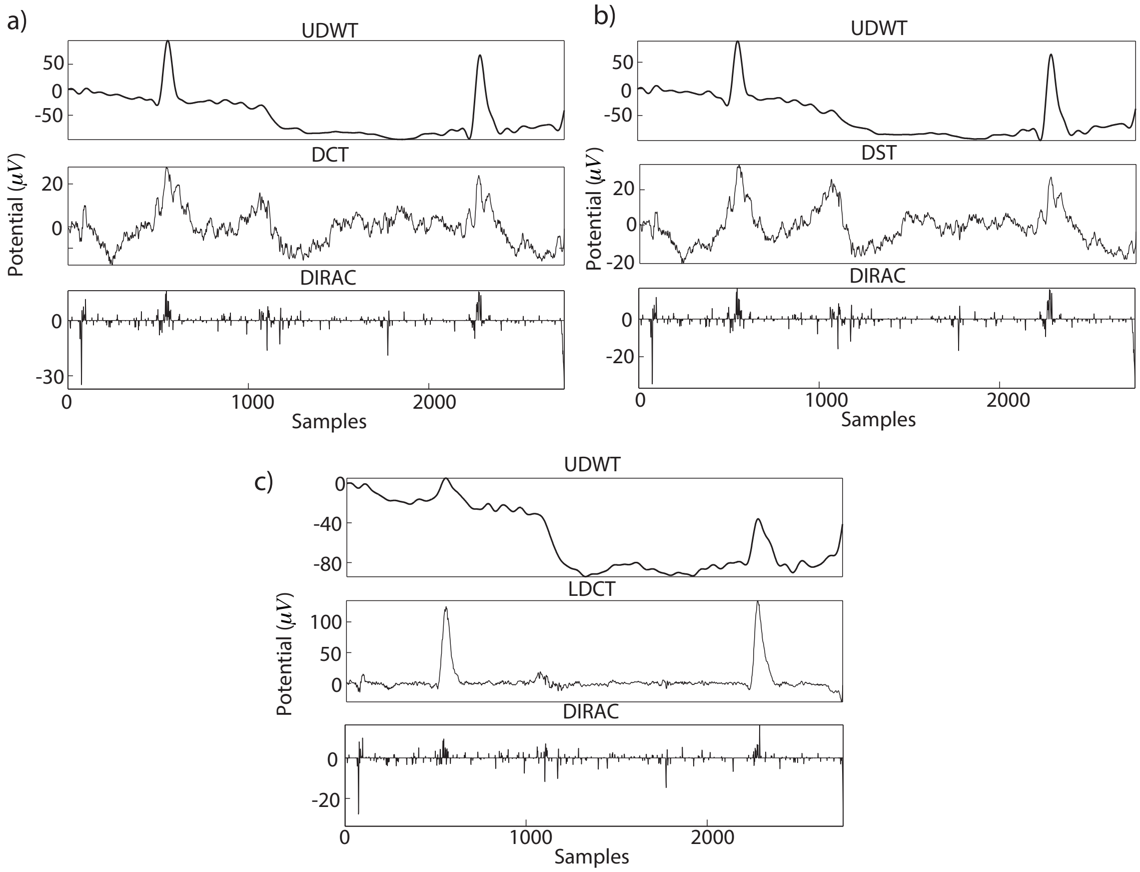

Figure 5-11: Component separated from EEG (Fp1 electrode) signal by explicit dictionaries a) UDWT-DCT-DIRAC, b) UDWT-DST-DIRAC, c) UDWT-LDCT-DIRAC respectively.

ogy. Accordingly, one can differentiate in decomposed components by over-complete dictionaries. The first component is decomposed by 'UDWT' of each over-complete dictionary was analyzed the slow and blink type morphology. The second component was decomposed by 'DCT', 'DST' and 'LDCT' and are analyzed the background of the signal which is similar to the EEG signal and third component was decomposed by 'DIRAC' and is analyzed the unexpected spike. The first over-complete dictionary is decomposed the EEG signal without changing the monomorphic, polymorphic and transient properties. The cc between the original signal and the summation of all decomposed component is close to one. Figure 5-12 showed the raw EOG signal taken from the vertical and horizontal channel and first decomposed component taken from Fp1, Fp2, Cz, O1, O2 respectively.

Table 5.1 showed individual cc of original signals and recomposed from the combination of components with respect to different channels and combinations of dictionaries. Table 5.2 showed the cc between filter raw EOG signal taken from vertical and horizontal channels and decomposed first component from Fp1, Fp2, Cz, O1 and O2 respectively.

Table 5.1: cc of original signal and sum of the decomposed components.

EEG channel	Correlation Coefficient		
	UDWT-DST-DIRAC	UDWT-DCT-DIRAC	UDWT-LDCT-DIRAC
Fp1	0.9921 0.014	0.9921 0.014	0.9932 0.013
Fp2	0.992 .017	0.9919 .018	0.9932 .014
Cz	0.9898 .01	0.9899 .01	0.9908 .009
O1	0.9836 .015	0.9836 .016	0.9869 .012
O2	0.9855 .013	0.9856 .013	0.9849 .015

5.7 Discussion

In neurobiological event diagnosis and neuroscientific research, the artifacts contamination in the EEG signal is the important issue. Therefore, various methods has been

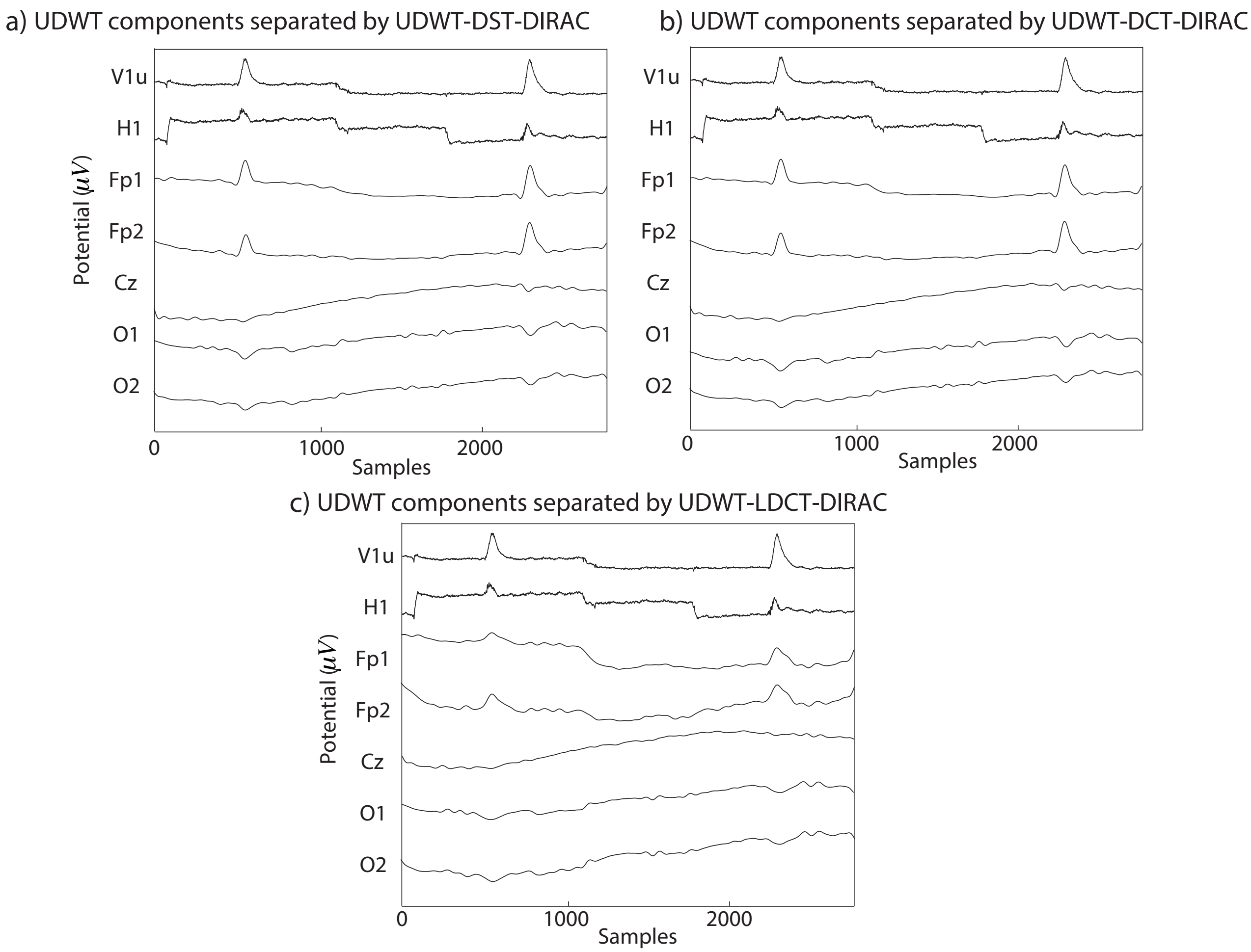

Figure 5-12: UDWT component taken from Fp1, Fp2, Cz, O1, O2 separated by UDWT-DCT-DIRAC, UDWT-DST-DIRAC, UDWT-LDCT-DIRAC respectively.

Table 5.2: cc between filtered EOG and UDWT component decomposed by UDWT dictionary.

		EOG Channels	EEG Channels				
			Fp1	Fp2	Cz	O1	O2
Correlation Coefficient	UDWT-DST-DIRAC	V1d	0.6777	0.657	0.7267	0.9223	0.6445
		V1u	0.6814	0.646	0.6606	0.9419	0.6354
		V2d	0.916	0.906	0.9402	0.882	0.5402
		V2u	0.2332	0.2268	0.2353	0.6388	0.8494
		H1	0.8582	0.847	0.8444	0.6902	0.5839
		H2	0.9419	0.9468	0.9559	0.7476	0.4752
	UDWT-DCT-DIRAC	V1d	0.6792	0.6595	0.68	0.9213	0.6352
		V1u	0.6835	0.6396	0.6424	0.9581	0.6585
		V2d	0.9193	0.902	0.9362	0.8764	0.5145
		V2u	0.2331	0.2183	0.2316	0.6639	0.8919
		H1	0.8593	0.8507	0.8626	0.6759	0.5376
		H2	0.9442	0.9465	0.9662	0.7266	0.4346
	UDWT-LDCT-DIRAC	V1d	0.6794	0.6403	0.7219	0.8892	0.65
		V1u	0.6443	0.6279	0.6459	0.8196	0.5381
		V2d	0.9142	0.9072	0.9395	0.9592	0.6506
		V2u	0.2351	0.2235	0.2383	0.3747	0.6804
		H1	0.8637	0.8449	0.8471	0.7638	0.5734
		H2	0.9586	0.9558	0.9577	0.8826	0.5598

used for removal of the artifacts [54, 63, 66, 67, 68, 70, 72, 73, 107, 131, 132]. Similarly, the decomposition based methods are also used to remove the EOG artifacts in EEG signals [68, 107, 130, 134, 142, 144]. However these methods have lack of the elucidation what the nature of EEG signals in the viewpoint of the signal analysis, and a systematic approach is required by treating the sparsity and non-linearity of the signal in the time domain.

This study is revealed the morphological nature contain in the original EEG signals in a sense, by using MCA. The UDWT is used to decompose the slow and bump morphology; The DCT, DST and LDCT transform is used to decompose the EEG signal; Spike type morphology is decomposed by DIRAC. The morphology of oscillatory activities are represented by the redundant transform of DCT and DST both has similar tendency. Therefore, we used the DCT, LDCT and DST dictionaries for validations of EEG signal. The significant difference of detail in morphology of DCT and DST are given in past studies [148, 149], while in this analysis there are no significant difference. The right combination of redundant transform to form over-complete dictionary is revealed the desired decomposition in principle.

The simulated EOG signal like 'Blocks', 'Bumps' are defined in past studies [102, 90, 91] as shown in Figure 5-4 and EEG data [122] are used for validation of the purposed method. The horizontal and vertical eye movements with abrupt changes are similar to the 'Blocks' that is described by past studies [52, 53]. The 'Bumps' are used to a representative signal form as eye blinks that happens in unexpected timings as illustrated in Figure 5-5 for the sake of simplicity in the present study. The separation of component by given dictionary is worked well in this evaluation but the further analysis is necessary in the evaluation of the signal decomposition with complex eye movements, which requires presumably various redundant dictionaries. In the verification of the component discrimination as shown in Figure 5-6 and 5-7, the accuracy of the averaged EOG component decomposition is above 90%, which suggests a plausible performance even in the complex eye movements. The combined DST and DIRAC dictionaries have better decomposition performance rather than others, while DST and DCT has theoretically no meaningful difference. The usage of iEEG to be the true EEG signal have a large benefit, which can be used for the performance test for past proposed method like ICA and PCA consistently. The proposed method is successfully demonstrated the performance in cc and the frequency profile especially, while in the serious discussion of the real EEG and EOG signals, the DST or DCT component exhibited a baseline fluctuation of the signal which are denote the persisting of the EOG component or other slow frequency artifacts noise, and the factor will be improved by the fine-tuned design of the DST or DCT dictionary with a band pass filter function. In addition, the threshold problem exits in the optimization algorithm and number of iteration [139].

The EEG decomposition have not up to mark with combination of second and third component of EEG signal decomposed by (DST, DCT, and LDCT) and DIRAC respectively based on the morphology. Therefore, the accurate combination in the further perspective will be considerable. Even the combination of all components and the mixed signal or real EEG signal have cc above 97% for all redundant transforms, as is analyzed in the frequency spectrum, the signal morphology has further meaning in the viewpoint of the signal transmission. The MCA method has such an extended and flexible availability for signal analyses.

Chapter 6

Bereitschaftspotential for Rise to Stand-Up Behavior

Around millions of people in the world are affected from some kind of central nervous system disorder (stoke, rapid loss due to blood circulation, multiple sclerosis or Parkinson's disease) or disable due to some form of accident(road traffic, sport practice). These disabilities are affected the daily work routine that leads the isolation from the social life. In this chapter, a very important gait rise to stand-up is consider for investigation. We are exploiting brain computer interface systems that assist neurocognitive disorder and motor-disabled persons. The electroencephalography (Bereitschaftspotential (BP)/readiness potential (RP), evoked before the onset of the rise) and electromyography are recorded for the rise to stand behaviour. In that the negative-going BP (RP) is associated with the preparation and execution of dynamic movement. This study revealed that the negative-going BP is evoked around 2 to 3 seconds before the onset of the rise in response to start cue. The BP has a negative peak before the onset of the movement. The potential is followed by premotor positivity, motor-related potential, and reafferent potential. BP negative peak values are correlated with the latency from the onset of the BP to the onset of the upper body, lower body movement and to the max amplitude of the quadriceps & hamstring electromyogram (EMG). BP for the rise to standing up is started around -3 seconds consisted of steeper negative slope (-.8 to -.001 seconds) before the onset of movement and steeper slope correlate with the hamstring EMG. The steepness of the late BP did not change in the trials. This chapter is comprised all above in details and the measured electroencephalography activities are widely used as input for non-invasive BCI systems for an example. It explains an experimental protocol for rise to stand-up and recorded signal from EEG, EOG and EMG.

6.1 Introduction

The human brain is a rich source of information associated with volition, actions, emotion and various aspects of the internal state. The capacity for any voluntary action is estimated from the performance of the task execution. The exploration is still going on to collect the scientific approach mechanism for the voluntary movement; how the brain is controlled the complex voluntary movement and adjust the posture through feedback by a visual, audio and sensory signal. The identification of cognitive behavior for voluntary movement is a new investigation therefore we discuss the brain state against the voluntary movement.

In our daily lives, we have been experiencing the unexpected event and most of the event is essential for survival; influencing the behavior. The complex voluntary movement is consist of several segments movement that influences the voluntary movement of a body segment is directly or indirectly accompanied with several other body segments and these expected or unexpected movements behavior are reflected by brain's response. The repeated occurrence of contingent's events are occurred with distinct brain responses. These events are time locked to specific external or internal event. They have been massive, physical stimuli, behavioral responses thoughts, and even emotional processes.

EEG signals are associated with movement-related cortical potentials (MRCPs) have been evaluated during the periods both preceding and following the voluntary movement [150, 151]. The type, sequence of movement [152], by eccentric / concentric of muscles contraction [153] and voluntary muscles activation [154] are affect the MRCPs in the voluntary movement. The movement related potential as general term that reflects the cortical activity for voluntary movement described as slowly rising negative potential. The BP or RP is a negative-going potential starting 1-2 seconds before the movement onset [155]. Pre-motion positivity (PMP) and negative motor potential (MP) are observed just before the movement [156]. A large positive potential (reafferent potential, RAP) [155] is following the movement onset and positive potential is associated to the type of movement [153] BP is maximal at the midline centro-parietal area, is symmetric, and is widely distributed over the scalp. A large positive potential (reafferent potential, RAP) [155] is associated to the type of movement [153] that follows the movement onset and positive potential. BP is maximal at the midline centro-parietal area, symmetric and widely distributed over the scalp. BP is divided in two components "BP1 (early BP)" and "BP2 (late BP)" [157]. The early BP is started in the SMA and includes pre-SMA and then progresses shortly to the lateral premotor cortices bilaterally has investigated in the past studies.

The early BP is involved in a slowly accumulative negative potential beginning between 1 and 2 seconds prior to the movement onset [150, 158]. The late BP is started in the M1 and the premotor cortex [159, 160] and has a steeper negative slope. It maximizes the negativity at the vertex, which lies over the supplementary motor area (SMA) [159, 160, 161, 162]. It is certain that both components are related to preparation and/or execution of voluntary movement. It provides the information for voluntary movement associated with several body segments and allows the evaluation of the cortical efferent process and other higher processes controlling voluntary movement [150, 163, 164]. The early BP is involved in the preparation of the voluntary movement. The type of movement and complexity of movement cannot be determined by the early BP [157]. Even it is not essential for simple movement. Early BP is similar to finger; elbow movements began between 1 and 2 seconds [157]. It is reflect the rising activity predominantly and associated with pre-movement preparatory process [165]. Late BP is very important for the type, complexity of muscle movement. It is associated with the time between SMA and motor cortex for selecting the muscle activation [157]. A number of studies revealed that the muscles forces are directly to proportional the MRCPs.

BP is observed during upper and lower extremity movements [150, 164] and have different morphology in terms of shape and magnitude during simple vs. complex movements [166]. So far, BPs have been recorded during mouth opening, finger, hand and foot movements [150, 151, 152, 156, 159, 160, 158, 161, 162, 163, 164, 167, 168, 169, 170]. The BP has been carried differential information for several type of movements that use upper and lower body extremities separately and BP for complex voluntary movements using both the upper and the lower body is not described in the past studies. The complex movements of the whole body is associated with several body segments in time [171]. The rise to stand is involved the upper and the lower body. The standing movement is a dynamic movement [172]. In this movement, the whole body, including the upper and the lower body, is used for the behavior [172]. Four phases are involved in the rise to standing. In the first phase, the flexion momentum is used to generate the initial momentum for rising. The second phase begins as the individual leaves the stool seat and ends at maximal dorsiflexion. In the third phase, the body rises to its full upright position. In the last, the whole body is stabilized. These phases are differentiated in terms of momentum and stability characteristics.

The preparatory process for the onset of the movement is modulated by temporal predictability and resolution of the imperative cue [152, 173]. The sequential movement is very crucial because it involved the sequencing of motor task in different order [174]. It has necessary to select order of movement trajectory and prior to movement the pre-SMA and SMA are involved [174] for rise to stand-up. The various cortical areas are associated for complex sequential finger movement than the simple movement [175]. Therefore, in this chapter we focused on the rise to stand behavior and studied BP during the movement. It is necessary to establish the BP dynamics of functional activities, such as rising to a stand position, in healthy individuals in order to improve abnormalities in individuals who have impairments [172, 176, 177]. Factors such as latency between the BP and surface EMG are seen in individuals with impairments. With start time the BP is gradually decreases and steepness of the late BP that suggests the behavior of movement (cue based and self-initiated).

This reflects the preparation for rising to stand and the construction of voluntary movement.

The decoding of the preparatory activity for voluntary movement may be helpful in various regards. As a result, brain computer interfaces (BCIs) have been incorporated into the motor cortex used to perform sitting and standing intention movements [178]. This helps during rehabilitation and expedites adaptation to BCI algorithms and robotic devices. The EEG signals were recorded from healthy participants while they were stand-up from a stool. The experimental paradigm was conventional and designed to record the scalp surface EEG during the preparation and execution of the rise to stand movement. We also recorded the gyro sensor signal at the participant's back and obtained quadriceps and hamstring EMGs to record the onsets of upper and lower body movements.

6.2 Materials

6.2.1 Participants

This study has included 10 unpaid healthy volunteers with no motor impairments in the experiment (10 males; age, 26.8 ± 3 [mean $\pm$ standard deviation [SD]] years) who provided written informed consent; the study is approved by the ethical committee of Kyushu Institute of Technology. The volunteers are highly motivated to perform the task. None have prior knowledge of the purpose of the study. The objective of the study and the procedure of the experiment are explained to all the participants just before the experiment.

6.2.2 Experimental procedure

The participants are requested to relax and sit on an armless, backless stool, which is adjusted according the participant's knee height. They are instructed to rise without moving their hands. The back of the participant is moved forward at first. Then their buttocks are leaved the stool.

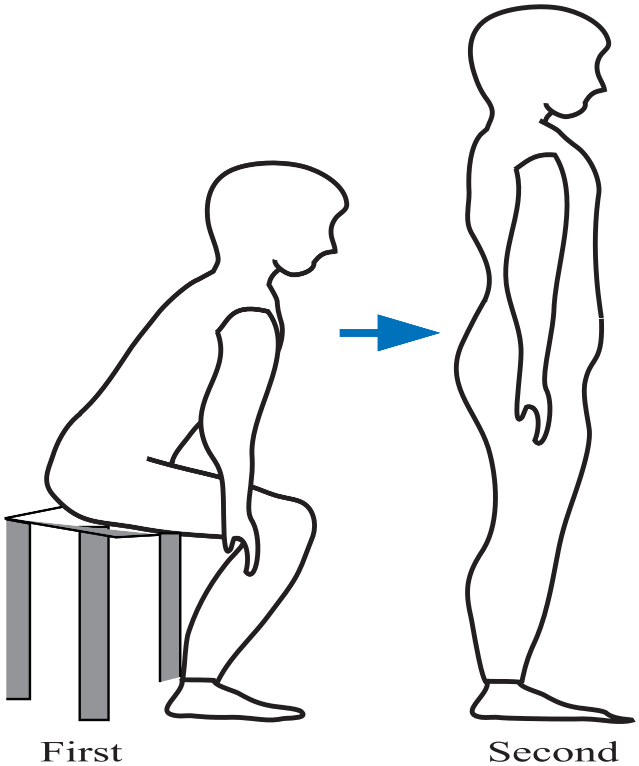

Figure 6-1: Schematic illustration of experiment postures.

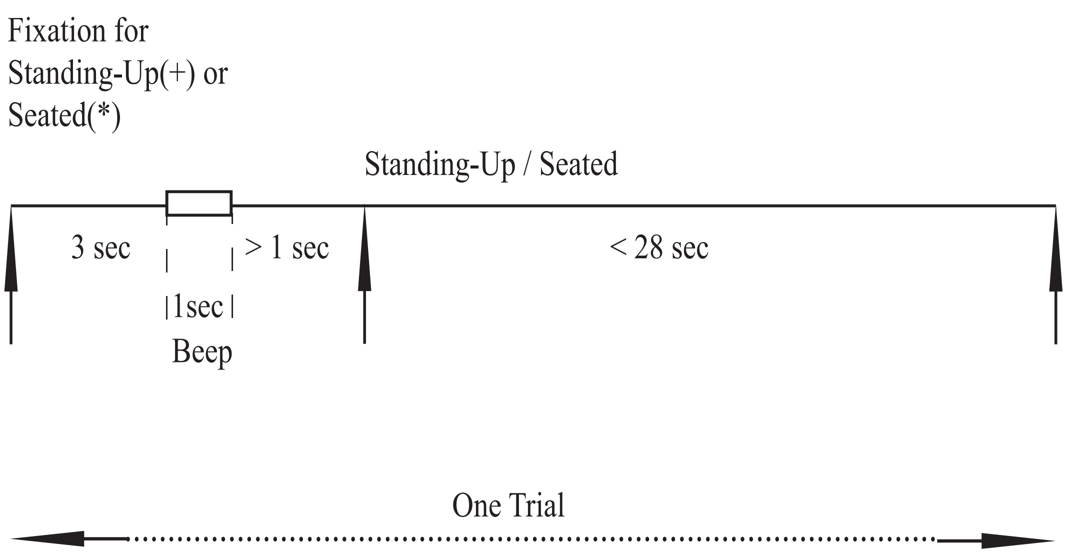

Figure 6-2: Experiment timing protocol.

Finally, the body is rise to its full upright position and the whole body is stabilized, as shown in the Figure 6-1. The participants are also requested to open their eyes and gaze toward the front during the rising movement.The pattern of the stand-up movement is complex and dynamic [172]. The schematic paradigm for the experimental procedure is shown in the Figure 6-2.

Each trial is lasted for 33 seconds and started with a visual fixation cue shown on the computer screen in front of the participants around 150 cm from their faces. There are two types of cues, "+" and "X". The "+" indicated that the participants are to stand up and the "X" indicated that is to be seated. After 3 seconds the visual cue, an auditory cue beep of 2 kHz stimulus is given to the participants for 1 second. After the beep, the participants are required to either stand up or to be seated. The participants have to wait more than 1 second after the beep, and then they are stand-up. The participants are seated until 30 seconds after the beep for the seated trial. A new trial Thirty seconds after the previous beep, a new cue appeared, and a new trial began. The participants are practiced before the actual recording started. They are asked to be 'attentive' to avoid their movements becoming automatic. Each participant performed a session of 50 trials. In each session, 30 trials for rising and 20 trials for being seated are administered to each participant randomly. The visual and auditory cues are presented by the Matlab (Mathworks Co., USA) program. In this session, 30 trials for rising without any external interference, subjects are performed the task according to their will.

6.2.3 EEG and EMG recordings

EEG signals are recorded from 6 Ag/AgCl electrodes; placed at F3, Fz, F4, C3, Cz, and C4 according to the international 10/20 system. All electrodes are referenced to mastoid electrodes, and the common ground signal is obtained at Fpz. A bandpass filter of 0.05-30 Hz is used for filtering the EEG signals and magnitude is amplified by an order of 1,000 (BIOamplifier, DIGITEX Lab. Co. Ltd., Japan). Electrode impedance does not exceed to 5 kΩ. EOGs are recorded using electrodes placed at the sides and the lower canthi of the left eye and used to remove blink and eye movement artifacts from the EEG. The surface EMGs are recorded from the lower body, as shown in Figure 6-3 during rise to stand movement.

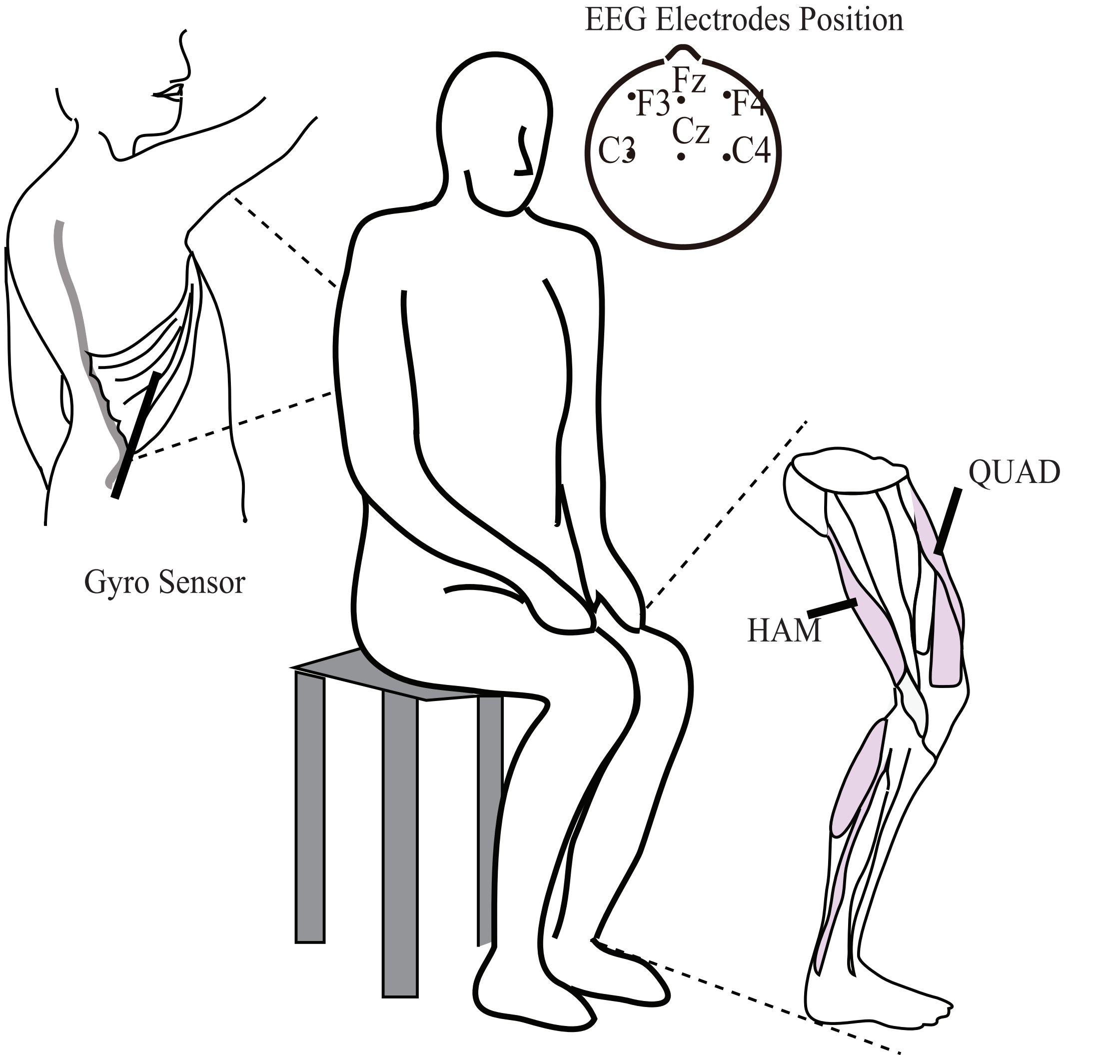

Figure 6-3: Electrode placements for EEG, EMG, the Gyro sensor, and the EOG recorded during the rise to stand movement. To detect the movement onset at the back of the upper body, a Gyro motion sensor was attached near the latissimus dorsi muscle on the back. QUAD and HAM stand for the quadriceps and hamstring.

A pair of electrodes are fixed approximately 3 cm apart over the quadriceps and the hamstring muscles of the left lower limb through an INTERCROSS-410 amplifier (Intercross Co. Ltd., Japan) for the surface EMGs. The EMG signals are recorded to detect the onset of lower body movement. EMG signals are are amplified by a magnitude of 1,000 and filtered using a bandpass filter of 5.3-250 Hz. A gyro sensor is placed near the latissimus dorsi to record the onset of upper body movement and the onset of the rise to stand movement. The signal is amplified by a magnitude of 380 and is DC-filtered (INTERCROSS-410 amplifier, Intercross Co. Ltd., Japan). All of the EEG, EMG, EOG, and gyro sensor signals are converged onto a PC through an A/D converter unit (AIO-16320FX-USB; CONTEC Co., Ltd., Japan) using the signal recording software LabDAQ (Matsuyama Advance Ltd., Japan). The signals are sampled at 1,000 Hz.

6.3 Data Analysis

6.3.1 Raw data

The EOG artifacts are identified by visual inspection and trials with artifacts are excluded. 4 participants EEG data have noise among 10 participants, so they are discarded and EEG data from 6 participants are remained. After the exclusions, 18 $\pm$ 5 trials remained (mean $\pm$ standard deviation [SD]) per participant. In the analysis, EEGs are high-cut filtered at 4 Hz using EEGLAB [179]. The onset of the activation of the quadriceps and hamstring EMGs (EMG onsets) or the onset of the gyro signal change (Gyro onset) is defined as time zero in the Figure 6-4. EEG data are extracted for 7 seconds in each trial. The time-frame of data is ranged from -4 to 3 seconds based on Gyro onset and from -5 to 2 seconds based on EMG onset. EEG signals are obtained between -4 to -3 seconds are used for baseline correction of the EEGs based on Gyro and between -5 to -4 seconds are used for baseline correction of the EEGs based EMG onsets. The EEG signals are averaged for the 30 standing up trials and the 20 seating trials. The Gyro onset is determined based on local estimation of noise spectra [180, 181]. In this method, mean and variance are computed from the energy of Gyro signal. Gyro onset satisfies the condition is given as:

$$|G_e(T+t) - N(T+t-1)| > k, 0 \leq t < 0.2sec$$

where $G_e(t)$ is the energy, $N(t-1)$ is estimated of initial energy of baseline signal just before the time window. k is a tunable threshold parameter, it's value is 1. σ is the variance of the Gyro signal $G_e(t)$ in the window. T is the value increased by 0.2 second.

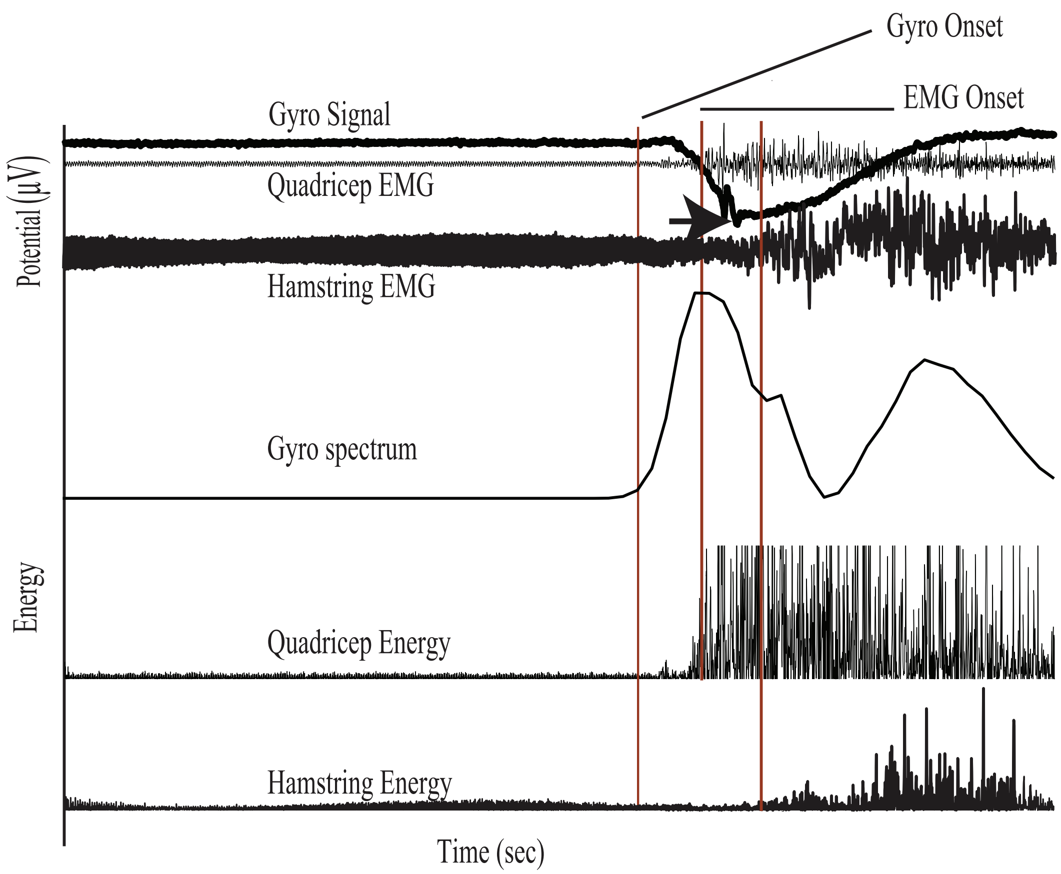

Figure 6-4: Schematic representation of the time course of the gyro, the quadriceps and hamstring EMGs, and the energy signals. An arrow indicates the negative peak of gyro signal.

The Teager-Kaiser energy (TKE) operator [182, 183] is used to determined the EMG onset. This nonlinear method can detect the surface EMG onset time of muscle activity. It is defined in the time domain as:

$$\Psi[x(t)] = x^2(t) - x(t-1)x(t+1),$$

where t is time. The TKE operator is proportional to the instantaneous amplitude and frequency of the EMG signal $x(t)$. Thus it has the advantage that it can consider the amplitude and frequency of the EMG simultaneously. The threshold used in the

TKE operator is determined by

$$T = \mu + h\sigma,$$

where μ and σ are the mean and standard deviation of the 2 seconds EMG signal before the onset of the EMG and h is a preset variable. $h = 15$ value is used in the present experiment. The operator is detected the EMG onset time accurately. Maximum EMG energies of the quadriceps and the hamstrings are calculated for 2 seconds after the EMG onset. BP is started between -3 and -2 second; Late BP (steeper negativity) is started between -1 and -.8 seconds before the onset of movement. A linear regression is used for the robust signal extraction [184]. It is given as

$$y(t) = \mu + \beta x(t) + \varepsilon,$$

Here μ, ε are 0. BP is divided by 0.1 seconds for detection of the starting BP and late BP. A slope of BP in the time of 0.1 seconds is calculated by least squares approximation. Early BP start time is determined by

$$-0.01 < \beta < -0.005,$$

Late BP start time is determined by

$$\beta < -0.01,$$

6.4 Results

To decompose the scalp EEG signal into different component in schematic manner by MCA procedure as shown in Figure 6-5. The Figure 6-6 shows the single trial raw EEG signal at Cz electrode position. The MCA method is applied to decompose the raw EEG signal with the explicit dictionaries such as UDWT, DST and DIRAC. The raw EEG data as shown in the Figure 6-6 are decomposed in three components

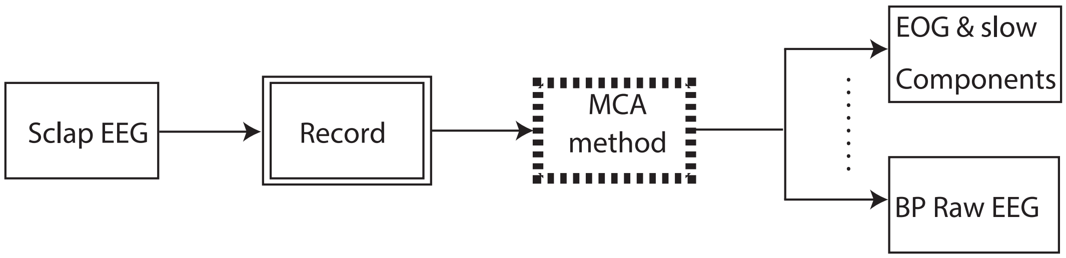

Figure 6-5: MCA method is applied to decompose the BP signal.

based on explicit dictionaries as mentioned above. The Figure 6-7 shows three different components separated by explicit dictionaries. The slow and EOG components are decomposed by UDWT redundant transform. The DST redundant transform is separated the raw EEG signal in a sense. The DIRAC transform is used to separate the unwanted spike artifacts is generated by different unknown sources. This results show that the MCA procedure can be work for single trial to decompose the BP component from the raw EEG signal for rise to stand-up behavior.

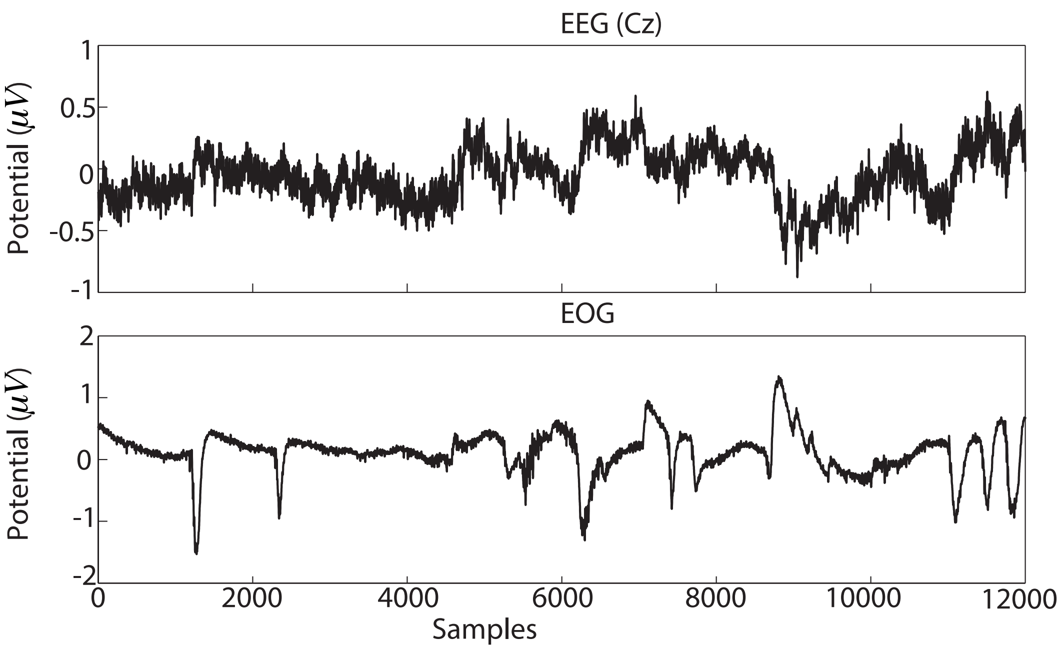

Figure 6-6: Single trial raw EEG signal at Cz electrode position based on gyro onset.

Even though EEG signals are high-cut filtered at 4 Hz using EEGLAB [179] for further analysis. The averaged EEG data results are shown in Figure 6-8 based on the Gyro onsets. Gyro onset is reflect the onset of upper body movement, while the EMG

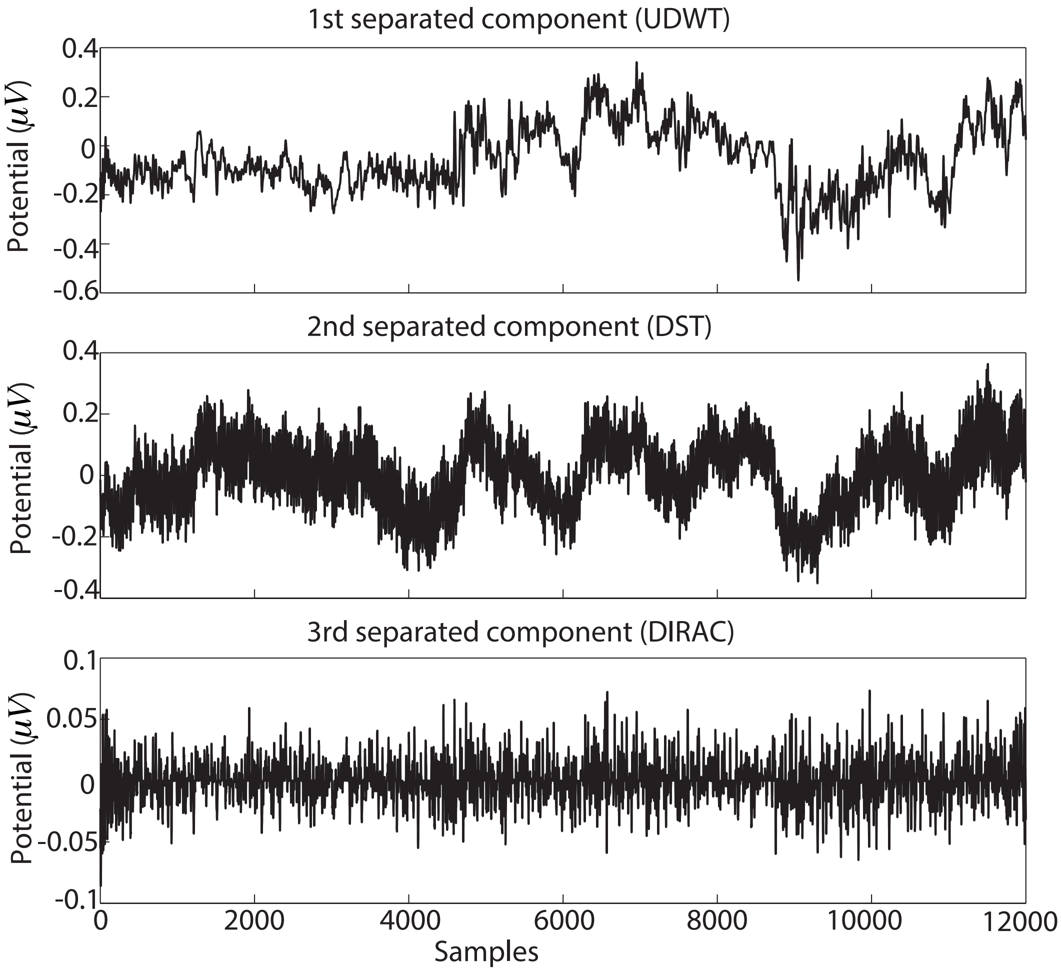

Figure 6-7: Component separated from raw EEG (Cz electrode) signal by UDWT-DST-DIRAC explicit dictionaries.

onset is reflect the onset of lower body limb movement. The grand averaged EEGs obtained at 6 locations among all of the subjects are shown in Figure 6-8 and 6-9 for cue based stand-up. Figure 6-9 shows the grand averaged EEGs based on EMG onset. A similar tendency to that in Figure 6-8 is observed, while the EEG signals are seem to be shifted to the left along the time axis. The gradual negative change is started around -4 seconds, which is earlier than -3 seconds, and the steeper change is started earlier than -1 second. The potential is reached the maximum negative peak at around -1 second. The time difference between the maximum negative peak time of the BP based on the Gyro and EMG onsets (ΔNPT) varied from 0.75 to 0.84 seconds. The EOG signal did not have a negative component from -4 to 3 seconds, as shown in Figure 6-8. The averaged value of BP start time are $2.95 \pm .54$ based on gyro onset from the entire subjects.

The potential is gradually decrease and reach the maximum negative peak around -.001 seconds as shown in Figure 6-8, around 3 seconds before the Gyro onset. The start time of the decrease (DT_{gyro}) and the negative peak time (NPT_{gyro}) are shown in Table 1. After that the potential is increased and reached a positive peak around 1.2 seconds after the Gyro onset. The potential changes at Fz and Cz are a little larger than those at the other electrode positions. BP has started around -3 second consist of two components: the initial slow component (early BP), and the late component, which has a steeper negative slope (late BP, also referred to as NS). The maximum negativity is determined the kind of complexity in movement. The potential at Cz has a steeper negative slope than before (gray arrow in Figure 6-8).

The decrease of start time is based on the Gyro and EMG onsets (DT_{EMG}) and the time of the negative peak of the BP (NPT_{gyro} and NPT_{EMG}) are defined in Figure 6-10, and the values are shown in Table 6.1. The time differences between BP based on Gyro onset and based on EMG onset ($\Delta DT = DT_{gyro} - DT_{EMG}$ or $\Delta NPT = NPT_{gyro} - NPT_{EMG}$) are also shown in Table 1. There is no significant difference between ΔDT and ΔNPT (unpaired t-test). ΔDT and ΔNPT are significantly correlated at all electrodes (r = 0.66, 0.71, 0.71, 0.69, 0.63, and 0.57 at F3, Fz, F4, C3, Cz, and C4, respectively; Spearman rank correlation test, $p < 0.001$).

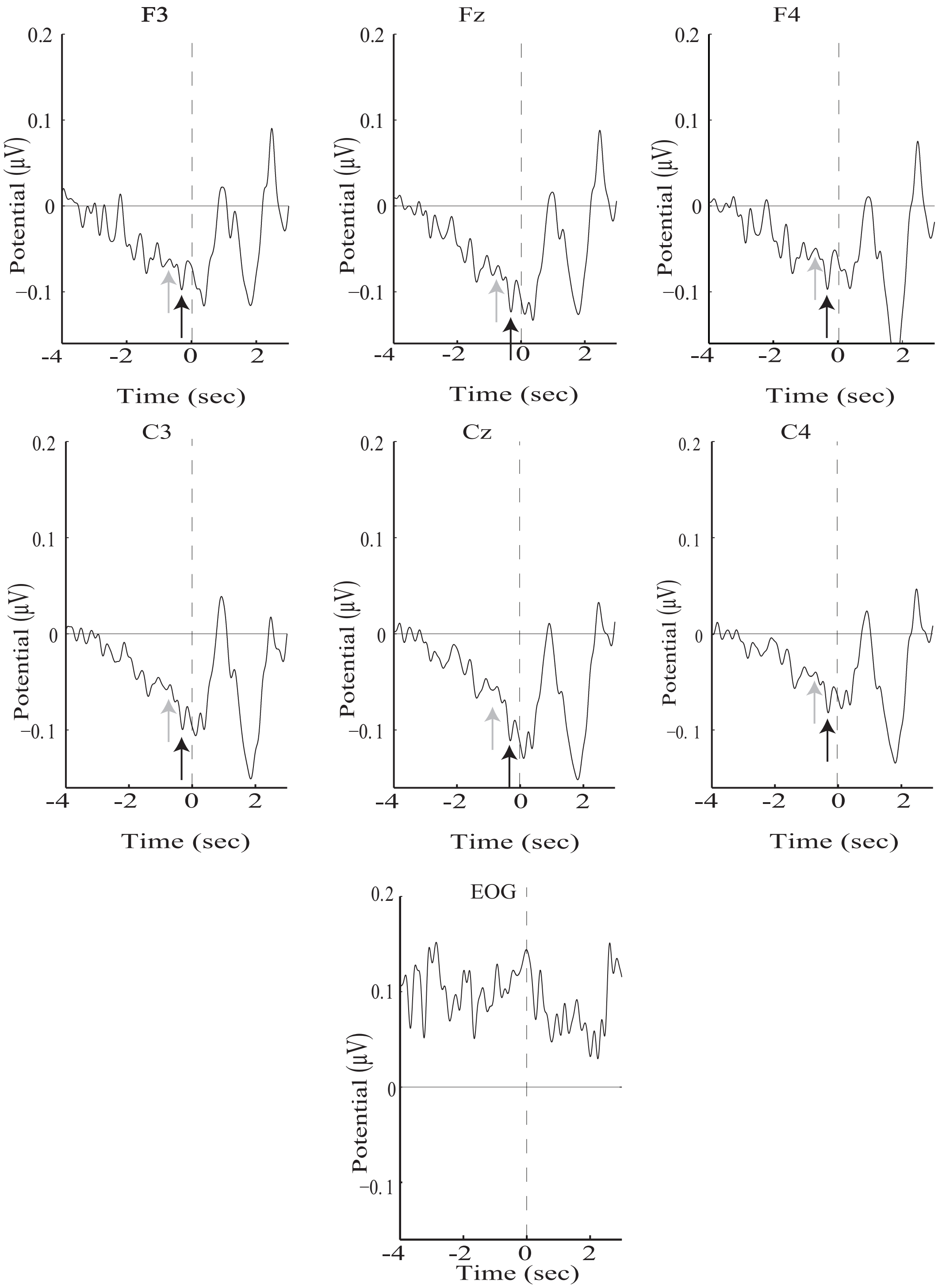

Figure 6-8: The averaged EEG extracted during standing up for all subjects based on Gyro onset. Time 0 indicates the Gyro onset. The gray and black arrows indicate the slope and the negative peak of the BP, respectively.

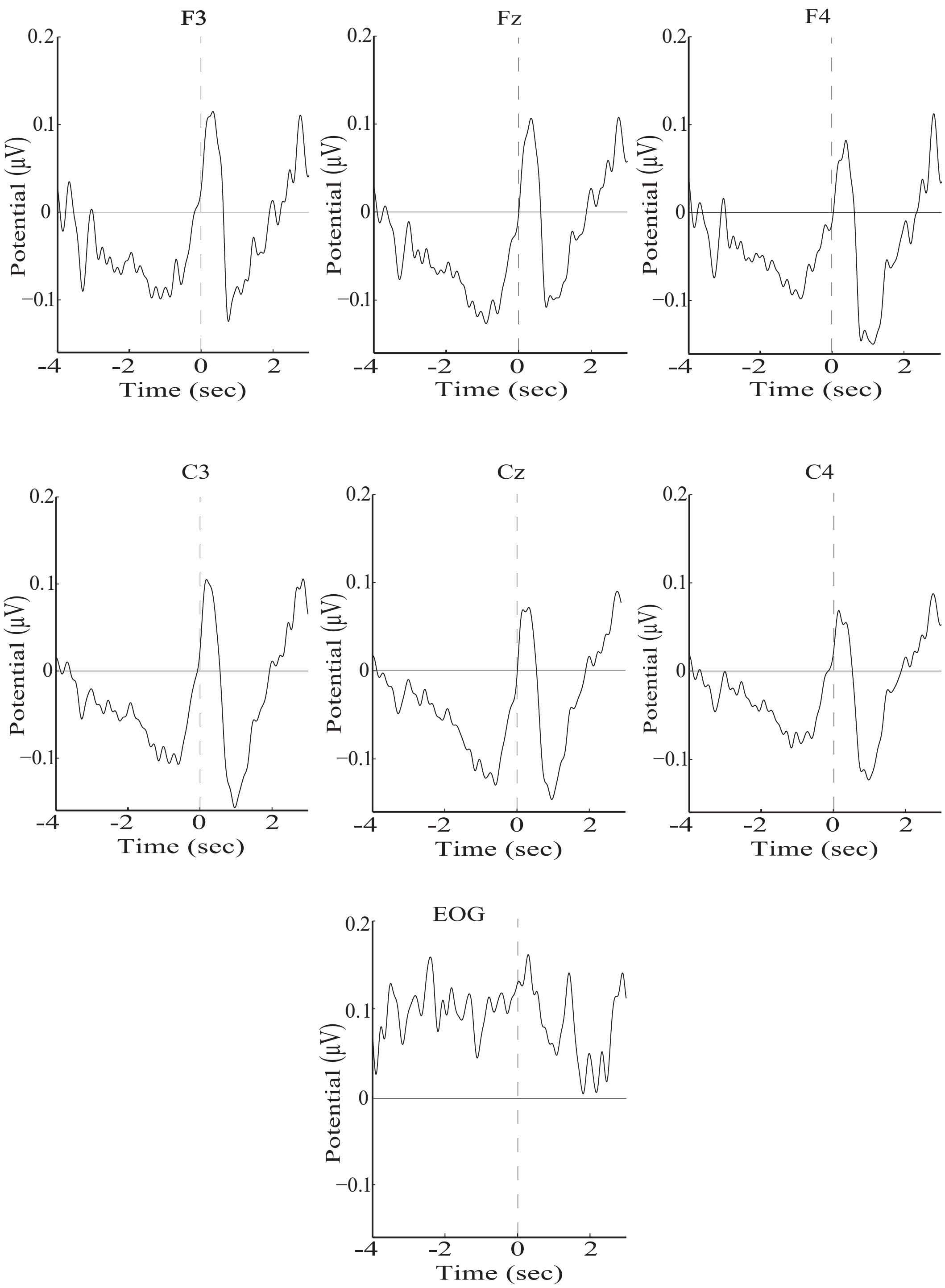

Figure 6-9: The averaged EEG extracted during standing up for all subjects based on the quadriceps EMG onset. Time 0 indicates the EMG onset. A similar tendency is observed to that in (Figure 6-8). The data are shifted to the left on the time axis, and the negative steeper slope starts earlier compared to (Figure 6-8) and reaches the maximum negative peak between -1 and -0.5 seconds. The onset of the upper body movement is much earlier than that of the lower body movement. The gray and black arrows indicate the slope and the negative peak of the BP, respectively.

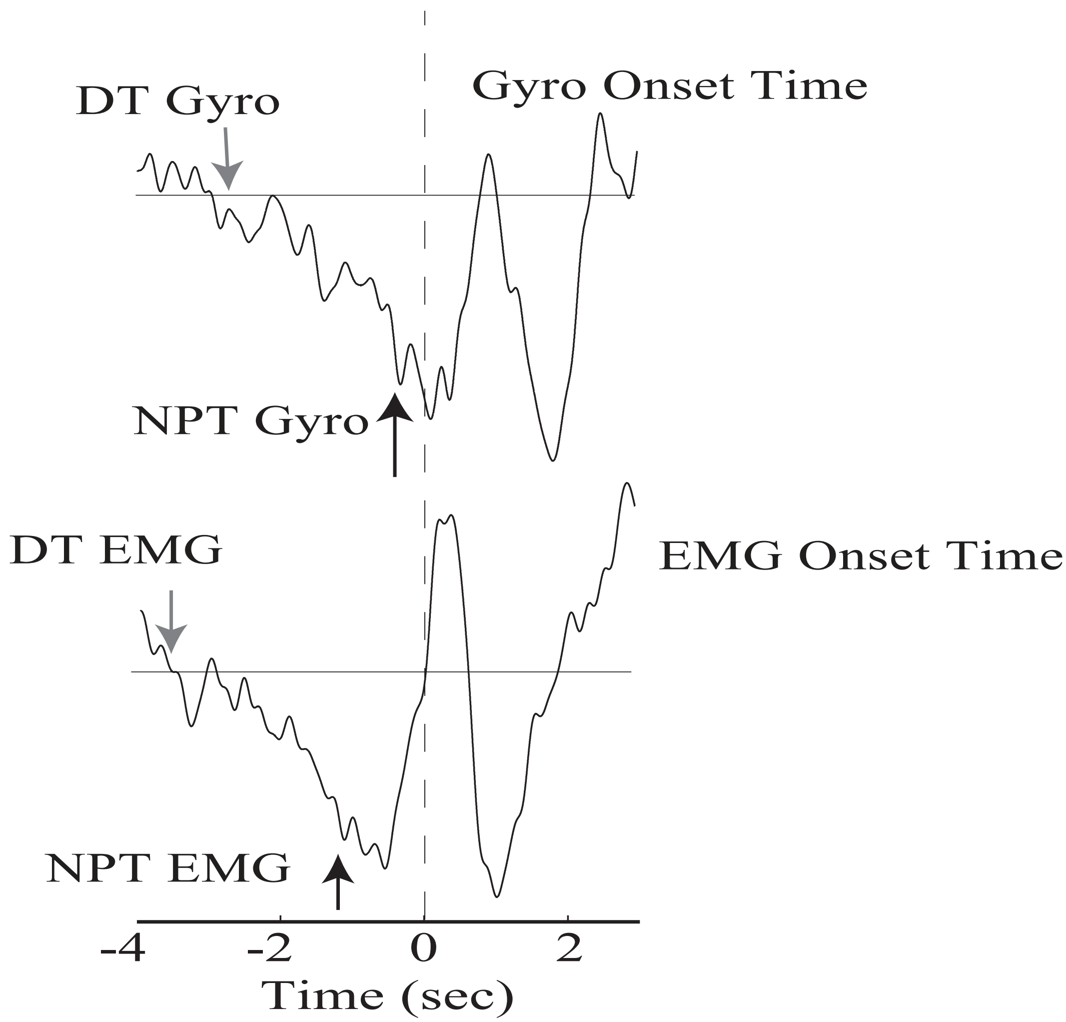

Figure 6-10: The definitions of the schematic representations: (↓) is the start of the decrement time (DT) and (↑) represents the negative peak time (NPT) based on Gyro onset and EMG onset.

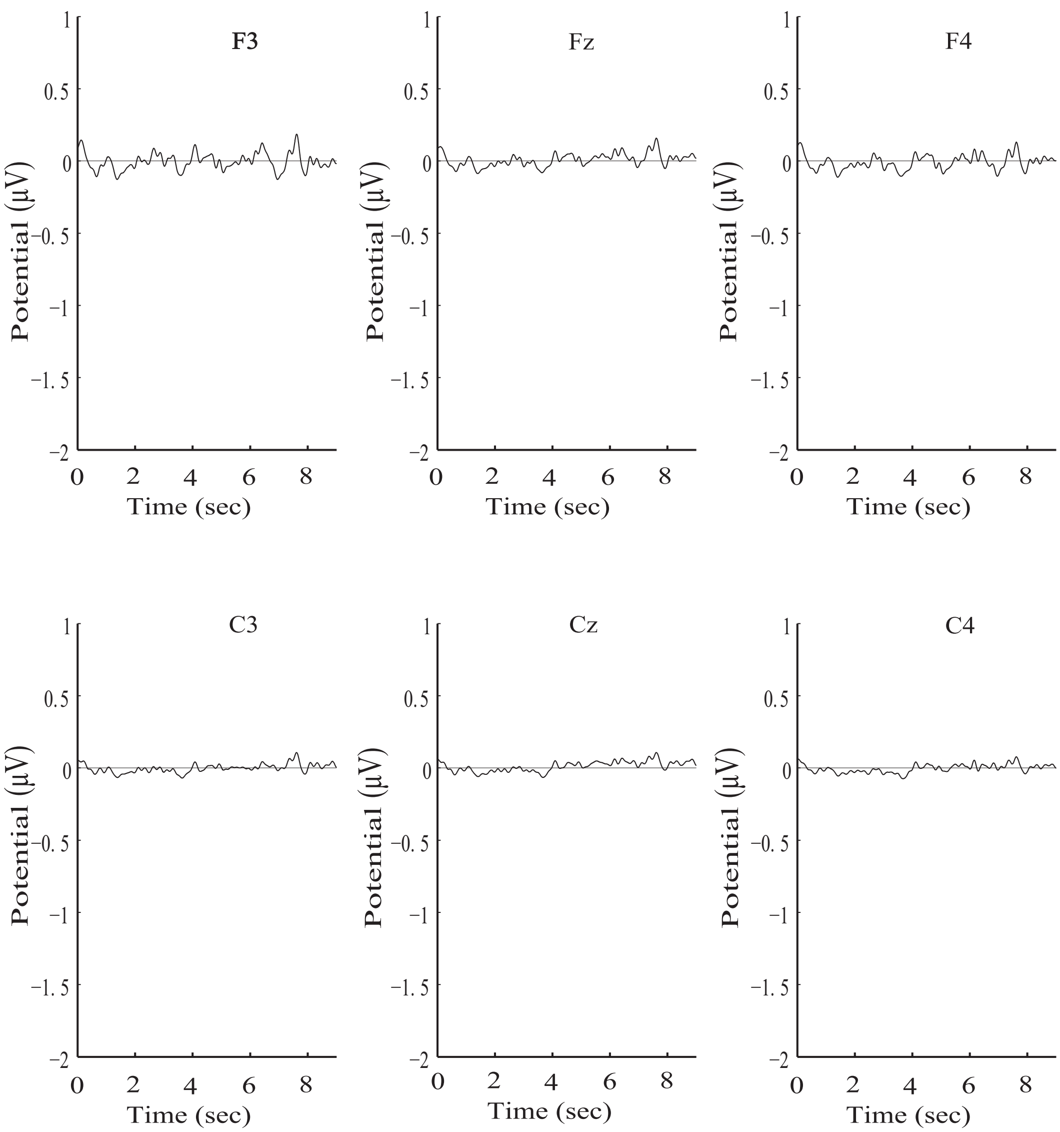

Figure 6-11: The averaged EEG during seating in all trials for all participants. Time zero indicates the onset of the visual fixation cue.

Table 6.1: DT_{gyro}, DT_{EMG}, NPT_{gyro} and NPT_{EMG}, and the time difference between DT_{gyro} and DT_{EMG}, and the time difference between NPT_{gyro} and NPT_{EMG} of the BP based on Gyro and EMG onsets.

	BP BASED ON GYRO ONSET		BP BASED ON EMG ONSET		TIME DIFFERENCE	
BP	DT_{gyro} (sec)	NPT_{gyro}	DT_{EMG} (sec)	NPT_{EMG} (sec)	Δ DT (sec)	Δ NPT (sec)
F3	-2.95 ± .53	-.31 ± .2	-3.84 ± .66	-1.06 ± .56	.89 ± .31	.75 ± .48
FZ	-2.87 ±.82	-.26 ± .19	-3.83 ± .66	-1.09 ± .45	.96 ± .67	.83 ± .37
F4	-2.95 ± .56	-.28 ± .26	-3.84 ± .69	-1.1 ± .41	.89 ± .29	.82 ± .36
C3	-2.92 ± .53	-.26 ± .25	-3.78 ± .65	-1.09 ± .42	.86 ± .27	.83 ± .36
Cz	-2.91 ± .55	-.26 ± .2	-3.77 ± .65	-1.07 ± .45	.86 ± .27	.82 ± .37
C4	-2.94 ± .59	-.23 ± .17	-3.79 ± .69	-1.07 ± .4	.85 ± .28	.84 ± .33

Figure 6-11 shows the grand average of seated EEGs among all participants. The zero indicates the onset time of the fixation cue. Negative and positive deflections are not observed in the averages. The previous studies has showed that the amplitude of BP was correlated with response speed and muscle force [185, 186]. Negative slope was changed according to participants will [187]; the start time and small or large value of negative slope was also depending upon the sequential and simultaneous [188]. Late BP may be related to the execution of the movement [151]. The slope of the BP was calculated between -0.8 and -.001 seconds of the BP based on Gyro and EMG onsets (gray arrows in Figure 6-8 and 6-9).

6.5 Discussion

The motor-related cortical potential is associated with the preparation for rising to stand up. To observe the patterns of the brain activity(mainly BP) is associated with the complex dynamic movement of rising to stand from a seated position in this investigation. The cortical potentials is associated with the voluntary movements of various body segments are known as MRCPs. The potentials is indicated the preparation and execution of controlled voluntary movement [155, 164]. The early and late BPs [151], PMP, MP, and RAP are the components of the potentials. A slow negative-going potential (BP) that one of the MRCPs is started before the preparation for the movement. BP is started 2 seconds before the onset of movement and suddenly increases its slope about 0.4 seconds before movement onset [151]. In past studies, the MRCPs have been based on mouth, finger, hand, and foot movements [150, 151, 152, 160, 156, 159, 158, 161, 162, 163, 164, 167, 168, 169, 170].

BP for the sequence of movement has also been recorded [188, 189]. BP for the sequential movements that includes both the upper and lower body have not yet been studied therefore this chapter included the rise to stand behavior. The whole body is divided into four phases for rise to stand-up behavior [172]. The flexion momentum is used in the first phase to generate the initial momentum for rising. The individual leaves the stool seat and ends at maximal dorsiflexion in the second phase. In the third phase, the body rises to its full upright position. The whole body is stabilized in the last phase. These phases occur automatically without the subject's realization. BP is started between 2 to 3 seconds and steepness in BP increased around 0.8 second before the onset of movement. This is the first study to describe the BP related to the rise to stand voluntary movement using both upper and lower body segments. The initial components and late components with steeper slopes are observed slow negative potential. These components correspond to the early BP and late BP, respectively, which are reported in previous studies [150, 151, 159, 160, 158, 161, 162, 163, 164, 167]. The sequence of the movement for rise to stand determined during the preparatory process (early BP) and for the successful execution of the movement, both the timing and the patterns of activation of all involved muscles need to be well-coordinated. The sequential movement that involved the many muscles forces is directly related to the late BP [153, 190]. The negative slope starts earlier and larger for the sequential movement [188], it also related to participants muscles contraction in the movement [153]. The negative slope is constant because the numbers of muscles involved are the same for the given task. The late BP negative slope is varied from sequential to simple movement, from fast to slow. The negative potential is not observed during seated behavior.

The amplitude of the BP is correlated with response speed and muscle force [190, 185, 186]. The increase in the negative peak value indicates that the larger number of cortical cell is involved in the sequential movement [154, 174]. These results suggest that the observed BP is related to the execution of the rise to stand. BP is generated in several cortical and subcortical structures that are linked with the motor area [159]. It is widely distributed on the scalp above the vertex, and central, prefrontal and parietal areas [151, 156, 158, 168]. It is thought that the potential may be related to the preparation and execution of voluntary movement. Our results indicate that the negative-going BP preceding the rise to stand is similar to the wave-form seen during voluntary movements in previous reports [150, 151, 152, 156, 159, 160, 158, 161, 162, 163, 164, 167, 168].

The negative peak of BP was significantly correlated with the max amplitude of the hamstrings EMG. The max amplitude of the quadriceps is greater than the hamstring EMG. Thus, the BP is correlated with the max amplitude of the hamstrings EMG. The negative slope of BP is correlated with the maximum energy of hamstring EMG. The time difference between quadriceps and hamstring EMG was around .05 second. The peak BP time is not significantly between peak time of max energy of quadriceps and hamstring EMG. The negative steepness determines the activation of muscles and it helps to define the behavior movement.

We found that BP for the rise to stand movement could be induced before the onset of the movement. We propose that it may be used for a stand-up support tool [176, 177]. It may take some time to detect and process the BP and to control the machines. BP can be induced about 3 seconds before the onset of the rise. Using the BP, we could then control the support tool for the person using the device to stand up. Thus, BP can be used as a support tool for standing up. In a previous study, it was argued that elderly persons may require different strategies for standing up than younger people [191]. Thus, in the future, we will study whether we can record BPs from elderly persons such as in the present study.

6.6 Summary

A realistic signal contamination procedure is consider for newly designed the EEG-EOG signal contamination model and proposed the two-stage wavelet shrinkage method with UDWT for quantitative validations to remove the EEGs artifacts. A hundred dataset of open-source clinical intracranial EEGs in each behavioral condition is used for the validation to be the 'true EEG' before the contamination of artificial EOGs. The EEG signal reconstruction is evaluated in the frequency spectrum to justify the quality, by how much the original specific brain-state profile is reproduced in the total manner. Numerical analyses demonstrated that the first stage is pursued abrupt changes with high amplitudes provided by assumed EOGs, and in the second stage the EEG spectrum is clearly reconstructed, which is exceeded the performance of the conventional shrinkage. And suggested that the threshold values are properly set depending on individual amplitudes of multiple signal sources in our proposed method. The present results are focused on actual amplitude-frequency structure in the polygenetic signal and provides the decomposition performance, simultaneously reveals the mixed procedure in the viewpoint of a new standard model for robust validations in the EEG-EOG signal contamination.

Secondly, MCA is applied on the simulated, semi-simulated and real EOG and EEG signal. It demonstrates the EOG and EEG signal decomposition into its morphological component successfully. It seems to be that the EEG signals and artifacts in EEG has represented by different explicit dictionaries. We analyzed the EEG signals involved with the EOG artifacts, which are influenced by task conditions. The DIRAC explicit dictionary was decomposed the EEG signal into spike-like activities, which may be related to transient property of EEG. UDWT explicit dictionary represents slow movement or bumps. DCT, DST and LDCT explicit dictionary represents dominant signal that represent EEGs signals as monomorphic and polymorphic activities. The results are suggested that the effective in removal of artifacts from the raw signal and EOG contains slow and smooth change in time as a main component. In the further analysis, the MCA is required to compare with other competing methods for the EEG and EOG signal decomposition.

The BP for the rise to stand-up movement is induced before the onset of the movement. We proposed that it may be used for a stand-up support tool that process the BP and to control the machines. BP may be induced about 3 seconds before the onset of the rise. Using the BP, we could then control the support tool for the person using the device to stand up. Thus, BP can be used as a support tool for standing up.

Bibliography

[1] Ghada Al-Hudhud. Affective command-based control system integrating brain signals in commands control systems. *Computers in Human Behavior*, 30:535–541, 2014.

[2] JL Sirvent Blasco, Eduardo Iáñez, Andrés Ubeda, and José Maria Azorín. Visual evoked potential-based brain–machine interface applications to assist disabled people. *Expert Systems with Applications*, 39(9):7908–7918, 2012.

[3] Hubert Cecotti. Spelling with non-invasive brain–computer interfaces–current and future trends. *Journal of Physiology-Paris*, 105(1):106–114, 2011.

[4] Ivan S Kotchetkov, Brian Y Hwang, Geoffrey Appelboom, Christopher P Kellner, and E Sander Connolly Jr. Brain-computer interfaces: military, neurosurgical, and ethical perspective. *Neurosurgical focus*, 28(5):E25, 2010.

[5] Louis Mayaud, Marco Congedo, Aurélien Van Laghenhove, D Orlikowski, M Figère, E Azabou, and F Cheliout-Heraut. A comparison of recording modalities of p300 event-related potentials (erp) for brain-computer interface (bci) paradigm. *Neurophysiologie Clinique/Clinical Neurophysiology*, 43(4):217–227, 2013.

[6] WANG Xing-Yu, JIN Jing, Yu Zhang, and WANG Bei. Brain control: human-computer integration control based on brain-computer interface approach. *Acta Automatica Sinica*, 39(3):208–221, 2013.

[7] Bin He. *Neural engineering*, volume 3. Springer Science & Business Media, 2007.

[8] Miguel AL Nicolelis. Actions from thoughts. *Nature*, 409(6818):403–407, 2001.

[9] Mijail D Serruya, Nicholas G Hatsopoulos, Liam Paninski, Matthew R Fellows, and John P Donoghue. Brain-machine interface: Instant neural control of a movement signal. *Nature*, 416(6877):141–142, 2002.

[10] Karsten Keller, Heinz Lauffer, and Mathieu Sinn. Ordinal analysis of eeg time series. *Chaos and Complexity Letters*, 2:247–258, 2007.

[11] Claudia Lainscsek, Manuel E Hernandez, Jonathan Weyhenmeyer, Terrence J Sejnowski, and Howard Poizner. Non-linear dynamical analysis of eeg time series distinguishes patients with parkinsons disease from healthy individuals. *Frontiers in neurology*, 4(200), 2013.

[12] K Lehnertz. Non-linear time series analysis of intracranial eeg recordings in patients with epilepsyan overview. *International Journal of Psychophysiology*, 34(1):45–52, 1999.

[13] Davide V Moretti, Claudio Babiloni, Giuliano Binetti, Emanuele Cassetta, Gloria Dal Forno, Florinda Ferreric, Raffaele Ferri, Bartolo Lanuzza, Carlo Miniussi, Flavio Nobili, et al. Individual analysis of eeg frequency and band power in mild alzheimer's disease. *Clinical Neurophysiology*, 115(2):299–308, 2004.

[14] Michael W Schwartz, Stephen C Woods, Daniel Porte, Randy J Seeley, and Denis G Baskin. Central nervous system control of food intake. *Nature*, 404(6778):661–671, 2000.

[15] Jonathan D Power, Damien A Fair, Bradley L Schlaggar, and Steven E Petersen. The development of human functional brain networks. *Neuron*, 67(5):735–748, 2010.

[16] David Meunier, Sophie Achard, Alexa Morcom, and Ed Bullmore. Age-related changes in modular organization of human brain functional networks. *Neuroimage*, 44(3):715–723, 2009.

[17] Gert Pfurtscheller, C Neuper, C Guger, WAHW Harkam, Herbert Ramoser, Alois Schlogl, BAOB Obermaier, MAPM Pregenzer, et al. Current trends in graz brain-computer interface (bci) research. *IEEE Transactions on Rehabilitation Engineering*, 8(2):216–219, 2000.

[18] Patrick Haggard. Human volition: towards a neuroscience of will. *Nature Reviews Neuroscience*, 9(12):934–946, 2008.

[19] Eugenijus Kaniusas and Eugenijus Kaniusas. Fundamentals of biosignals. *Biomedical Signals and Sensors I: Linking Physiological Phenomena and Biosignals*, pages 1–26, 2012.

[20] D. Purves, D. Fitzpatrick, L.C. Katz, A.S. Lamantia, J.O. McNamara, S.M. Williams, and G.J. Augustine. *Neuroscience*. Sinauer Associates, 2001.

[21] L. Squire, F.E. Bloom, N.C. Spitzer, L.R. Squire, D. Berg, S. du Lac, and A. Ghosh. *Fundamental Neuroscience*. Fundamental Neuroscience Series. Elsevier Science, 2008.

[22] Gerald Hahn, Alejandro F Bujan, Yves Frégnac, Ad Aertsen, and Arvind Kumar. Communication through resonance in spiking neuronal networks. *PLoS Comput Biol*, 10(8):e1003811, 2014.

[23] Jonathan Cannon, Michelle M McCarthy, Shane Lee, Jung Lee, Christoph Börgers, Miles A Whittington, and Nancy Kopell. Neurosystems: brain rhythms and cognitive processing. *European Journal of Neuroscience*, 39(5):705–719, 2014.

[24] Michel Le Van Quyen and Anatol Bragin. Analysis of dynamic brain oscillations: methodological advances. *Trends in neurosciences*, 30(7):365–373, 2007.

[25] Fernando Lopes da Silva. Eeg: origin and measurement. In *EEG-fMRI*, pages 19–38. Springer, 2009.

[26] Fernando Lopes da Silva. Eeg and meg: relevance to neuroscience. *Neuron*, 80(5):1112–1128, 2013.

[27] Zhongming Liu, Lei Ding, and Bin He. Integration of eeg/meg with mri and fmri in functional neuroimaging. *IEEE engineering in medicine and biology magazine: the quarterly magazine of the Engineering in Medicine & Biology Society*, 25(4):46, 2006.

[28] Philip J Allen, Oliver Josephs, and Robert Turner. A method for removing imaging artifact from continuous eeg recorded during functional mri. *Neuroimage*, 12(2):230–239, 2000.

[29] David Cohen and B Neil Cuffin. Eeg versus meg localization accuracy: theory and experiment. *Brain topography*, 4(2):95–103, 1991.

[30] HJ Wieringa, MJ Peters, and FH Lopes da Silva. The estimation of a realistic localization of dipole layers within the brain based on functional (eeg, meg) and structural (mri) data: a preliminary note. *Brain topography*, 5(4):327–330, 1993.

[31] FH Lopes da Silva, HJ Wieringa, and MJ Peters. Source localization of eeg versus meg: empirical comparison using visually evoked responses and theoretical considerations. *Brain topography*, 4(2):133–142, 1991.

[32] F Amzica and M Steriade. Electrophysiological correlates of sleep delta waves. *Electroencephalography and clinical neurophysiology*, 107(2):69–83, 1998.

[33] Thien Thanh Dang-Vu, Martin Desseilles, Steven Laureys, Christian Degueldre, Fabien Perrin, Christophe Phillips, Pierre Maquet, and Philippe Peigneux. Cerebral correlates of delta waves during non-rem sleep revisited. *Neuroimage*, 28(1):14–21, 2005.

[34] M Steriade. Grouping of brain rhythms in corticothalamic systems. *Neuroscience*, 137(4):1087–1106, 2006.

[35] Dennis JLG Schutter and Jack van Honk. An electrophysiological link between the cerebellum, cognition and emotion: frontal theta eeg activity to single-pulse cerebellar tms. *Neuroimage*, 33(4):1227–1231, 2006.

[36] René Scheeringa, Karl Magnus Petersson, Robert Oostenveld, David G Norris, Peter Hagoort, and Marcel CM Bastiaansen. Trial-by-trial coupling between eeg and bold identifies networks related to alpha and theta eeg power increases during working memory maintenance. *Neuroimage*, 44(3):1224–1238, 2009.

[37] Phan Luu, Don M Tucker, and Scott Makeig. Frontal midline theta and the error-related negativity: neurophysiological mechanisms of action regulation. *Clinical Neurophysiology*, 115(8):1821–1835, 2004.

[38] José L Cantero, Mercedes Atienza, Rosa M Salas, and Carlos M Gómez. Alpha eeg coherence in different brain states: an electrophysiological index of the arousal level in human subjects. *Neuroscience Letters*, 271(3):167–170, 1999.

[39] Jose L Cantero, Mercedes Atienza, and Rosa M Salas. Human alpha oscillations in wakefulness, drowsiness period, and rem sleep: different electroencephalographic phenomena within the alpha band. *Neurophysiologie Clinique/Clinical Neurophysiology*, 32(1):54–71, 2002.

[40] Chiara Spironelli and Alessandro Angrilli. Developmental aspects of language lateralization in delta, theta, alpha and beta eeg bands. *Biological psychology*, 85(2):258–267, 2010.

[41] Michael L Perlis, Helli Merica, Michael T Smith, and Donna E Giles. Beta eeg activity and insomnia. *Sleep medicine reviews*, 5(5):365–376, 2001.

[42] SP Fitzgibbon, KJ Pope, Lorraine Mackenzie, CR Clark, and JO Willoughby. Cognitive tasks augment gamma eeg power. *Clinical Neurophysiology*, 115(8):1802–1809, 2004.

[43] Selim R Benbadis. Eeg artifacts.

[44] Pekka Tallgren, Sampsa Vanhatalo, Kai Kaila, and Juha Voipio. Evaluation of commercially available electrodes and gels for recording of slow eeg potentials. *Clinical Neurophysiology*, 116(4):799–806, 2005.

[45] Jorma O Ollikainen, Marko Vauhkonen, Pasi A Karjalainen, and Jari P Kaipio. Effects of electrode properties on eeg measurements and a related inverse problem. *Medical engineering & physics*, 22(8):535–545, 2000.

[46] Thomas C Ferree, Phan Luu, Gerald S Russell, and Don M Tucker. Scalp electrode impedance, infection risk, and eeg data quality. *Clinical Neurophysiology*, 112(3):536–544, 2001.

[47] Wesley C Clapp, Michael T Rubens, and Adam Gazzaley. Mechanisms of working memory disruption by external interference. *Cerebral Cortex*, page bhp150, 2009.

[48] Anne S Berry, Theodore P Zanto, Aaron M Rutman, Wesley C Clapp, and Adam Gazzaley. Practice-related improvement in working memory is modulated by changes in processing external interference. *Journal of neurophysiology*, 102(3):1779–1789, 2009.

[49] G Srivastava, S Crottaz-Herbette, KM Lau, GH Glover, and V Menon. Ica-based procedures for removing ballistocardiogram artifacts from eeg data acquired in the mri scanner. *Neuroimage*, 24(1):50–60, 2005.

[50] Irina I Goncharova, Dennis J McFarland, Theresa M Vaughan, and Jonathan R Wolpaw. Emg contamination of eeg: spectral and topographical characteristics. *Clinical neurophysiology*, 114(9):1580–1593, 2003.

[51] Mehrdad Fatourechi, Ali Bashashati, Rabab K Ward, and Gary E Birch. Emg and eog artifacts in brain computer interface systems: A survey. *Clinical neurophysiology*, 118(3):480–494, 2007.

[52] Patrick Berg and Michael Scherg. A multiple source approach to the correction of eye artifacts. *Electroencephalography and clinical neurophysiology*, 90(3):229–241, 1994.

[53] Patrick Berg and Michael Scherg. Dipole models of eye movements and blinks. *Electroencephalography and clinical Neurophysiology*, 79(1):36–44, 1991.

[54] RJ Croft and RJ Barry. Removal of ocular artifact from the eeg: a review. *Neurophysiologie Clinique/Clinical Neurophysiology*, 30(1):5–19, 2000.

[55] Otavio G Lins, Terence W Picton, Patrick Berg, and Michael Scherg. Ocular artifacts in eeg and event-related potentials i: Scalp topography. *Brain topography*, 6(1):51–63, 1993.

[56] Markus Junghöfer, Thomas Elbert, Don M Tucker, and Brigitte Rockstroh. Statistical control of artifacts in dense array eeg/meg studies. *Psychophysiology*, 37(4):523–532, 2000.

[57] James Pardey, Stephen Roberts, and Lionel Tarassenko. A review of parametric modelling techniques for eeg analysis. *Medical engineering & physics*, 18(1):2–11, 1996.

[58] J-L Starck, Y Moudden, J Bobin, M Elad, and DL Donoho. Morphological component analysis. In *Optics & Photonics 2005*, pages 59140Q–59140Q. International Society for Optics and Photonics, 2005.

[59] Elaheh Imani, Hamid-Reza Pourreza, and Touka Banaee. Fully automated diabetic retinopathy screening using morphological component analysis. *Computerized Medical Imaging and Graphics*, 43:78–88, 2015.

[60] Elaheh Imani, Malihe Javidi, and Hamid-Reza Pourreza. Improvement of retinal blood vessel detection using morphological component analysis. *Computer methods and programs in biomedicine*, 118(3):263–279, 2015.

[61] Jean-Luc Starck, Michael Elad, and David Donoho. Redundant multiscale transforms and their application for morphological component separation. *Advances in Imaging and Electron Physics*, 132:287–348, 2004.

[62] Jérôme Bobin, Jean-Luc Starck, Jalal Fadili, and Yassir Moudden. Sparsity and morphological diversity in blind source separation. *IEEE Transactions on Image Processing*, 16(11):2662–2674, 2007.

[63] Jose Antonio Urigüen and Begoña Garcia-Zapirain. Eeg artifact removalstate-of-the-art and guidelines. *Journal of neural engineering*, 12(3):031001, 2015.

[64] Chella Kamarajan and Bernice Porjesz. Advances in electrophysiological research. *Alcohol research: current reviews*, 37(1):53, 2015.

[65] Luis Fernando Nicolas-Alonso and Jaime Gomez-Gil. Brain computer interfaces, a review. *Sensors*, 12(2):1211–1279, 2012.

[66] PK Sadasivan and D Narayana Dutt. Svd based technique for noise reduction in electroencephalographic signals. *Signal Processing*, 55(2):179–189, 1996.

[67] Ricardo Nuno Vigário. Extraction of ocular artefacts from eeg using independent component analysis. *Electroencephalography and clinical neurophysiology*, 103(3):395–404, 1997.

[68] Carrie A Joyce, Irina F Gorodnitsky, and Marta Kutas. Automatic removal of eye movement and blink artifacts from eeg data using blind component separation. *Psychophysiology*, 41(2):313–325, 2004.

[69] Anestis Antoniadis. Wavelets in statistics: a review. *Journal of the Italian Statistical Society*, 6(2):97–130, 1997.

[70] Amjed S Al-Fahoum and Ausilah A Al-Fraihat. Methods of eeg signal features extraction using linear analysis in frequency and time-frequency domains. *ISRN neuroscience*, 2014, 2014.

[71] Michael Plöchl, José Pablo Ossandón, and Peter König. Combining eeg and eye tracking: identification, characterization, and correction of eye movement artifacts in electroencephalographic data. *Frontiers in human neuroscience*, 6:278, 2012.

[72] Weidong Zhou and Jean Gotman. Automatic removal of eye movement artifacts from the eeg using ica and the dipole model. *Progress in Natural Science*, 19(9):1165–1170, 2009.

[73] Reza Sameni and Cédric Gouy-Pailler. An iterative subspace denoising algorithm for removing electroencephalogram ocular artifacts. *Journal of neuroscience methods*, 225:97–105, 2014.

[74] Ping He, G Wilson, and C Russell. Removal of ocular artifacts from electroencephalogram by adaptive filtering. *Medical and biological engineering and computing*, 42(3):407–412, 2004.

[75] Hong Zeng, Aiguo Song, Ruqiang Yan, and Hongyun Qin. Eog artifact correction from eeg recording using stationary subspace analysis and empirical mode decomposition. *Sensors*, 13(11):14839–14859, 2013.

[76] Patrick Flandrin, Gabriel Rilling, and Paulo Goncalves. Empirical mode decomposition as a filter bank. *IEEE signal processing letters*, 11(2):112–114, 2004.

[77] Md Khademul Islam Molla, Rabiul Islam, Toshihisa Tanaka, Tomasz M Rutkowski, et al. Artifact suppression from eeg signals using data adaptive time domain filtering. *Neurocomputing*, 97:297–308, 2012.

[78] Fay S. Tyner, John Russell Knott, and W. Brem Mayer Jr. *Fundamentals of EEG Technology: Vol. 1: Basic Concepts and Methods.* Raven Press: New York, 1983.

[79] S Noachtar, C Binnie, J Ebersole, F Mauguiere, A Sakamoto, and B Westmoreland. A glossary of terms most commonly used by clinical electroencephalog-

raphers and proposal for the report form for the eeg findings. the international federation of clinical neurophysiology. *Electroencephalography and clinical neurophysiology. Supplement*, 52:21, 1999.

[80] SJM Smith. Eeg in neurological conditions other than epilepsy: when does it help, what does it add? *Journal of Neurology, Neurosurgery & Psychiatry*, 76(suppl 2):ii8–ii12, 2005.

[81] Ling Zou, Hui Pu, Qi Sun, and Wenjin Su. Analysis of attention deficit hyperactivity disorder and control participants in eeg using ica and pca. In *International Symposium on Neural Networks*, pages 403–410. Springer, 2012.

[82] Rong-Chi Chen, Song-Yen Tsai, Yang-Chyuan Chang, and Horng-Huei Liou. Seizure frequency affects event-related potentials (p300) in epilepsy. *Journal of clinical neuroscience*, 8(5):442–446, 2001.

[83] Guohun Zhu, Yan Li, and Peng Paul Wen. Epileptic seizure detection in eegs signals using a fast weighted horizontal visibility algorithm. *Computer methods and programs in biomedicine*, 115(2):64–75, 2014.

[84] Sandra K Loo and Scott Makeig. Clinical utility of eeg in attention-deficit/hyperactivity disorder: a research update. *Neurotherapeutics*, 9(3):569–587, 2012.

[85] Wu Ting, Yan Guo-zheng, Yang Bang-hua, and Sun Hong. Eeg feature extraction based on wavelet packet decomposition for brain computer interface. *Measurement*, 41(6):618–625, 2008.

[86] Andre Luvizotto, César Rennó-Costa, and Paul FMJ Verschure. A wavelet-based neural model to optimize and read out a temporal population code. *Frontiers in computational neuroscience*, 6, 2012.

[87] U Rajendra Acharya, S Vinitha Sree, Peng Chuan Alvin Ang, Ratna Yanti, and Jasjit S Suri. Application of non-linear and wavelet based features for the

automated identification of epileptic eeg signals. *International journal of neural systems*, 22(02):1250002, 2012.

[88] Gyanendra K Verma and Uma Shanker Tiwary. Multimodal fusion framework: A multiresolution approach for emotion classification and recognition from physiological signals. *NeuroImage*, 102:162–172, 2014.

[89] Oliver Faust, U Rajendra Acharya, Hojjat Adeli, and Amir Adeli. Wavelet-based eeg processing for computer-aided seizure detection and epilepsy diagnosis. *Seizure*, 26:56–64, 2015.

[90] Markus Lang, Haitao Guo, Jan E Odegard, C Sidney Burrus, and Raymond O Wells. Noise reduction using an undecimated discrete wavelet transform. *IEEE Signal Processing Letters*, 3(1):10–12, 1996.

[91] J-L Starck, Jalal Fadili, and Fionn Murtagh. The undecimated wavelet decomposition and its reconstruction. *Image Processing, IEEE Transactions on*, 16(2):297–309, 2007.

[92] T Bernas, EK Asem, JP Robinson, and B Rajwa. Application of wavelet denoising to improve compression efficiency while preserving integrity of digital micrographs. *Journal of microscopy*, 231(1):81–96, 2008.

[93] Aglika Gyaourova, Chandrika Kamath, and Imola K Fodor. Undecimated wavelet transforms for image de-noising. *Report, Lawrence Livermore National Lab., CA*, 18, 2002.

[94] James E Fowler. The redundant discrete wavelet transform and additive noise. *Signal Processing Letters, IEEE*, 12(9):629–632, 2005.

[95] David L Donoho. Wavelet shrinkage and wvd: A 10-minute tour. In *Presented on the International Conference on Wavelets and Applications, Tolouse, France*, 1992.

[96] David L Donoho and Jain M Johnstone. Ideal spatial adaptation by wavelet shrinkage. *Biometrika*, 81(3):425–455, 1994.

[97] David L Donoho, Iain M Johnstone, Gérard Kerkyacharian, and Dominique Picard. Wavelet shrinkage: asymptopia? *Journal of the Royal Statistical Society. Series B (Methodological)*, pages 301–369, 1995.

[98] David L Donoho and Iain M Johnstone. Adapting to unknown smoothness via wavelet shrinkage. *Journal of the american statistical association*, 90(432):1200–1224, 1995.

[99] David L Donoho. De-noising by soft-thresholding. *IEEE transactions on information theory*, 41(3):613–627, 1995.

[100] David L Donoho, Iain M Johnstone, et al. Minimax estimation via wavelet shrinkage. *The annals of Statistics*, 26(3):879–921, 1998.

[101] Albert Cohen, Ingrid Daubechies, Björn Jawerth, and Pierre Vial. Multiresolution analysis, wavelets and fast algorithms on an interval. *Comptes rendus de l'Académie des sciences. Série 1, Mathématique*, 316(5):417–421, 1993.

[102] Ronald R Coifman and David L Donoho. *Translation-invariant de-noising*. Springer, 1995.

[103] Sven Erik G Nilsson and Björn E Andersson. Corneal dc recordings of slow ocular potential changes such as the erg c-wave and the light peak in clinical work. *Documenta ophthalmologica*, 68(3-4):313–325, 1988.

[104] Terence W Picton, Patricia van Roon, Maria L Armilio, Patrick Berg, Nicole Ille, and Michael Scherg. The correction of ocular artifacts: a topographic perspective. *Clinical Neurophysiology*, 111(1):53–65, 2000.

[105] Steven J Luck. *An introduction to the event-related potential technique*. MIT press, 2014.

[106] Alon S Keren, Shlomit Yuval-Greenberg, and Leon Y Deouell. Saccadic spike potentials in gamma-band eeg: characterization, detection and suppression. *Neuroimage*, 49(3):2248–2263, 2010.

[107] Garrick L Wallstrom, Robert E Kass, Anita Miller, Jeffrey F Cohn, and Nathan A Fox. Automatic correction of ocular artifacts in the eeg: a comparison of regression-based and component-based methods. *International journal of psychophysiology*, 53(2):105–119, 2004.

[108] Sangita Dandekar, Claudio Privitera, Thom Carney, and Stanley A Klein. Neural saccadic response estimation during natural viewing. *Journal of neurophysiology*, 107(6):1776–1790, 2012.

[109] Olivier David, James M Kilner, and Karl J Friston. Mechanisms of evoked and induced responses in meg/eeg. *Neuroimage*, 31(4):1580–1591, 2006.

[110] Damien Debatisse, Etienne Pralong, Amir R Dehdashti, and Luca Regli. Simultaneous multilobar electrocorticography (mecog) and scalp electroencephalography (scalp eeg) during intracranial vascular surgery: a new approach in neuromonitoring. *Clinical neurophysiology*, 116(12):2734–2740, 2005.

[111] Amit Ray, James X Tao, Susan M Hawes-Ebersole, and John S Ebersole. Localizing value of scalp eeg spikes: a simultaneous scalp and intracranial study. *Clinical neurophysiology*, 118(1):69–79, 2007.

[112] Tonio Ball, Markus Kern, Isabella Mutschler, Ad Aertsen, and Andreas Schulze-Bonhage. Signal quality of simultaneously recorded invasive and non-invasive eeg. *Neuroimage*, 46(3):708–716, 2009.

[113] Madoka Yamazaki, Don M Tucker, Ayataka Fujimoto, Tomohiro Yamazoe, Tohru Okanishi, Takuya Yokota, Hideo Enoki, and Takamichi Yamamoto. Comparison of dense array eeg with simultaneous intracranial eeg for interictal spike detection and localization. *Epilepsy research*, 98(2):166–173, 2012.

[114] Yahya Aghakhani, Craig A Beers, Daniel J Pittman, Ismael Gaxiola-Valdez, Bradley G Goodyear, and Paolo Federico. Co-localization between the bold response and epileptiform discharges recorded by simultaneous intracranial eeg-fmri at 3 t. *NeuroImage: Clinical*, 7:755–763, 2015.

[115] Guangyi Ai, Naoyuki Sato, Balbir Singh, and Hiroaki Wagatsuma. Direction and viewing area-sensitive influence of eog artifacts revealed in the eeg topographic pattern analysis. *Cognitive Neurodynamics*, pages 1–14, 2016.

[116] Nicole M Long, John F Burke, and Michael J Kahana. Subsequent memory effect in intracranial and scalp eeg. *Neuroimage*, 84:488–494, 2014.

[117] V Naga Prudhvi Raj and Tad Venkateswarlu. Denoising of medical images using undecimated wavelet transform. In *Recent Advances in Intelligent Computational Systems (RAICS), 2011 IEEE*, pages 483–488. IEEE, 2011.

[118] Md Mamun, Mahmoud Al-Kadi, and Mohd Marufuzzaman. Effectiveness of wavelet denoising on electroencephalogram signals. *Journal of applied research and technology*, 11(1):156–160, 2013.

[119] Geeta Kaushik, HP Sinha, and Lillie Dewan. Biomedical signals analysis by dwt signal denoising with neural networks. *Journal of Theoretical and Applied Information Technology*, 62(1), 2014.

[120] M Balamareeswaran and D Ebenezer. Denoising of eeg signals using discrete wavelet transform based scalar quantization. *Biomedical and Pharmacology Journal*, 8(1):399–406, 2015.

[121] Saleha Khatun, Ruhi Mahajan, and Bashir I Morshed. Comparative study of wavelet-based unsupervised ocular artifact removal techniques for single-channel eeg data. *IEEE Journal of Translational Engineering in Health and Medicine*, 4:1–8, 2016.

[122] Ralph G Andrzejak, Klaus Lehnertz, Florian Mormann, Christoph Rieke, Peter David, and Christian E Elger. Indications of nonlinear deterministic and finite-

dimensional structures in time series of brain electrical activity: Dependence on recording region and brain state. *Physical Review E*, 64(6):061907, 2001.

[123] Department of Epileptology at the University Hospital of Bonn. Eeg time series download, http://epileptologie-bonn.de/cms/. `http://epileptologie-bonn.de/cms/front_content.php?idcat=193`.

[124] John P Donoghue, Jerome N Sanes, Nicholas G Hatsopoulos, and Gyöngyi Gaál. Neural discharge and local field potential oscillations in primate motor cortex during voluntary movements. *Journal of neurophysiology*, 79(1):159–173, 1998.

[125] M Breakspear and JR Terry. Detection and description of non-linear interdependence in normal multichannel human eeg data. *Clinical neurophysiology*, 113(5):735–753, 2002.

[126] Rajendra Acharya, Oliver Faust, N Kannathal, TjiLeng Chua, and Swamy Laxminarayan. Non-linear analysis of eeg signals at various sleep stages. *Computer methods and programs in biomedicine*, 80(1):37–45, 2005.

[127] LI Aftanas and SA Golocheikine. Non-linear dynamic complexity of the human eeg during meditation. *Neuroscience letters*, 330(2):143–146, 2002.

[128] M Jalal Fadili, Jean-Luc Starck, Jérôme Bobin, and Yassir Moudden. Image decomposition and separation using sparse representations: an overview. *Proceedings of the IEEE*, 98(6):983–994, 2010.

[129] Katarzyna J Blinowska and Piotr J Durka. Unbiased high resolution method of eeg analysis in time-frequency space. *Acta Neurobiologiae Experimentalis*, 61(3):157–174, 2001.

[130] Michael Zibulevsky and Barak A Pearlmutter. Blind source separation by sparse decomposition in a signal dictionary. *Neural computation*, 13(4):863–882, 2001.

[131] Nazareth P Castellanos and Valeri A Makarov. Recovering eeg brain signals: artifact suppression with wavelet enhanced independent component analysis. *Journal of neuroscience methods*, 158(2):300–312, 2006.

[132] Jidong Hou, Kyle Morgan, Don M Tucker, Amy Konyn, Catherine Poulsen, Yasuhiro Tanaka, Erik W Anderson, and Phan Luu. An improved artifacts removal method for high dimensional eeg. *Journal of neuroscience methods*, 268:31–42, 2016.

[133] SM Gordon, V Lawhern, AD Passaro, and K McDowell. Informed decomposition of electroencephalographic data. *Journal of neuroscience methods*, 256:41–55, 2015.

[134] Daniel Studer, Ulrich Hoffmann, and Thomas Koenig. From eeg dependency multichannel matching pursuit to sparse topographic eeg decomposition. *Journal of neuroscience methods*, 153(2):261–275, 2006.

[135] Piotr J Franaszczuk, Gregory K Bergey, Piotr J Durka, and Howard M Eisenberg. Time–frequency analysis using the matching pursuit algorithm applied to seizures originating from the mesial temporal lobe. *Electroencephalography and clinical neurophysiology*, 106(6):513–521, 1998.

[136] Piotr J Durka, Artur Matysiak, Eduardo Martínez Montes, Pedro Valdés Sosa, and Katarzyna J Blinowska. Multichannel matching pursuit and eeg inverse solutions. *Journal of neuroscience methods*, 148(1):49–59, 2005.

[137] Piotr J Durka, Dobieslaw Ircha, and Katarzyna J Blinowska. Stochastic time-frequency dictionaries for matching pursuit. *IEEE Transactions on Signal Processing*, 49(3):507–510, 2001.

[138] Xinyi Yong, Rabab K Ward, and Gary E Birch. Generalized morphological component analysis for eeg source separation and artifact removal. In *2009 4th International IEEE/EMBS Conference on Neural Engineering*, pages 343–346. IEEE, 2009.

[139] Balbir Singh, Guangyi Ai, and Hiroaki Wagatsuma. An electrooculography analysis in the time-frequency domain using morphological component analysis toward the development of mobile bci systems. In *International Conference*

on Universal Access in Human-Computer Interaction, pages 528–537. Springer, 2015.

[140] Scott Shaobing Chen, David L Donoho, and Michael A Saunders. Atomic decomposition by basis pursuit. *SIAM review*, 43(1):129–159, 2001.

[141] David L Donoho and Xiaoming Huo. Uncertainty principles and ideal atomic decomposition. *IEEE Transactions on Information Theory*, 47(7):2845–2862, 2001.

[142] Fumikazu Miwakeichi, Eduardo Martınez-Montes, Pedro A Valdés-Sosa, Nobuaki Nishiyama, Hiroaki Mizuhara, and Yoko Yamaguchi. Decomposing eeg data into space–time–frequency components using parallel factor analysis. *NeuroImage*, 22(3):1035–1045, 2004.

[143] KJ Friston, CD Frith, PF Liddle, and RSJ Frackowiak. Functional connectivity: the principal-component analysis of large (pet) data sets. *Journal of Cerebral Blood Flow & Metabolism*, 13(1):5–14, 1993.

[144] Scott Makeig, Tzyy-Ping Jung, Anthony J Bell, Dara Ghahremani, and Terrence J Sejnowski. Blind separation of auditory event-related brain responses into independent components. *Proceedings of the National Academy of Sciences*, 94(20):10979–10984, 1997.

[145] Biomedical signal. Website. `www.medicine.mcgill.ca/physio/vlab/biomed_signals/eeg_n.htm`.

[146] Ira J Rampil. A primer for eeg signal processing in anesthesia. *The Journal of the American Society of Anesthesiologists*, 89(4):980–1002, 1998.

[147] S Sardy, A Bruce, and P Tseng. Block coordinate relaxation methods for nonparametric signal denoising with wavelet dictionaries. Technical report, Citeseer, 1998.

[148] Markus Püschel and José MF Moura. The algebraic approach to the discrete cosine and sine transforms and their fast algorithms. *SIAM Journal on Computing*, 32(5):1280–1316, 2003.

[149] Xuancheng Shao and Steven G Johnson. Type-iv dct, dst, and mdct algorithms with reduced numbers of arithmetic operations. *Signal Processing*, 88(6):1313–1326, 2008.

[150] CHM Brunia and WEJ Van den Bosch. Movement-related slow potentials. i. a contrast between finger and foot movements in right-handed subjects. *Electroencephalography and clinical neurophysiology*, 57(6):515–527, 1984.

[151] Hiroshi Shibasaki and Mark Hallett. What is the bereitschaftspotential? *Clinical neurophysiology*, 117(11):2341–2356, 2006.

[152] Rongqing Cui and Colum D MacKinnon. The effect of temporal accuracy constraints on movement-related potentials. *Experimental brain research*, 194(3):477–488, 2009.

[153] Yin Fang, Vlodek Siemionow, Vinod Sahgal, Fuqin Xiong, and Guang H Yue. Greater movement-related cortical potential during human eccentric versus concentric muscle contractions. *Journal of Neurophysiology*, 86(4):1764–1772, 2001.

[154] Vlodek Siemionow, Guang H Yue, Vinoth K Ranganathan, Jing Z Liu, and Vinod Sahgal. Relationship between motor activity-related cortical potential and voluntary muscle activation. *Experimental Brain Research*, 133(3):303–311, 2000.

[155] Hans H Kornhuber and Lüder Deecke. Hirnpotentialänderungen bei willkürbewegungen und passiven bewegungen des menschen: Bereitschaftspotential und reafferente potentiale. *Pflüger's Archiv für die gesamte Physiologie des Menschen und der Tiere*, 284(1):1–17, 1965.

[156] Lüder Deecke, Peter Scheid, and Hans H Kornhuber. Distribution of readiness potential, pre-motion positivity, and motor potential of the human cerebral

cortex preceding voluntary finger movements. *Experimental Brain Research*, 7(2):158–168, 1969.

[157] James G Colebatch. Bereitschaftspotential and movement-related potentials: Origin, significance, and application in disorders of human movement. *Movement Disorders*, 22(5):601–610, 2007.

[158] Ivan Rektor, Martin Bareš, and Dagmar Kubová. Movement-related potentials in the basal ganglia: a seeg readiness potential study. *Clinical neurophysiology*, 112(11):2146–2153, 2001.

[159] Akio Ikeda, HANS O LÜDERS, Richard C Burgess, and Hiroshi Shibasaki. Movement-related potentials recorded from supplementary motor area and primary motor area. *Brain*, 115(4):1017–1043, 1992.

[160] Shogo Yazawa, Akio Ikeda, Takeharu Kunieda, Shinji Ohara, Tatsuya Mima, Takashi Nagamine, Waro Taki, Jun Kimura, Tomokatsu Hori, and Hiroshi Shibasaki. Human presupplementary motor area is active before voluntary movement: subdural recording of bereitschaftspotential from medial frontal cortex. *Experimental brain research*, 131(2):165–177, 2000.

[161] L Deecke. Bereitschaftspotential as an indicator of movement preparation in supplementary motor area and motor cortex. In *Ciba Foundation Symposium 132-Motor Areas of the Cerebral Cortex*, pages 231–250. Wiley Online Library, 1987.

[162] Ming-Kuei Lu, Noritoshi Arai, Chon-Haw Tsai, and Ulf Ziemann. Movement related cortical potentials of cued versus self-initiated movements: Double dissociated modulation by dorsal premotor cortex versus supplementary motor area rtms. *Human brain mapping*, 33(4):824–839, 2012.

[163] Niels Birbaumer, Thomas Elbert, Anthony G Canavan, and Brigitte Rockstroh. Slow potentials of the cerebral cortex and behavior. *Physiological reviews*, 70(1):1–41, 1990.

[164] H Shibasaki, G Barrett, Elise Halliday, and AM Halliday. Cortical potentials associated with voluntary foot movement in man. *Electroencephalography and clinical neurophysiology*, 52(6):507–516, 1981.

[165] Ross Cunnington, Robert Iansek, John L Bradshaw, and Jim G Phillips. Movement-related potentials associated with movement preparation and motor imagery. *Experimental brain research*, 111(3):429–436, 1996.

[166] M Simonetta, M Clanet, and O Rascol. Bereitschaftspotential in a simple movement or in a motor sequence starting with the same simple movement. *Electroencephalography and Clinical Neurophysiology/Evoked Potentials Section*, 81(2):129–134, 1991.

[167] S Yoshida, K Nakazawa, E Shimizu, and I Shimoyama. Anticipatory postural adjustments modify the movement-related potentials of upper extremity voluntary movement. *Gait & posture*, 27(1):97–102, 2008.

[168] Kazuya Yoshida, Ryuji Kaji, Toshiaki Hamano, Nobuo Kohara, Jun Kimura, and Tadahiko Iizuka. Cortical distribution of bereitschaftspotential and negative slope potential preceding mouth-opening movements in humans. *Archives of oral biology*, 44(2):183–190, 1999.

[169] Lüder Deecke, Berta Grözinger, and HH Kornhuber. Voluntary finger movement in man: cerebral potentials and theory. *Biological cybernetics*, 23(2):99–119, 1976.

[170] Ming-Kuei Lu, Patrick Jung, Barbara Bliem, Hsu-Tzu Shih, Yi-Ting Hseu, Yu-Wan Yang, Ulf Ziemann, and Chon-Haw Tsai. The bereitschaftspotential in essential tremor. *Clinical Neurophysiology*, 121(4):622–630, 2010.

[171] Apostolos P Georgopoulos. Neural aspects of cognitive motor control. *Current opinion in neurobiology*, 10(2):238–241, 2000.

[172] Margaret Schenkman, Richard A Berger, Patrick O Riley, Robert W Mann, and W Andrew Hodge. Whole-body movements during rising to standing from sitting. *Physical Therapy*, 70(10):638–648, 1990.

[173] Anthony N Carlsen and Colum D MacKinnon. Motor preparation is modulated by the resolution of the response timing information. *Brain research*, 1322:38–49, 2010.

[174] Jun Tanji. Sequential organization of multiple movements: involvement of cortical motor areas. *Annual review of neuroscience*, 24(1):631–651, 2001.

[175] Christian Gerloff, Brian Corwell, Robert Chen, Mark Hallett, and Leonardo G Cohen. The role of the human motor cortex in the control of complex and simple finger movement sequences. *Brain*, 121(9):1695–1709, 1998.

[176] Masafumi Sone and Hiroaki Wagatsuma. A stress-generated backlash power in s-shaped plates for the development of robotic plastic muscles. In *Proceedings of the 21st annual conference of the Japanese Neural Networks Society, JNNS*, pages 188–189, 2011.

[177] M Sone, H Wagatsuma, K Tachibana, and K Sakamoto. Robotic rehabilitation tool supporting up and down motions in the bathroom–analyses of the catapultassisted taking-off mechanism. In *Proceedings of 9th International Conference on Disability, Virtual Reality and Associated Technologies, ICDVRAT*, 2012.

[178] Thomas C Bulea, Saurabh Prasad, Atilla Kilicarslan, and Jose L Contreras-Vidal. Sitting and standing intention can be decoded from scalp eeg recorded prior to movement execution. *Frontiers in neuroscience*, 8:376, 2014.

[179] Arnaud Delorme and Scott Makeig. Eeglab: an open source toolbox for analysis of single-trial eeg dynamics including independent component analysis. *Journal of neuroscience methods*, 134(1):9–21, 2004.

[180] Christophe Ris and Stéphane Dupont. Assessing local noise level estimation methods: Application to noise robust asr. *Speech Communication*, 34(1):141–158, 2001.

[181] G Nisha Meenakshi and Prasanta Kumar Ghosh. Robust whisper activity detection using long-term log energy variation of sub-band signal. *IEEE Signal Processing Letters*, 22(11):1859–1863, 2015.

[182] Stanislaw Solnik, Patrick Rider, Ken Steinweg, Paul DeVita, and Tibor Hortobágyi. Teager–kaiser energy operator signal conditioning improves emg onset detection. *European journal of applied physiology*, 110(3):489–498, 2010.

[183] Xiaoyan Li, Ping Zhou, and Alexander S Aruin. Teager–kaiser energy operation of surface emg improves muscle activity onset detection. *Annals of biomedical engineering*, 35(9):1532–1538, 2007.

[184] P Laurie Davies, Roland Fried, and Ursula Gather. Robust signal extraction for on-line monitoring data. *Journal of Statistical Planning and Inference*, 122(1):65–78, 2004.

[185] Shuji Hashimoto, Hisae Gemba, and Kazuo Sasaki. Premovement slow cortical potentials and required muscle force in self-paced hand movements in the monkey. *Brain research*, 197(2):415–423, 1980.

[186] Brigitte Rockstroh, Thomas Elbert, Werner Lutzenberger, and Niels Birbaumer. The effects of slow cortical potentials on response speed. *Psychophysiology*, 19(2):211–217, 1982.

[187] Hiroaki Masaki, Noriyoshi Takasawa, and Katuo Yamazaki. Enhanced negative slope of the readiness potential preceding a target force production task. *Electroencephalography and Clinical Neurophysiology/Evoked Potentials Section*, 108(4):390–397, 1998.

[188] Jun-ichi Kitamura, Hiroshi Shibasaki, Akiteru Takagi, Hideo Nabeshima, and Akira Yamaguchi. Enhanced negative slope of cortical potentials before sequen-

tial as compared with simultaneous extensions of two fingers. *Electroencephalography and clinical neurophysiology*, 86(3):176–182, 1993.

[189] R Benecke, JPR Dick, JC Rothwell, BL Day, and CD Marsden. Increase of the bereitschaftspotential in simultaneous and sequential movements. *Neuroscience letters*, 62(3):347–352, 1985.

[190] Steven C Cramer, Robert M Weisskoff, Judith D Schaechter, Gereon Nelles, Mary Foley, Seth P Finklestein, and Bruce R Rosen. Motor cortex activation is related to force of squeezing. *Human brain mapping*, 16(4):197–205, 2002.

[191] MA Hughes, DK Weiner, ML Schenkman, RM Long, and SA Studenski. Chair rise strategies in the elderly. *Clinical Biomechanics*, 9(3):187–192, 1994.